Stiffness Design of Laminated Composites

Efficient Conversion of Lamination Parameters into Stacking Sequences

Master of Science Thesis

Rakshith Manikandan

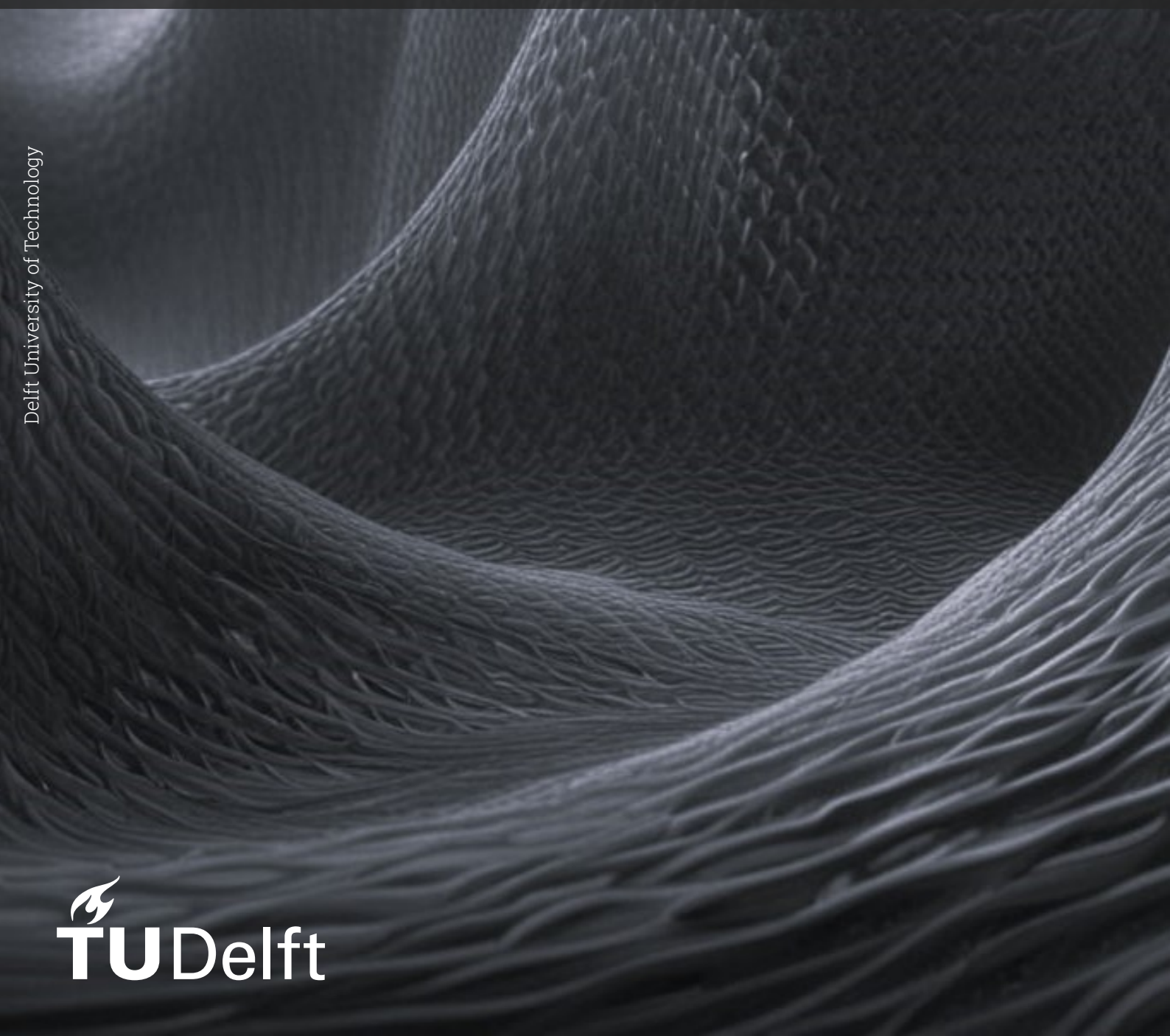

Delft University of Technology

TU Delft

Stiffness Design of Laminated Composites

Efficient Conversion of Lamination Parameters into Stacking Sequences

by

Rakshith Manikandan

to obtain the degree of Master of Science
at the Delft University of Technology,

Student Number:	5466210
Supervisors:	Dr. D.M.J. Peeters, and Dr. J.M.J.F. van Campen
Course Code:	AE5711-Thesis Aerospace Structures & Materials
Duration:	16/01/2023 - 21/11/2023
Location:	Faculty of Aerospace Engineering, Delft

Cover:	AI art made using NightCafe Studio representing sinusoidal surface waves made of fibre-reinforced laminates
Style:	TU Delft Report Style, with modifications by Daan Zwaneveld

TU Delft

Delft University of Technology
Faculty of Aerospace Engineering
Department of Aerospace Structures and Materials

GRADUATION COMMITTEE

Dated: 21-11-2023

Chair holder:

Dr.ing. S.G.P.(Saullo) Castro

Committee members:

Dr.ir. J.M.J.F.(Julien) van Campen

Dr.ir. D.M.J.(Daniël) Peeters

Dr. N.(Nan) Yue

Preface

While placed at the beginning, this was the last piece of text I wrote in this thesis. Writing these lines carried certain emotional weight, as it marks the end of my Master's study in this beautiful city of Delft. While I do not know what the future holds, I will remember the last two years for all the highs and lows. This experience has made me a better engineer and, more importantly, a better person. It seems I expressed this sentiment at the end of every milestone in my life till now, but I am happy about my progress, nonetheless. At the same time, no accomplishment is solely one's own, and I have a lot of people to thank for it. I offer my apologies in advance if I forget to mention someone.

I firmly believe that exciting and formidable challenges have always been the driving force behind human greatness on numerous fronts. In our collective pursuit for a sustainable future, researchers worldwide are working on many such exciting problems. One such problem in the field of lightweight composite design is to efficiently determine fibre orientations in a laminate for predefined stiffness targets- an enigma often called as the 'Inverse Problem'. It is here that I would like to thank Yasser M. Meddaikar, my internship supervisor at DLR-Göttingen, for introducing me to this problem. Your guidance and unwavering support ever since have been invaluable to me.

My academic and practical ventures, including this Master's degree, enriched me with valuable knowledge and technical skills. With these tools, I aimed to better navigate the complex design space offered by laminated composites. Here, I extend my profound gratitude to Dr.ir J.M.J.F. (Julien) van Campen and Dr.ir D.M.J. (Daniël) Peeters for helping frame my topic and supervising me throughout this odyssey. I thank you for the countless hours you have spent with me, and always be there to shine your wisdom. While we may have had our share of disagreements (e.g., 'designed layers'), I cannot overstate your influence on both my scientific and personal growth. By observing how you approach a problem, question-presented data, and organise your thoughts, you have made me more patient, diligent, and a better problem solver. You have elevated the quality of my work to heights I had never imagined for myself. While the inverse problem remains a problem, your guidance has brought me closer to understanding it. I eagerly anticipate how this study will be pursued by others, or perhaps by myself, in the near future.

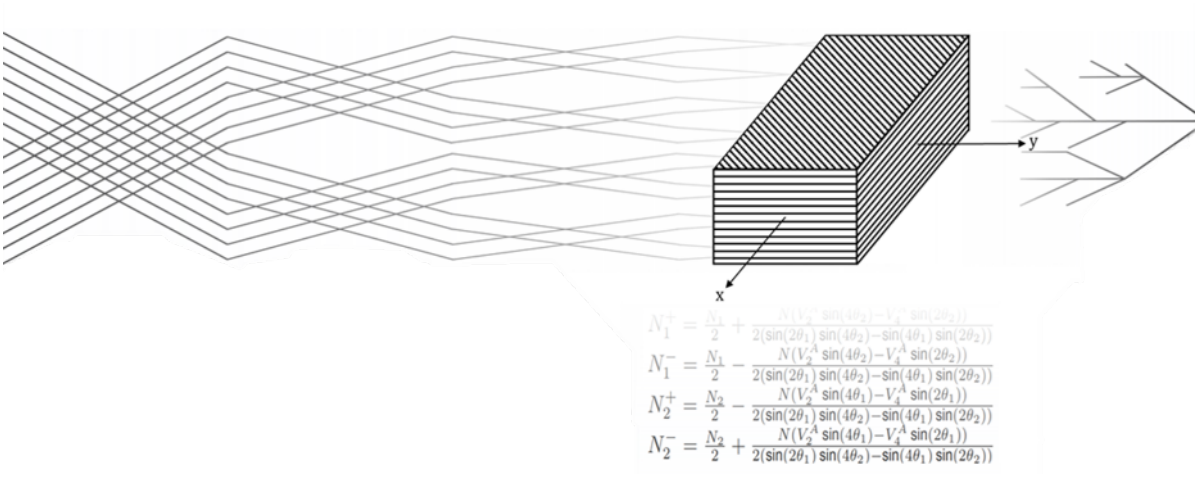

My heartfelt thanks goes to my family and friends. Atharva, Avyadhish, George Popi, Georgia, Kübra, Ritika, Sovit, Swapan, Tanuj, Thom, Vikram, and Yi-Hsiu - your unwavering support has been my anchor. Thanks for tolerating my quirks. From cooking together, travelling cross-country, and cherished evenings, you guys are the best friends I could have asked for. Swapan, you might not be aware, but we are dubbed the 'Lamination Parameter Bros'. I will cherish our discussions about higher dimensional space, neural networks, home food, and, well, all things LPs. We south Indians have a thing for LPs, though the reasons escape me. Thank you for being there during challenging times and never discouraging me from taking the difficult road.

Moreover, to all my friends in the MSc workspace—Filippo, Javier, Mateo, Shreyasi, and Stephan—thank you for your presence. It was really fun sharing our insights into each other's problems. Your insightful questions always helped me challenge my assumptions. Dr. ing S.G.P. (Saullo) Castro, although I regrettably did not attend any of your courses or lectures, I am sincerely grateful for your continued support and guidance throughout my Master's journey. I treasure your motivational talks and am happy to see you on my graduation assessment committee alongside Dr. N. (Nan) Yue. Working with DARE during this thesis journey has been a pleasure. I thank Marcel for the enjoyable moments spent working on the buckling of composite shells with cutouts. More than the lack of experimental data to validate our FEM, ANSYS, I must say, has been our formidable adversary at times.

The solutions to a lot of our problems exists, but they may not always take the form we expect. As such, with this thesis, I drew upon wisdom from the realm of signal processing to design composites more efficiently. I could not have reached this point without each one of you. This thesis stands as a testament to your invaluable contributions, and it is dedicated to all of you.

Rakshith
Delft, November 2023

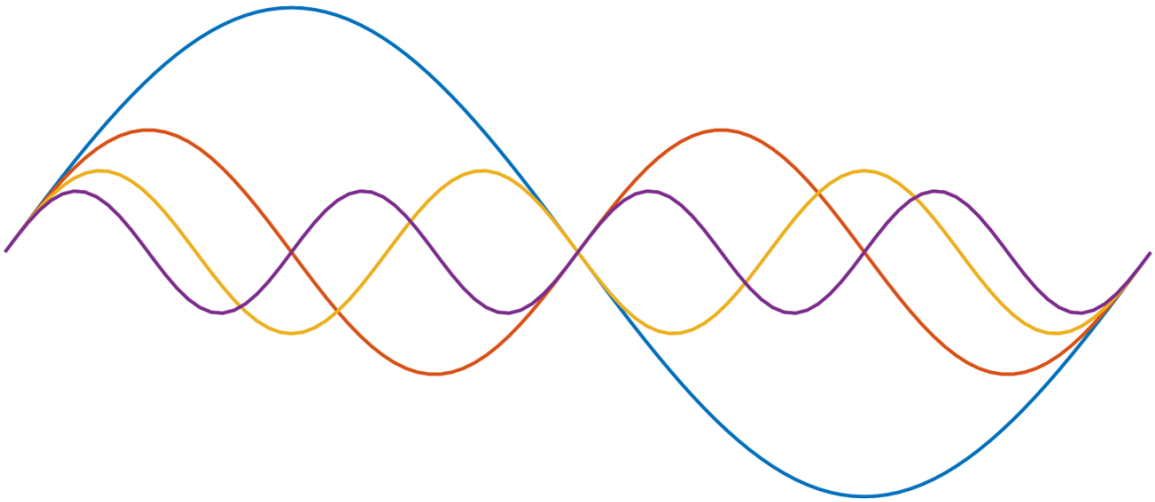

Abstract

Fibre-reinforced laminated composites are constructed layer-by-layer, allowing their material properties to be easily tailored relative to their isotropic counterparts (metallic alloys). Moreover, a composite structure with variable stiffness (VS) can be made by spatially tailoring stiffness across a laminate. This permits better load distribution within a structure, efficiently using a given material, and allow for lighter construction. Typically, the design of VS structures follows a bi-level procedure: first, the structure's stiffness distribution is optimised using lamination parameters (LPs), and second, the stacking sequences (SS) of differently oriented fibres are designed to achieve the desired stiffness distribution. However, the designs envisioned using LPs are only sometimes exactly matched by the designed SS. The shortcomings faced during this conversion are called the 'Inverse Problem'. Upon reviewing the existing techniques in literature to handle the inverse problem, it was understood that converting LPs into SS is challenging without incurring substantial computational costs or imposing significant restrictions on allowable fibre orientations in the design. Such restrictions tend to under-utilise the directional properties of the fibres. Thus, there was a need to explore and develop better stiffness design methods for laminated composites by bridging the gap between LPs and SS in a computationally efficient way.

In response to this challenge, a hierarchical design framework was proposed to handle the Inverse Problem. Diverging from conventional methods that directly design the SS and try to match a given set of LPs, this framework divides the problem into two distinct stages. Initially, the focus is to use the In-Plane LPs and determine the number of layers in each orientation within a laminate, also called the Fibre Angle Distribution (FAD). Subsequently, the FAD serves as an interim solution, and the SS can be designed by using the Out-of-Plane LPs along with it. This problem partitioning enhances computational efficiency and offers potential benefits in solving the Inverse Problem more effectively. Given the time constraints inherent to a master thesis, the primary undertaking of this study was to efficiently design the FAD while accommodating a wide range of possible fibre orientations. To address this, a novel method using the Fast-Fourier Transform (FFT) was developed to facilitate FAD design with ply angle multiples of 15° (or $[\Delta 15^\circ] = [0, \pm 15, \pm 30, \pm 45, \pm 60, \pm 75, 90]$). Moreover, empirical guidelines for SS design, such as the Symmetry and Balancing rule, were incorporated into the design step.

The primary contribution of this report is introducing an FFT-based method to design FADs, a novel addition to the existing body of research. Upon extensive testing, it was shown that this implementation could convert LPs into multiple unique FAD solutions in less than 0.3 seconds on a regular office laptop, outperforming other methods in literature by at least ten times. Furthermore, the implementation was also used to demonstrate the benefits of designing laminated composites using $[\Delta 15^\circ]$ over the conventional $[\Delta 45^\circ]$ orientations (or $[0, \pm 45, 90]$). In light of the positive results, it is pointed out that the In-Plane LPs (and consequently the In-Plane stiffness) are known to be sensitive only to the FAD and not their SS. As such, the readers of this thesis are presented with a very computationally efficient approach for designing laminated composites for In-Plane Stiffness.

However, it is crucial to acknowledge the method's limitations in designing unbalanced FADs with more than three-ply orientations. Although possible with manual effort, the framework is not robust enough to be automatically set up for smaller ply angle increments, such as $[\Delta 5^\circ]$. Hence, the report concludes by elaborating on these points and presenting recommendations to make the hierarchical SS design framework more complete and robust.

Executive Summary

Structural design using fibre-reinforced laminated composites allows for lighter construction than metallic alloys. This can be attributed to the layer-by-layer construction of these materials, allowing better use of their specific strength and tailoring their stiffness for a given application by altering fibre orientations in each layer. Furthermore, a designer also has the freedom to tailor stiffness across the structure to handle uniform or non-uniform load distributions. This redistributes loads within a structure, efficiently uses a given composite material, and consequently allows for lighter designs. The design of such variable stiffness structures is commonly handled using an effective bi-level procedure instead of designing every single layer's orientation in a structure. First, the stiffness distribution of a structure is described by a set of 12 non-dimensional variables ($V_{1,2,3,4}^{A,B,D}$) known as lamination parameters (LPs). Then, the Stacking Sequence (SS) of plies with different orientations are designed. However, designing an SS with the same stiffness described by LPs is a complex task. They are hence termed the 'Inverse Problem' in the literature. Upon reviewing the challenges faced by existing solutions for this problem, the following was realised: currently-used techniques to convert LPs to SS become computationally expensive when designing with ply orientations beyond the conventional set of $[0, \pm 45, 90]$ (or, $[\Delta 45^{\circ}]$). Hence, the objective of this thesis was to develop an efficient technique to design laminates with a set of non-conventional orientations ($[\Delta 15^{\circ}] = [0, \pm 15\ , \pm 30, \pm 45, \pm 60, \pm 75, 90]$). To achieve this, a novel approach inspired by signal processing methods was put forward.

Upon numerically analysing the relation used to calculate LPs for a given SS, it was understood that they are a weighted sum of sinusoids of the angles in the SS. Hence, the objective of the inverse problem is to split the LPs into a sum of sinusoids, such that an SS can be inferred from them. As such, they resembled the working of the Fast Fourier Transform (FFT) algorithm in signal processing. Using FFTs, a given harmonic signal can be represented as a sum of sinusoidal signals with different frequencies. This is performed to know a given signal's constituent frequencies and their respective amplitudes. LPs were then represented in the time domain to utilise FFTs to design laminated composites.

A mathematically feasible way to represent LPs in time was by parameterising ply orientations as frequency, and the corresponding sum of their weighting terms (Sum of Weights) in the LP formulations as amplitudes. Although all LPs are correlated, they are made using two different sinusoids (sin and cos) and correspond with three different stiffness matrices (ABD) through different weights. Hence, multiple signals are required to represent a set of LPs. As this thesis limited itself to designing symmetric laminates, the coupling stiffness matrix $B = 0$ (and $V_{1,2,3,4}^{B} = 0$). Thus, four different laminate signals $L_{1,2}^{A,D}$ was parameterised to represent the remaining 8 LPs ($V_{1,2,3,4}^{A,D}$). L_1^A represents the two In-Plane Cosine based LPs ($V_{1,3}^{A}$), L_2^A represents the two In-Plane Sine based LPs ($V_{2,4}^{A}$), L_1^D represents the two Out-of-Plane Cosine based LPs ($V_{1,3}^{D}$), and L_2^D represents the two Out-of-Plane Sine based LPs ($V_{2,4}^{D}$).

Given the parameterisation, it was understood that performing an FFT on laminate signals yields the Sum of Weights for all ply orientations in a laminate. However, the Sum of Weights varies for every signal $L_{1,2}^{A,D}$. Upon examining what these quantities mean, it was realised that the Sum of Weights obtained from L_1^A and L_2^A corresponds to the number of plies belonging to different orientations in a laminate (Fibre-Angle Distribution (FAD)). In contrast, the Sum of Weights from L_1^D and L_2^D does not intuitively relate to the laminate. Initially, it was hypothesised that the information about FAD and the out-of-plane sum of weights could be used together to design an SS. However, later in this thesis, it was realised that performing FFTs on the sine-based signals (L_2^A and L_2^D) and reliably obtaining outputs from L_1^D was not a viable task. Therefore, FFTs were only performed on L_1^A. Moreover, the FAD obtained from L_1^A corresponds to $|\theta|$ (insensitive to the sign $+$ or $-$). The even nature of cosine functions inside L_1^A explains this characteristic.

Based on the attainable information from FFTs, it was decided that a set of LPs would be converted

into an SS using a step-by-step procedure. This was termed the Hierarchical SS Design Framework, and they work as follows: Initially, $V^A_{1,2,3,4}$ is used to design the FAD, after which they are rearranged to match the $V^D_{1,2,3,4}$.

For the design of Symmetric-Balanced FAD, the LPs $V^A_{2,4} = 0$. Hence, they can be designed only considering $V^A_{1,3}$. This was achieved by performing FFT on L^A_1. In a balanced FAD, the off-axis ply counts of any $+\theta$ and $-\theta$ are equal. Therefore, the FAD solution from L^A_1 provides ply counts of $|\theta|$, which are then equally split between $+\theta$ and $-\theta$. Since the Inverse Problem is multi-modal, multiple unique laminates can have the same LPs. Consequently, many different L^A_1 exist for the same $V^A_{1,3}$. Nevertheless, the signal parameterisation helped visualise the temporal behaviour of different L^A_1 with the same LPs. They exhibited several symmetries and repetitions. These repeating patterns were parameterised in terms of the known LPs($V^A_{1,3}$). As such, they were termed 'Signal Patterns'. Using them, multiple interpretations of L^A_1 could be described for the same $V^A_{1,3}$. Consequently, performing FFTs on them helped obtain multiple unique FADs corresponding to the same $V^A_{1,3}$. However, it has to be said that a subset of these patterns was mathematically derived for a given set of three orientations from a $[\Delta\theta]$, and the rest were manually identified with the help of FADs that belong to different parts of the $V^A_{1,3}$ space. These patterns were termed 'Exact Patterns' and 'Approximate Patterns', respectively. They formed a pool of pre-observed signal patterns. Moreover, an open-source genetic algorithm was used to design the FADs for manual pattern identification. As such, in this thesis, 58 signal patterns were made for $[\Delta 15°]$. Each can design closely matching FADs at different parts of the $V^A_{1,3}$ space.

For the case of Symmetric-Unbalanced FADs, the ply counts belonging to a $|\theta|$ need to be unequally split between $+\theta$ and $-\theta$ to match a target $V^A_{2,4}$ value. Hence, for unbalanced designs, the known $|\theta|$ ply counts (FAD) from the FFT of L^A_1 and the target $V^A_{2,4}$ were used to construct a System of Equations. This system was then used to determine how to unequally split a maximum of three off-axis $|\theta|$. As such, this step concluded the design of FADs in the implementation. For completeness, it must be said that an FFT or a System of Equations by themselves cannot design FADs that contain integer ply counts. Hence, these procedures and a series of post-processing steps were implemented. With the time constraints of the master thesis, the conversion of FAD to SS to match a set of $V^D_{1,2,3,4}$ was not implemented. Regardless, based on the learnings from the literature review, it was understood that a combinatorial optimiser is best suited to handle this step. Thus, a layerwise optimisation method using decision trees is suggested to complete the hierarchical framework.

As it stands, the hierarchical framework can design FADs using an FFT-based method. Hence, their capabilities were thoroughly tested for FAD design. Through the results of these tests, it was understood that for both the design of Symmetric-Balanced and Symmetric-Unbalanced FADs, the implementation is very efficient, as it is capable of designing multiple unique solutions within a blink of an eye (less than 0.4s). Combined with their solution accuracy, this outperformed all other design procedures in the literature that handle the Inverse Problem, at least by a ten-fold margin. Moreover, the implementation demonstrated the benefits of using non-conventional $[\Delta 15°]$ ply orientations over the conventional $[\Delta 45°]$. By using $[\Delta 15°]$, more of the feasible $V^A_{1,3}$ design space can be matched with a FAD with less number of N, paving the way for lighter designs.

Nevertheless, it is crucial to address the limitations of the current implementation. In the case of Symmetric-Unbalanced FADs, the current implementation can design them with a maximum of three off-axis $|\theta|$'s. Hence, the solution accuracy of this framework is inferior to a GA for $V^A_{1,2,3,4}$ combinations that can only be achieved with more than three off-axis orientations. Furthermore, the hierarchical framework is currently set up to design laminates with $[\Delta 15°]$, but they lack the robustness to automatically accommodate $[\Delta 5°]$ orientations in design. This is because an exhaustive and manual pattern-finding operation has to be performed to make Approximate Patterns. Therefore, future work should focus on overcoming these limitations, making the implementation more robust, and extending the framework's capabilities to design SS, all while considering the empirical design guidelines.

The MATLAB implementation of the FFT-based method and the benchmark datasets used for validations can be accessed from a GitHub repository (`https://github.com/rakshith-m1505/LP2FAD`).

Contents

Nomenclature

Symbols

Symbol	Definition
$[a, b, c]$	Coefficients to solve for Exact Patterns
ABD	Extensional, Coupling, and Flexural Stiffness Matrix
h	Laminate thickness
L	Laminate Signal
n	Number of off-axis ply orientations in a laminate
N	Number of Plies (in the symmetric half (from chapter 7))
T	Fictitious Time-Domain of Laminate Signals
V	Lamination Parameters
$V^A_{1,2,3,4}$	Four In-Plane Lamination Parameters
$V^B_{1,2,3,4}$	Four Coupled Lamination Parameters
$V^D_{1,2,3,4}$	Four Out-of-Plane Lamination Parameters
z	Through-thickness location in a laminate
ε	Mismatch error between target LPs and designed LPs
Γ	Material Invariant matrices
ν	Volume Fraction of plies belonging to a orientation
ω	Frequency(s) in a harmonic signal
θ	Ply Orientation
$[\Delta\theta]$	Set of ply orientations that are multiples of θ
$\mathcal{N}$	Number of Time-Domain Samples of a signal
$\mathcal{O}$	Computational Complexity

Abbreviations

Term	Definition
2D/4D	2-Dimensional/4-Dimensional
ABD	Collective name of Extensional, Coupling, and Flexural Stiffness matrix
AFP	Automated Fibre Placement
DFT	Discrete Fourier Transform
FAD	Fibre Angle Distribution
FBB	Fractal Branch and Bound
FEA	Finite Element Analysis
FFT	Fast Fourier Transform
GA	Genetic Algorithm
LO	Layerwise Optimisation
LP	Lamination Parameter
NUFFT	Non-uniform Fast Fourier Transform
PHC	Polynomial Homotopy Continuation
SFVS	Straight Fiber Variable Stiffness
SS	Stacking Sequence
SST	Stacking Sequence Table
VS	Variable Stiffness
QI	Quasi-Isotropy

Glossary

Term	Definition/Explanation
2D-Benchmark	Self-made benchmark dataset with $V_{1,3}^{A}$ targets (2-Dimensional entities). It is used while making L_1^A signal patterns and test design performance for Symmetric-Balanced FADs (see section 10.1).
4D-Benchmark	Self-made benchmark dataset with $V_{1,2,3,4}^{A}$ targets (4-Dimensional entities). It is used while testing design performance for Symmetric-Unbalanced FADs (see subsection 10.3.2).
Approximate Pattern	Describes the behaviour of L_1^A signals belonging to FADs with more than three $\lvert\theta\rvert$'s. The patterns are made by manually approximating L_1^A values at different timestamps as a function of $V_{1,3}^{A}$ (see subsection 7.1.2).
Balanced Laminate (or Balanced SS)	Laminates with a stacking sequence (SS), whose off-axis θ's (orientations apart from 0 and 90) always occur as a balanced pair of $+\theta$ and $-\theta$.
Conventional Orientations	Collective name to address the ply orientations $[0, \pm 45, 90]$ or $[\Delta 45^{\circ}]$. In the early years, for manufacturing convenience, plies were decided to be oriented only along these four directions.
Convex and Non-Convex design space	A design space is convex if one were to connect any two points within this space with a straight line, and every point along that line would also fall within the confines of the space. Design spaces that do not obey this property are known to be non-convex. In this thesis, the lamination parameters (LPs) mathematically describe a convex design space of laminate stiffness, while the stacking sequence (SS) describes a non-convex design space of laminate stiffness.
Cosine and Sine-based LPs	Out of the 12 lamination parameters(LPs), six consist of sine functions, while the other six consist of cosines. As such, in certain parts of this thesis, the LPs are addressed based on the sinusoidal function present within them.
Discrete Fourier Transform (DFT)	A mathematical operation whose inputs are time-domain samples of a signal, and their outputs present the amplitudes and phase differences of all the frequencies present in the signal.
Decision tree paradigm	A graphical representation used in problem-solving, where a complex issue is systematically broken down into a series of interconnected questions or decisions. As each question is answered by making a decision, it leads to further branching questions, creating a tree-like structure. This method is employed to navigate a design space to arrive at a viable solution through a step-by-step decision-making process. In this thesis, the literature review discusses various research works that use this decision tree paradigm to design composites (in subsection 3.2.3).

Term	Definition/Explanation
DFT Coefficients	For every frequency present in a signal, a discrete Fourier transform (DFT) can provide their corresponding amplitudes and phase differences. These entities are represented collectively within an array of complex numbers, and each value in this array is termed a DFT coefficient.
Empirical Design Guidelines	The rules commonly followed while designing laminated composite for them to be manufacturable and have structural integrity. A complete list of these guidelines can be referred from section A.3.
Error Distribution	A plot illustrating a distribution of mismatch errors incurred when a set of lamination Parameters(LPs) were attempted to be matched using laminates for different numbers of layers (N).
Error Profile	Visually represents the capability of this thesis implementation to design laminates at different parts of the $V^A_{1,3}$ design space.
Exact Pattern	Describes the behaviour of L^A_1 signals belonging to FADs with less than or equal to three $\|\theta\|$'s. The patterns are mathematically derived for three given $\|\theta\|$'s, and they can describe values at different timestamps as a function of $V^A_{1,3}$ (see subsection 7.1.1).
Fibre Angle Distribution (FAD ($\forall\|\theta\|$ or θ))	Describes the number of plies belonging to every $\|\theta\|$ or θ in a laminated composite.
Feasible design domain of LPs	All lamination parameters (LPs) are individually defined. However, they are mathematically correlated since they all need to correspond to the same laminate. Hence, the value of LPs is mathematically bound by certain feasible domains. The feasible domain of certain LPs is also called Miki's diagram in literature (as seen in Figure 3.1).
Fast Fourier Transform (FFT)	An efficient algorithm used to perform the discrete Fourier transform (DFT).
Fast Fourier Transform (FFT)-based method	An FFT inspired approach to design a laminate's Fibre-Angle Distribution using lamination parameters (LPs).
Frequency and amplitude of a laminate Signal	The laminate signals were parameterised such that their frequencies numerically correspond to ply orientations present in a laminate, and their respective amplitudes were the Sum of Weighted terms that make up their LP values.
Frequency bins	Each discrete Fourier Transform (DFT) coefficient corresponds to a frequency. Hence, every position within the array of DFT coefficients is called a 'frequency bin'.
Frequency Spectrum of a signal	A plot describing the frequencies present in the signal and their corresponding amplitudes.
Fundamental Frequency (of a harmonic signal)	It is defined as the frequency corresponding to the difference between multiple frequencies present within a harmonic signal. They are numerically quantified as their greatest common divisor of the present frequencies.
Genetic Algorithm	An optimisation technique inspired by the idea of Darwinian evolution. It starts with a population of randomly generated solutions. Over many iterations, they are combined and mutated into a new set of solutions, which is repeated till the best solution, according to a predefined objective, is found.
Harmonic Signal	A signal that repeats itself at specific intervals throughout infinity (in time). It is important to note that such signals may comprise various frequencies within them

Term	Definition/Explanation
Hierarchical SS design procedure/framework	Design approach through which the laminate's Fibre-Angle Distribution (FAD) is designed first, after which their Stacking Sequence (SS) is designed. This framework works contrary to what is commonly found in literature, which directly attempts to design SS to match a set of LPs. The FAD design is performed by the FFT-based method.
Integer Ply Counts	Laminated composites are built layer-by-layer, while each could consist of plies of different orientations. Hence, it is evident that the count of these different plies must always be an integer value. This definition is provided because the solutions from this thesis implementation often required post-processing such that they do not design laminates with non-integer ply count values.
Inverse Problem	The conversion of lamination parameters into stacking sequence earned the name 'Inverse Problem' in literature due to their nature and complexity.
Lamination Parameters	A set of 12 continuous non-dimensional values, which, along with the laminate thickness, can fully describe the stiffness properties of a laminate (see subsection 2.1.1).
LP Mismatch	The discrepancy between the lamination parameters of the designed stacking sequence and the lamination parameters that are determined to be optimum. They can be measured in many different ways. In this thesis, the mismatch is measured using Euclidean Distance (see Equation 7.4)
Miki's diagram	Refer to the definition of 'Feasible design domain of LPs'.
Multi-Modality	From a mathematical optimisation perspective, a problem is multi-modal when it has multiple optimum solutions. For example, a set of lamination parameters can correspond with multiple different laminates (see Table 7.2).
Non-Conventional Orientations	Collective name to address the ply orientations that are not restricted to $[\Delta 45^\circ]$ (or $\theta \in (-89, 90]$). By using such sets of θ, a fibre can be effectively utilised in many other directions, allowing for lighter designs.
NUFFT	Procedure to implement a fast Fourier transform for a set of time-domain samples that are non-uniformly distributed in time. The version used in this thesis involves interpolating samples such that a uniform set of samples is obtained. Then, a regular fast Fourier transform is performed.
Number of Samples	Fast Fourier transform (FFT) needs to be performed on discrete time-domain samples of a signal. The number of these samples is determined by the signal's fundamental frequency.
Off-axis Ply Orientation	Orientations that are not 0° or 90° ($\lvert\theta\rvert \in (0, 90)$). For example, the off-axis orientations within $[\Delta 15^\circ]$ are $[\pm 15, \pm 30, \pm 45, \pm 60, \pm 75]$.
Ply angle delta ($[\Delta\theta]$)	Set of possible ply orientations when the minimum allowable difference between them is θ. For example: $[\Delta 15^\circ] = [0, \pm 15, \pm 30, \pm 45, \pm 60, \pm 75, 90]$.
Pool of Signal Patterns	Since different signal patterns correspond to signals made with different sets of frequencies, many such patterns were pre-observed. These patterns were collectively called the 'Pool of Signal Patterns'.
Rounding Procedure	Set of activities performed to convert non-integer FAD solutions into integers. They are required because techniques like the FFT or the System of Linear equations do not always produce integer solutions.

Term	Definition/Explanation
Sampling Rate	The rate at which a signal needs to be sampled for their FFT results to be reliable. The Nyquist-Shannon Sampling theorem suggests that the sampling rate must be decided based on the maximum detectable frequency within the signal (see subsection 4.2.2)
Signal Pattern	Help describes the value of a harmonic signal in terms of LPs at various timestamps. Depending on the frequencies within the periodic signal, their behaviour changes, and consequently, the pattern governing them changes. Hence, multiple signal patterns exist to describe the values of many different signals. In the FFT-based design method used in this thesis, the frequencies correspond to ply orientations. So, by describing signals using many such patterns, composite laminates with different sets of ply orientations were designed.
Signal Periodicity	Harmonic signals tend to repeat themselves at specific intervals. These intervals are known as a signal's periodicity, and they can be numerically quantified using their fundamental frequency.
Stacking Sequence	A common way to represent the sequence in which fibres of different orientations are stacked within a laminated composite material.
Sum of Weights	The lamination parameters (LPs), while being non-dimensional entities, can be calculated for a given laminate as a weighted sum of sinusoidal functions. The implementation presented in this thesis is capable of finding the sum of these weighting terms that are multiplied to the sinusoidal function of different ply orientations that make up the LP value.
Symmetric Laminate (or Symmetric SS)	Laminates with a stacking sequence (SS) that mirror itself symmetrically about their middle-plane.

1

Introduction

Vehicles such as automobiles, trains, ships and aircraft are the inevitable mode of transportation for any long-distance travel. Such vehicles are powered primarily by fossil fuels, contributing to almost a quarter of the world's greenhouse gas emissions [1]. These emissions promote the greenhouse effect in the atmosphere, which traps more heat and increases the surface temperature of our planet. Moreover, the availability of fossil fuels is ever-reducing. In this regard, there is a push within the scientific community to limit greenhouse gas emissions, reduce vehicle fuel consumption, and find alternate energy sources. One significant approach for reducing a vehicle's fuel consumption is efficiently designing structures with minimal material usage. As such, this master thesis centres on improving fuel efficiency by developing a method to design lightweight structures with laminated composites.

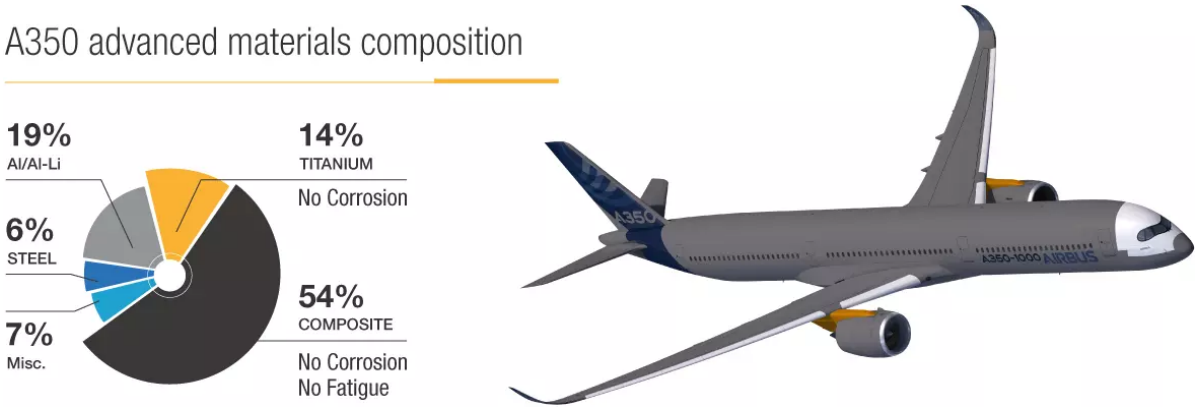

Figure 1.1: Material composition of the Airbus A350 [2]

Today, more than half the structural weight of modern aircraft comprises fibre-reinforced laminated composite materials [2, 3], owing to their superior specific strength relative to metallic alloys. The weight-saving benefits of using them can be attributed to their layer-by-layer construction, allowing better use of their specific strength. Furthermore, the work of Hyer et al. [4] showed more weight-saving potential by locally tailoring stiffness throughout a composite structure. Such tailoring was achieved by optimising the orientation of the fibres within the laminate locally, allowing better load redistribution within a structure. However, the benefits from stiffness tailoring are hard to realise in reality, as optimising such structures is more challenging and computationally expensive, given the enlarged design space that the tailoring notion provided. Hence, structural design is always performed in two stages to circumvent optimisation difficulties: First, the structure's stiffness is optimised to handle the given load case(s), and then fibre orientations are designed to realise these stiffnesses.

Nevertheless, it is sometimes complex to design laminates with a set of fibre orientations to exactly match the designed stiffness properties. This is commonly called the 'Inverse problem', and it affects

the structural feasibility of a design. Upon conducting a literature review, it was understood that many solutions had been proposed to handle this; however, their computational efficiency needs improvement. As such, this gave the impetus to research stiffness design methods of laminated composite materials. Regardless, it was then realised that the description of the inverse problem was very close to that of the Fast-Fourier transforms, an algorithm used in the frequency decomposition of signals. Hence, this thesis proposes a new design framework containing a novel technique inspired by signal processing techniques. They show promise to efficiently design a laminated composite to match a given set of directional stiffness properties.

Report Layout

This report is split into three parts. The first part consists of a literature review that introduces the design of laminated composites and then explains the challenges faced by already proposed solutions to handle the inverse problem. These challenges helped shape the focus of this thesis. The similarities between signal processing techniques and the inverse problem were then elucidated before stating the research goals for this master thesis. The second part elaborates on the mathematical implementation of the proposed design framework and its limitations. The third part will validate the implementation and compare their computational efficiency and accuracy with the state-of-the-art. Then, the report concludes all findings and states recommendations for future work.

Part I

Literature Review

2

Design of Laminated Composites

Unlike their isotropic counterparts, the macro-mechanical behaviour of composites (laminate stiffness) is not only influenced by their global sizing (length, width, and thickness). Their layer-by-layer construction allows stiffness[1] to be a variable of individual layer(ply) thickness and the orientation of reinforcing fibres within them [5]. Therefore, a laminate is defined by the stacking sequence (SS) of plies[2] with different fibre orientations within them.

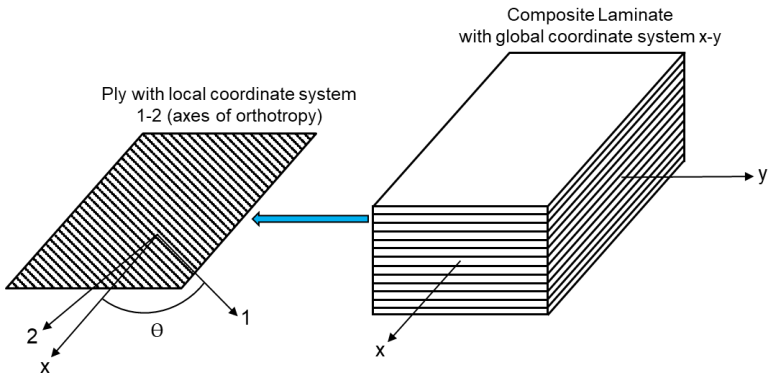

Figure 2.1: Layer-by-layer construction of laminated composite materials

In the early years when composites were introduced to the aerospace industry, for analytical and manufacturing convenience, all plies were designed to have the same thickness, and fibres were oriented only along multiples of 45° [6]: $\theta \in [0, \pm 45, 90]$. Such laminates are termed 'Conventional' and are still commonly used in the aerospace industry owing to several years of experience making aircraft with them. However, such a practice implies that a fibre's directional properties cannot be effectively used outside the aforementioned four directions. As such, more structural weight reduction can be theoretically achieved using 'Non-Conventional' orientations: $\theta \in (-90, 90]$.

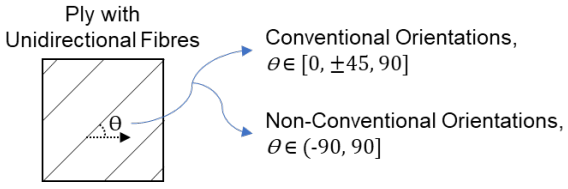

Figure 2.2: Classification of laminates based on allowable ply orientations

[1] Classical laminated plate theory describes laminate stiffness in a three-fold manner (ABD matrix): A- Extensional Stiffness, B- Coupling Stiffness, and D- Flexural Stiffness. Their formulations can be referred from the Appendix (in section A.1)

[2] Unless mentioned otherwise, a ply in this report refers to a layer of continuous and unidirectional fibres

Furthermore, engineers can capitalise on the layer-by-layer construction of laminates and design structures by spatially tailoring their stiffness. Such tailoring was shown by Hyer et al. [4] to allow material to be more efficiently used in a structure while handling various load cases (uniform or non-uniform load distributions). This study was one of the earliest to highlight the benefits of stiffness tailoring, and their potential for reducing weight was promising. As such, it served as a catalyst and promoted all future research in variable stiffness (VS) laminates.

The research to effectively design and adopt structures made of VS laminates and non-conventional orientations in the aerospace industry is gaining more significance, given that reducing aircraft fuel consumption and emissions has been the foundation of several worldwide climate-neutral development ventures [1, 7]. Therefore, to effectively utilise the design freedom provided by VS laminates, engineers resort towards mathematical optimisation techniques [6, 8]. The following sections will explain how these techniques are implemented in practice.

2.1. Bi-Level Design Procedures

As previously mentioned, the construction of laminated composite materials allows stiffness to be tailored across a structure (VS laminates). For this, a preliminary step of discretisation is performed over a structure of known geometry[3], as shown with an example of a plate with a cutout, in Figure 2.3.

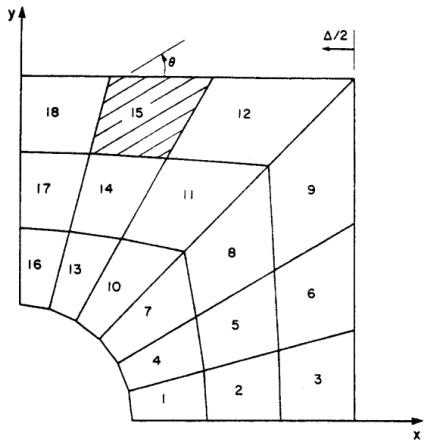

Figure 2.3: Discretising structure into segments with different material properties (Figure Courtesy:[4])

The plate shown in Figure 2.3 is loaded under compression along the x-direction, and only a quarter of it is designed upon considering symmetry in geometry and mechanical response. From here, a design procedure would find the optimal SS for each segment so the plate can handle the compression load. Nevertheless, such an arrangement is not practically scalable for large-scale structures with several components within them [8, 10, 11, 12]. This is because designing orientations for N layers in a structure (considering SS of all segments) is a N-dimensional problem, and the design space they describe for laminate stiffness is highly nonlinear. Hence, the design of VS laminates is usually partitioned into two stages and methodically dealt with to reduce computational effort. This is commonly called the bi-level procedure in literature, as illustrated in Figure 2.4.

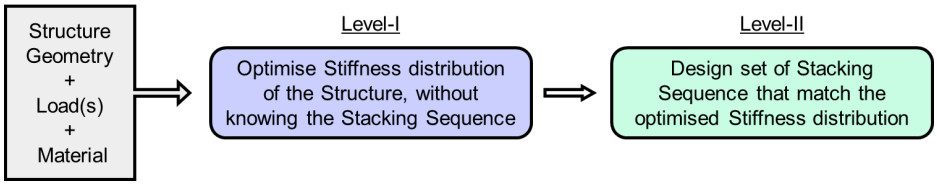

Figure 2.4: Bi-level procedure followed to design structures made of laminated composites

[3]A structure with unknown geometry can also be designed using composites by adding artificial densities as design variables to each design segment [9]. For brevity, explanations in this thesis will only focus on cases with known geometry.

Independent of the allowable ply orientations (in Figure 2.2), for a given material, geometry, and load case(s), the bi-level procedure works as follows: at level-I, the stiffness distribution of a structure is optimised for given load(s), and during level-II, the SS required to match the desired stiffness distribution is found. This approach is well-regarded in literature as it guarantees the effective use of laminated composite materials in a VS structure, when performed properly [8, 13].

For the practical implementation of Level-I, lamination parameters (LPs) [14] are used, allowing one to calculate the stiffness (ABD) without an SS. By optimising these LPs, one could optimise laminate stiffness, as discussed further in subsection 2.1.1. Following that, in Level-II, the SS is designed to match the optimum stiffness (described by the LPs in Level-I). However, this is a complex step, as the optimised LPs cannot always be exactly matched using a SS [8]. This is commonly referred to as the 'Inverse Problem,' for which several solutions have been proposed. Furthermore, there are multiple different fibre-stacking methods, using which SS can be varied across a structure and achieve VS. Hence, subsection 2.1.2 introduces different Fibre-Stacking methods, and section 2.2 will explain the Inverse Problem and the difficulties caused by them in the design process.

2.1.1. Stiffness Modelling using Lamination Parameters

To determine an optimum stiffness distribution for a structure, the directional stiffness values (ABD matrix) of every discretised design segment can be used as design variables of level-I optimisation. However, the terms within ABD are highly interrelated, making arbitrary assignment of their values difficult. Hence, Tsai et al.[14] parameterised ply material properties using trigonometric identities to linearly describe ABD using laminate height h and 12 non-dimensional quantities known as the LPs. This representation of laminate stiffness for a structure is summarised in Figure 2.5.

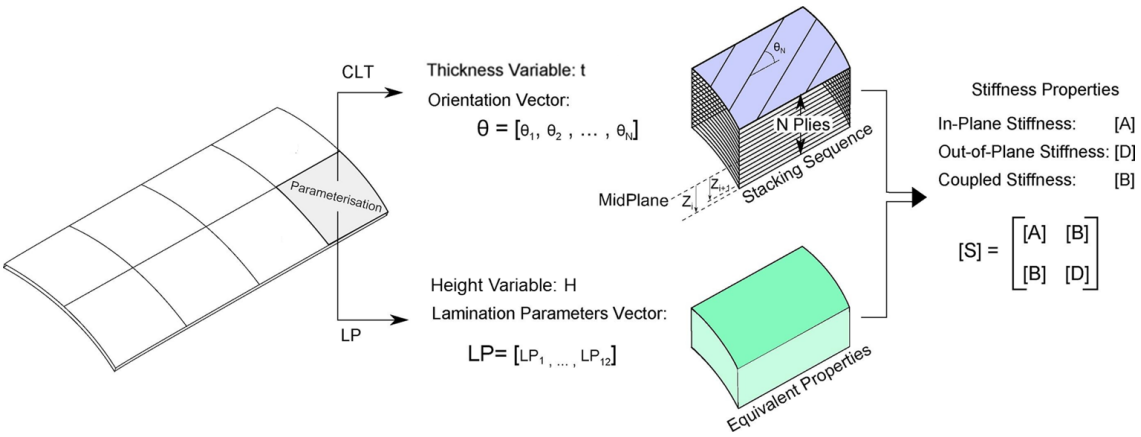

Figure 2.5: Stiffness of discretised segments in a structure, parameterised using classical laminated plate Theory (CLT) and lamination parameters (LP) (Figure modified from Macquart et al.[15])

As seen here, parameterising stiffness with LPs significantly reduces the optimisation problem dimensionality, as the number of design variables is always 12 and not dependent on N. Regardless, the ABD matrix can be mathematically described using LPs as follows:

$$\begin{aligned} A &= h(\Gamma_0 + \Gamma_1 V_1^A + \Gamma_2 V_2^A + \Gamma_3 V_3^A + \Gamma_4 V_4^A) \\ B &= \frac{h^2}{4}(\Gamma_1 V_1^B + \Gamma_2 V_2^B + \Gamma_3 V_3^B + \Gamma_4 V_4^B) \\ D &= \frac{h^3}{12}(\Gamma_0 + \Gamma_1 V_1^D + \Gamma_2 V_2^D + \Gamma_3 V_3^D + \Gamma_4 V_4^D) \end{aligned} \tag{2.1}$$

Here, the Γ entities are matrices of ply material properties that are invariant to orientation[4], and $V_{[1,2,3,4]}^{\{A,B,D\}}$

[4]Relations used to calculate the Material Invariant properties can be referred from the Appendix(section A.2)

are the LPs. For a given SS with equi-thickness plies, they can be calculated as follows:

$$V_{[1,2,3,4]}^{\{A,B,D\}} = \frac{1}{\left\{N, \frac{N^2}{2}, \frac{N^3}{4}\right\}} \sum_{k=1}^{N} \left\{1, \left(\tfrac{N}{2}-k+1\right)^2 - \left(\tfrac{N}{2}-k\right)^2, \left(\tfrac{N}{2}-k+1\right)^3 - \left(\tfrac{N}{2}-k\right)^3\right\} [\cos 2\theta_k, \sin 2\theta_k, \cos 4\theta_k, \sin 4\theta_k] \quad (2.2)$$

The compact notation used above means that V_2^D, for example, can be calculated as:

$$V_2^D = \frac{4}{N^3} \sum_{k=1}^{N} \left\{ \left(\frac{N}{2}-k+1\right)^3 - \left(\frac{N}{2}-k\right)^3 \right\} [\sin 2\theta_k]$$

Here, t represents the ply thickness, and θ_k represents the orientation of the k^{th} ply. The definitions for LPs vary across literature based on convenience, and no universally accepted notation exists. The version presented above is when LPs are appropriately normalised with h, so they are confined within the domain $V_{[1,2,3,4]}^{\{A,B,D\}} \in [-1, 1]$ (maximum and minimum values of the trigonometric functions) [6]. For completeness, it has to be mentioned here that the use of LPs is valid only for the design of laminates or sandwich structures [16], with plies and/or core, respectively, made of the same material.

The LPs are mathematically described in a continuous and convex[5] design space. Such properties of a design space allow the use of time-efficient gradient-based optimisation algorithms. However, that does not easily assure optimality, as the optimisation objectives (structural responses such as buckling, strain failure criterion, aeroelastic requirements, etc..[5]) need not be convex. As a consequence, several studies can be found in the literature that use different gradient-based methods to optimise the stiffness of a structure, within one of three paradigms: Finite Element Analysis (FEA) [18], Cellular Automaton (CA) [19], or Isogeometric framework [20]. These paradigms are different mathematical frameworks to represent a discretised structure, and their unique properties are utilised during optimisation.

It was established earlier that the ABD matrix terms are highly interrelated, and their values cannot be arbitrarily assigned. Similarly, all LPs are related to each other, as they all consist of the same trigonometric functions. Hence, appropriate optimisation constraints need to be used to describe the convex feasible domains of LPs and correlations between certain LPs[6]. This is an actively studied topic in literature, and an appropriate list of constraints can be referred from [13, 19]. After optimising a structure's ideal stiffness distribution in the form of LPs, an engineer can move on to level-II (Figure 2.4) and plan how to realise them in the form of SS(s).

2.1.2. Fibre Stacking Methods

In literature, the widely-used technique to convert LPs into SS is the genetic algorithms (GAs) due to their ease in handling discrete design variables (different fibre angles to be present in different layers) [13]. So, upon optimising the stiffness distribution of a structure (in level-I), they are realised by designing SS for different parts of the structure (in level-II). This design can be visualised as follows:

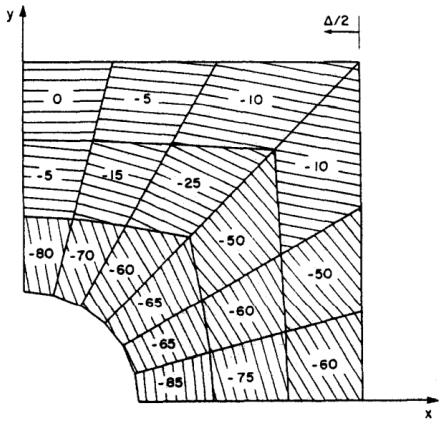

Figure 2.6: Assigning different SS to each design segment (Figure Courtesy:[4])

[5]Convexity is a unique property of a design space which contains only one optimum (minima or maxima) [17]

[6]To date, no single equation correlates all 12 LPs together and describe their feasible design space, making it an active research topic. The developments in this front are briefly summarised in the work of Macquart et al.[15].

Hence, stiffness can be tailored throughout the structure by allowing the fibre orientation to change every segment. Such VS designs allow for better load redistribution than constant stiffness laminates, giving them a lighter construction. However, placing fibres with entirely different orientations beside each other will cause stress concentrations. This is because the load transfer between segments will solely occur through the matrix (butted edges). Hence, over the years, researchers have focused on developing methods to stack fibres and design VS laminates without affecting the structural integrity [13]. Such designs can be manufactured by steering fibres into different orientations across the structure (Steered Fibre Variable Stiffness [12]), or by patching together straight-fibre plies (Straight Fibre Variable Stiffness [21]).

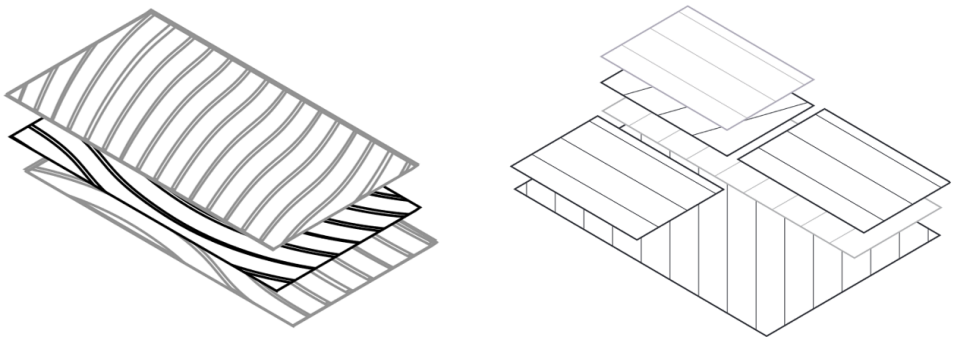

(a) Steered Fibre Designs (b) Straight Fibre Designs

Figure 2.7: Achieving variable stiffness designs using: (a) Steered fibres ; (b) Straight fibres (Figure modified from Ijsselmuiden [18])

By allowing or restricting the change in fibre orientations within a ply, the amount by which the laminate stiffness can be tailored will vary. Consequently, the methods used to design these VS laminates have varying capabilities to match a given stiffness distribution. These methods will be discussed briefly in the remainder of this section.

Steered Fibre Variable Stiffness Designs

By utilising the advances made in automated fibre placement (AFP) technologies, not only can fibres be laid in any direction, but they can be steered into other directions [22, 23]. Therefore, steering allows layer stiffness to be spatially varied. Such steered fibres are illustrated in Figure 2.8.

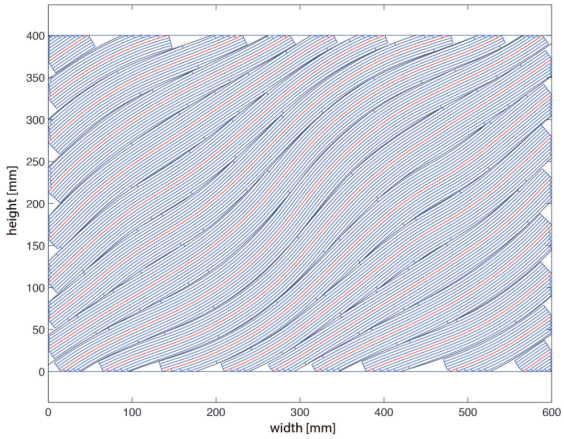

Figure 2.8: Steered fibres within a layer (Figure Courtesy:[23])

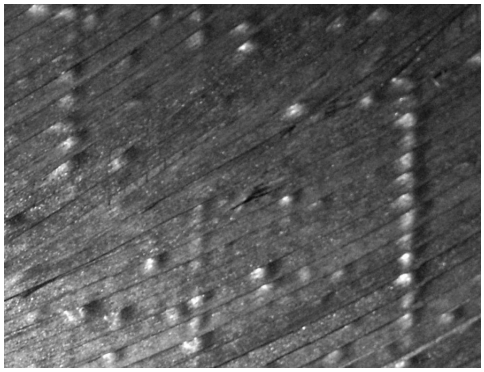

Figure 2.9: Out-of-plane wrinkling of tows while steering (Figure Courtesy:[24])

Nevertheless, it must be understood that to steer and change the angle of a set of straight fibres (tows), they need to be bent, which affects their load-bearing capacity [25]. When fibres are steered (bent) along a direction, one edge is compressed, and the other is under tension. However, as seen in Figure 2.9, beyond a certain point, the fibres under compression tend to buckle locally. This phenomenon

is commonly referred to as wrinkling, and to avoid it, a minimum steering radius limit is imposed for AFP. Based on the material and equipment, this limit usually varies from 400 to 1000 mm [23]. Such a limit can be completely repealed by embroidering fibres onto a surface, but their slow deposition rate makes it an infeasible approach for large-scale applications [26].

To manufacture these steered laminates, the AFP machine must be provided with the towpaths. These paths are generated by analysing the SS of all design segments[7]. For a given layer, every SS contains different ply orientations, and they are converted into the centre lines of a towpath. However, even when towpaths abide by steering radius limits, they can contribute to the formation of defects: when gaps exist between laid tows within a layer, they act as resin pockets and cause stress concentration; when one tow overlaps over another (in order to match a fibre angle distribution effectively), it causes a local thickness build-up. Hence, to generate manufacturable[8] towpaths that closely match a desired fibre angle distribution, while minimising the presence of these defects and thickness variations, several solutions are present in literature [20, 28]. Among them, the most successful solution has been the 'streamline' methodology pioneered by Blom [24], and recently enhanced by Hijne [27].

As an alternative to conventional steering, shearing tows, when laid, can allow for tighter towpath curvatures (40mm [29]) and fill layers with fewer defects. This practice is known as the continuous tow-shearing method. However, shearing will affect the thickness of laid tows. Although the thickness change due to tow-shearing is predictable, generating feasible fibre paths to achieve a pre-determined stiffness distribution will be a complicated task.

Straight Fibre Variable Stiffness Designs

By allowing a ply of one orientation to span across the structure and drop them wherever not desired, the laminate stiffness can be varied from one point to another. As such, a Straight-Fibre Variable Stiffness (SFVS) can be designed. To assure ply continuity throughout the structure while doing this, a more firm set of rules, now known as blending, was established by Kristinsdottir et al. [30]. Over the years, these rules evolved into many variations based on design and manufacturing convenience. However, the guide-based blending implementation of Adams et al. [31] has been the most successful definition as it is widely regarded for its computational efficiency. Their work introduced the term 'guide-stack', a master SS, from which SS of all the other structure segments is derived by turning on/off the presence of certain layers.

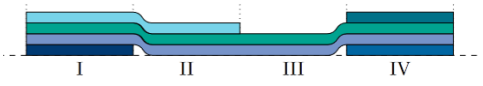

Figure 2.10: Guide-based blending definitions of Adams et al. [31]: (Figure Courtesy: [32])

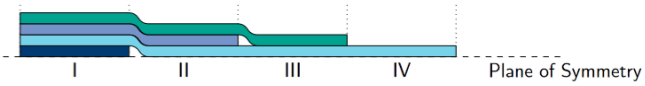

Figure 2.11: Generalised Blending definition of Van Campen et al.[33] (Figure Courtesy: [32])

As illustrated in Figure 2.10, guide-based blending can be achieved by dropping only the innermost plies (in regions I to II) or the outermost plies (in regions II to III). However, this severely restricts the achievable stiffness values to a smaller set. Hence, Van Campen et al.[33] proposed a 'generalised' blending rule to enlarge this set. This allowed plies to be dropped in any sequence as illustrated in Figure 2.11 (ply drop sequence from region I to IV). In literature, SFVS laminates using both the guide-based and generalised blending approach have been efficiently designed using a GA to match a pre-determined stiffness distribution [13, 31, 34, 35].

It was initially established that two completely different SS cannot be placed next to each other, as butted edge formations cause stress concentrations. However, by allowing the ply of one layer to continue in another while preventing the formation of butted edges, such laminates can be considered completely blended. As such, Van Campen et al.[33] introduced the 'relaxed generalised' blending rule. They can be visualised by observing the following ply drop sequence (especially from region III to IV):

[7] In a bi-level design context, an optimised stiffness distribution is converted into a set of SS by using a GA (visualised in Figure A.4).

[8] Minimum allowable length of tows to be placed, and other steering constraints arising from mould geometry [27].

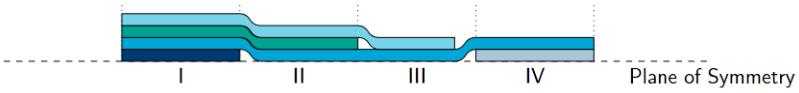

Figure 2.12: Relaxed Generalised Blending definition of Van Campen et al.[33] (Figure Courtesy: [32])

As such, the relaxed generalised blending rule allows for more stiffness variability between segments compared to the aforementioned guide-based approaches. To blend a set of SS[9] together using 'relaxed generalised blending', Van den Oord [36] pioneered a CA-based algorithm, which was later improved by the work of Roepman [32]. However, when Gomaa [21] manufactured an SFVS laminate using this blending rule, geometric imperfections (of a saddle shape) were observed in the cured laminates. These were attributed to the changes in the coefficient of thermal expansion across the laminate. Since the SFVS laminate, in this case, was made by blending 25 different SS, each of them expanded and contracted at different rates over the manufacturing process (curing and cooling). These thermal incompatibilities caused residual stress build-up, ultimately resulting in an out-of-plane deformation and the introduction of geometric imperfections. Consequently, for future designs, a thermal stress model was suggested to be used for predicting the curing behaviour of an SFVS laminate and account for thermal incompatibilities [32].

Nevertheless, the notion of dropping plies in SFVS laminates also comes with unwanted artefacts: resin-pocket formations and stress raisers. Moreover, the ability of a laminated composite to resolve loads by coupling responses across one plane (stretch-shearing coupling and bend-twist coupling) or two planes (in-plane & out-of-plane coupling) induces thermal residual stresses in the structure while curing them to shape in an autoclave [5, 6]. These latter effects commonly apply to SS made of both straight or steered fibres. Hence, SS design commonly follows empirical design guidelines [5, 37, 38]. Some of them are listed below:

i. To nullify in-plane and out-plane coupling stiffness (B matrix), mid-plane **symmetry** of a stacking sequence can be enforced. Eliminating coupling behaviour without mid-plane symmetry is explored by the work of York et al. [39].
ii. To nullify coupling responses within the A matrix (extension-shear coupling), the off-axis plies (orientations apart from 0 and 90) need to be **balanced**, that is, every $+\theta$ should have a $-\theta$. Eliminating In-Plane coupling effects without balancing is explored by Montemurro et al. [40].
iii. To nullify coupling responses within the D matrix (bend-twist coupling), the SS can be **anti-symmetric** about midplane. Since this guideline cannot be realised along with the symmetry guideline, the coupling effect is usually minimised by closely placing all balanced pairs ($+\theta$ and $-\theta$) [41].

A complete list of these guidelines is presented in the Appendix (insection A.3) for brevity. To circumvent complex design procedures to handle guidelines, the industry primarily uses pre-defined sub-laminates[10] for sub-optimal but quick designs.

2.2. Inverse Problem

In section 2.1, the bi-level procedure used to design VS laminates was introduced. In level-I, the stiffness distribution of the structure is optimised using LPs, and in level-II the stiffness distribution is realised by designing SS for different parts of a structure. However, in subsection 2.1.2, it can be understood that the capability to match a designed stiffness distribution (from level-I) depends on the fibre stacking method used to make the VS laminate. This implies that stiffness targets obtained in level-I need not always be realisable. Hence, many studies can be found in the literature that helps account for a fibre stacking method and make LP targets more realisable[11]. With that being said, the bi-level procedure (shown in Figure 2.4) can be expanded as follows to account for different fibre

[9] In a bi-level design context, this will be a set of SS designed to match the stiffness distribution from level-I closely.

[10] Sub-laminates consist of certain angles in a certain sequence that satisfy empirical guidelines. Building laminates with them as a building block is a common industrial practice to satisfy empirical guidelines. The recent work on Double-Double laminates established a methodical procedure to design such sub-laminates [42].

[11] To optimise/repair stiffness distributions, a continuous blending constraint from Macquart et al. [43] could be used for generalised blended designs, and a curvature control method from Hong et al.[44] could be utilised for steered fibre designs.

stacking methods (Guide-based blending, Generalised blending, Relaxed generalised blending, and fibre steering):

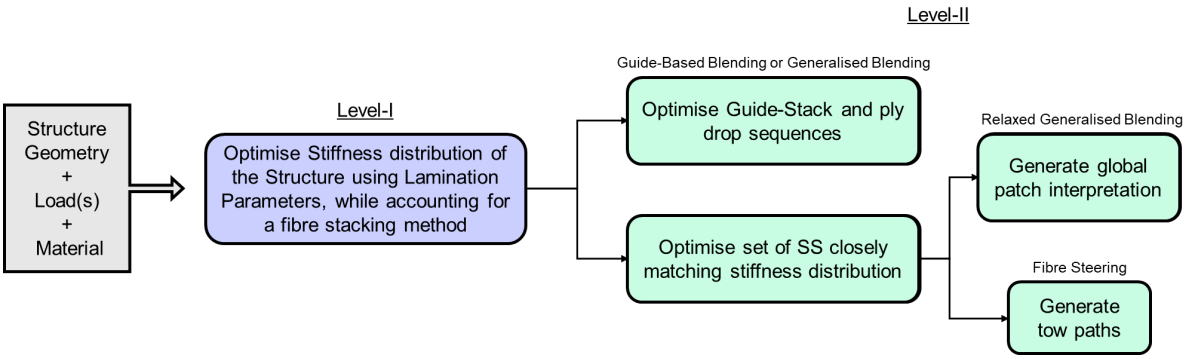

Figure 2.13: Bi-level procedure expanded for multiple fibre stacking methods

In literature, it is commonly stated that using a bi-level procedure allows efficient use of laminated composite materials [13]. Their effectiveness can be attributed to the fact that the two stages of the design problem are handled by optimisation algorithms best suited for the application. Time-efficient gradient-based methods handle stiffness optimisation containing LPs, which are convex and continuous design variables. Furthermore, GAs handle the SS design containing discrete design variables and a non-convex nature. However, there always tends to be a performance loss between the design envisioned in level-I and realised in level-II [32, 44, 45]. This loss is often cited towards multiple reasons. However, the shortcomings in handling the inverse problem (converting LPs to SS) have been one consistent reason, irrespective of the fibre stacking method used (blending or steering).

When an SS cannot be designed to closely match the stiffness targets (in the form of designed LPs), one of the following two steps are performed: 1) The same SS is used at the cost of structural infeasibility, and a knockdown factor is applied over the load case(s); 2) More layers are added to the SS at the cost of increased structural weight, to add more stiffness and allow their LPs to closely match the designed LPs. However, none of these two steps is practically favourable. Therefore, moving forward, more attention was given to the inverse problem. The upcoming (chapter 3) discusses different solutions proposed in the literature to handle them. These solutions will be discussed independently of the fibre stacking methods whenever possible.

3

Concurrent Solutions for the Inverse Problem

As established in chapter 2, LPs are described in a linear and continuous design space, while SS is described in a nonlinear and discrete design space. However, the jump between these two design spaces (converting LPs to SS) is commonly referred to as the 'inverse problem, ' and it has been a complex problem to address during the stiffness design of laminated composites. Many solutions have been proposed in the literature over the last few decades to address them. These solutions can be divided into two broad types: Direct procedures (in section 3.1) and Iterative procedures (in section 3.2). They are briefly explained in the upcoming sections.

3.1. Direct Procedures

Laminate stiffness parameterised using SS of a discrete number of layers yields a highly nonlinear design space. In practice, such nonlinear problems could be handled by analytical methods (upon making multiple assumptions and simplifications) or through rigorous pre-computing to enumerate a design space. These two avenues have been explored in the literature to attempt handling the inverse problem, and they are summarised in the following subsections:

3.1.1. Analytical Methods

In 1982, Miki described the feasible region of in-plane and out-of-plane LPs [46, 47]. This feasible space is commonly known as Miki's diagram in literature, which for a long time stood as a graphical solution to the inverse problem (for balanced laminates) as seen below in Figure 3.1.

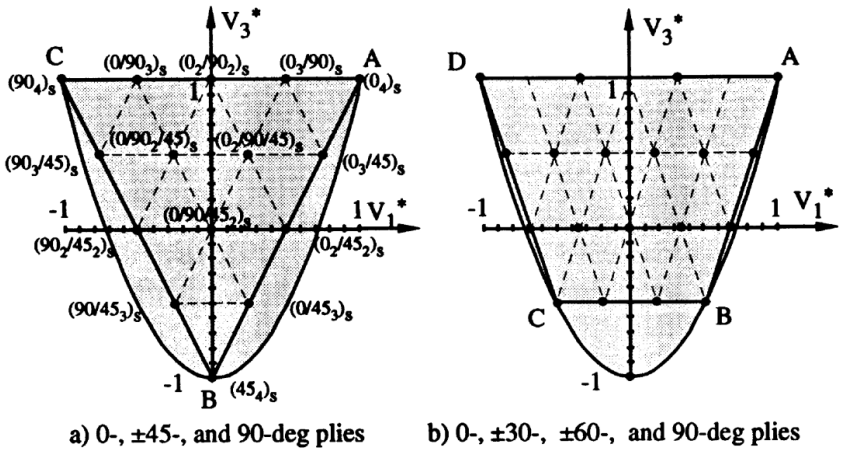

Figure 3.1: Miki's diagram for In-Plane LPs, with feasible values of a 4-layer SS with two different allowable orientation sets (Figure Courtesy:[48])

For conventional orientations $[0, \pm 45, 90]$ the design space is triangular, and for $[0, \pm 30, \pm 60, 90]$ the design space is trapezoidal. This meant that the allowable orientation angles could describe the apices of the polygonal design space. Depending on the number of layers in the laminate, the density of feasible points within the polygon increases and arranges themselves in a uniform and predictable fashion[1]. This also holds for the coupled and out-of-plane lamination parameters, except for the fact that the feasible points are not uniformly spaced[2]. Miki's study also published a closed-form solution to circumvent these tedious graphical procedures and design In-Plane stiffness properties of a Symmetric-Balanced laminate. The relations shown below (Equation 3.1) are for an SS up to three orientations ($[\pm\theta_1, \pm\theta_2, \theta_3 = 0°]$) each with a user-defined volume fraction v (fraction of plies in a laminate with certain orientations):

$$\theta_1 = \frac{1}{2}\cos^{-1}\left(\frac{V_1 - v_2\Theta - v_3}{v_1}\right), \quad \theta_2 = \frac{1}{2}\cos^{-1}\Theta \tag{3.1}$$

$$\Theta = \frac{-K_b \pm \sqrt{K_b^2 - K_a K_c}}{K_a},$$
$$K_a = 2v_2\left(v_1 + v_2\right), \quad K_b = 2v_2\left(v_3 - V_1^*\right),$$
$$K_c = 2v_3^2 + 2\left(v_1 - 2V_1^*\right)v_3 - \left(1 + V_3^*\right)v_1 + 2V_1^{*2}$$

By following certain empirical guidelines, certain LPs always remain zero. Using the symmetry and balanced rule, one could nullify the LPs $V^B_{1,2,3,4}$ and $V^A_{2,4}$, respectively. Hence, only two in-plane LPs are present in these closed-form solutions. For completeness, the simplifications used to ignore certain LPs based on design guidelines are mathematically explained in Table A.1. However, this method cannot design an SS simultaneously for both In-Plane and Out-of-plane LPs. As such, Van Campen et al.[49] proposed a method designing SS of form $[\pm\theta_1, \pm\theta_2]_S$. This study highlights that a feasible set of known LPs of one kind of stiffness(in-plane or out-of-plane) only corresponds with a handful of the other kind.

Another class of analytical approaches observed in the literature view the inverse problem as a square system (equal number of known and unknowns). As such, Fukunaga et al.[50, 51] retrieved four-layer SS while solving for four in-plane or out-of-plane LPs. Similarly, Hammer et al.[52] and Autio [53] showed that a three-layer SS is enough to match four in-plane LPs, while a two-layer SS was enough to match four out-of-plane LPs. However, these solutions were practically infeasible, as they allowed ply thickness to be a continuous design variable. By working along these lines, Sprengholz et al.[54] produced a more feasible solution with the square system approach. They showed that 12 LPs can always be matched using 12 equi-thickness plies that assume arbitrary orientation ($\theta \in (-90, 90]$). This approach, however, is limited to 12 layers. The authors indeed propose a theorem stating that it is theoretically possible for the solution of a square system (N=12) to be up-scaled for any arbitrary N. Having said that, such up-scaling procedures were not published in this study.

The modelling of any problem using polynomial(not trigonometric equations) and solving them comes with great appeal due to their ease of handling and the availability of mature software packages to do the same. Many advances have been made in kinematics using Polynomial Homotopy Continuation (PHC): a fully deterministic root finding technique, where all real solutions of a system of equations can be precisely solved for, albeit with a large number of unknowns [55]. Viquerat et al.[56] capitalised on them to attempt to solve the inverse problem, where LPs were rewritten in polynomial form using the tan half-angle formulae. In PHC, solutions for a system of equations are found by solving nearby systems [56]. Here, a nearby system is a starting system of equations of known solutions and the same dimensionality. The ability to reliably find all possible real solutions of a system of equations [55, 56] is not something any other optimisation technique guarantees. Therefore, among the direct procedures, the PHC method appears effective for designing laminates considering all 12 LPs. However, the performance of PHC is susceptible to the construction of the starting system of equations with known

[1] The exact space division rule for feasible design points can be referred from [48]

[2] For brevity, the non-uniformly spaced feasible points of the B and D LPs are shown in the Appendix (in Figure A.5)

solutions. Albeit better than the other analytical methods, PHC is time-consuming. Solving a square system (12 layer-12 LPs) in this study takes two hours on a regular office laptop. Moreover, solving a non-square system with many layers and having constraints to enforce design guidelines may take substantially longer.

3.1.2. Database Methods

Since LPs are defined only by geometric properties (fibre orientation and position with respect to midplane), their corresponding SS are not material dependent. Hence, the inverse problem has also been solved in literature by utilising pre-computed laminate databases (collection of SS with different number of layers and their associated LPs) [57]. However, this need not necessarily yield perfect SS matches for a set of designed LPs, as these databases are usually created considering a finite set of ply orientations and/or design guidelines. For example, a database for a 14-layer symmetric laminate (seven designed layers) with allowable orientations being a multiple of 15° will contain almost 36 million SS. This constitutes a substantial computational effort for generating these databases and calculating their LPs. To improve the process on this front, Bohrer et al.[58] proposed a method to make laminate databases for a given number of layers(N) by combining two existing databases of laminates with N_1 and N_2 layers, respectively, given that N_1 and N_2 add up to N (i.e., $N_1 + N_2 = N$). Nonetheless, the large amount of computer disk space used by different databases (for different N) is an inevitable drawback for this procedure, limiting their practical feasibility.

3.2. Iterative Procedures

In literature, the inverse problem has been attempted to be solved using iterative procedures. This is usually done by exploring a design space for the optimal solution, which can be done using a single initial solution, a set of initial solutions, or the iterative construction of a solution. Moreover, these searches can be guided by informed objectives (gradient information of objective or specific properties of LP space) or by simple nature-inspired heuristics. The proposed solutions, based on the search method used, are summarised in the upcoming sections.

3.2.1. Gradient driven search

Laminate stiffness, when parameterised by LPs (in Equation 2.1), is preferred to be designed using gradient-based methods due to their linear and convex nature [13]. However, when written in terms of SS, LPs are nonlinear (Equation 2.2). By following a bi-level procedure (in section 2.1) and designing LPs beforehand, Grédiac attempted to optimise a SS as a minimisation problem [59]. The objective function for this problem was written as a least squares sum :

$$F(\Theta) = \sum_{1}^{12} (V(\Theta) - V_{Design})^2 \tag{3.2}$$

Here, V_{Design} is the designed set of LPs, $V(\Theta)$ is the LPs for a given SS (Θ), which is a vector of size N (number of layers in a designed laminate). In his work, Grédiac minimised F using the steepest-gradient descent algorithm [59, 60]. Nonetheless, this process can be made faster by replacing the objective function with an approximation scheme (a primary problem is replaced with a series of approximate sub-problems). Peeters et al.[61] used such an approach, and the objective function was now a convex quadratic approximation that described compliance[3] in terms of an SS:

$$f^{II}(\Theta) \approx f_0^I + \mathbf{g} \cdot \Delta\Theta + \frac{1}{2}\Delta\Theta^T \cdot \mathbf{H} \cdot \Delta\Theta \tag{3.3}$$

Here, a second-order Taylor series expansion was used about the point of designed compliance f_0^I, with exact first-order (gradient **g**) and second-order (hessian **H**) information. To optimise compliance, the 'method of moving asymptotes' was used [61]. Nevertheless, with increasing dimensionality (number of layers in SS), a gradient-driven search method faces issues in being trapped in local minima. Moreover, it also risks becoming computationally expensive due to the utilisation of expensive structural response information. To avoid the former, work has been attempted to continuously seed a gradient-driven procedure with the help of a genetic algorithm (a technique to be explained in subsection 3.2.2) [62]. However, with increased problem dimensionality, even this procedure becomes computationally expensive.

[3] For approximating structural responses such as buckling and stress, one can refer to the PhD thesis of Peeters [23].

3.2.2. Metaheuristic Methods

For solving the inverse problem, exploring design space with heuristics (a simple set of rules inspired by concepts such as evolution, swarm intelligence, or metallurgical annealing [63]) instead of using expensive gradient information, has received the most interest in academia and industry alike [8, 13]. Such procedures are known as metaheuristics, and their popularity can be attributed to their problem-independent nature and the consequent ease of use. These metaheuristics are population-based techniques, meaning they involve randomly sampling the design space to create an initial pool of solutions, which are then iteratively evolved. Governed by rules followed by different metaheuristics, they simultaneously explore different parts of the design space. This process is illustrated in Figure 3.2.

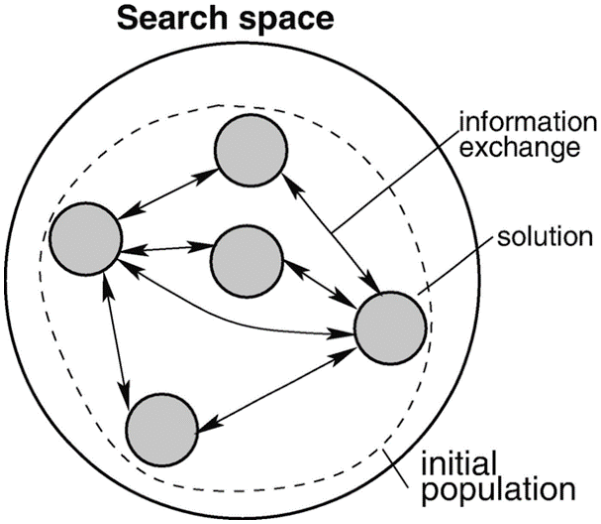

Figure 3.2: General schematic of a population-based metaheuristic (Figure Courtesy:[63])

The metaheuristic that is governed by Darwinian evolution-inspired rules are the genetic algorithms (GAs). Compared to other techniques[4], GAs are known to take advantage of particular properties of a given problem easily and tend to escape a local-minima relatively better [8, 63]. As such, GAs have been the most widely used metaheuristic to solve the inverse problem. They are an abstract model of biological evolution: the initial pool of solutions evolves over multiple cycles (generations) through nature-inspired selection and replacement operations. Candidates in a population (randomly generated SS) are encoded to allow these operations using biological notations such as chromosomes and genes. Laminates have been encoded in many such ways in literature, and their detailed description can be inferred from [33, 45].

In a GA, the initial population's fitness is evaluated based on an objective, and only some of the fittest solutions survive (elitists). The 'selection' phase then passes certain traits (genes) from parent solutions to newly generated ones. By inducing stochastic variations to the search population over many such selection and replacement operations, design space exploration moves towards well-performing regions. Nonetheless, the efficiency of a GA depends on how laminates are encoded and which nature-inspired selection and replacement operators are used [5].

Kogiso et al.[66] was the first to use GAs to solve the inverse problem using LP as targets. Furthermore, as previously mentioned (in chapter 2), the guide-based approach of Adams et al.[31] can efficiently use a GA to design SFVS laminates following the 'Inner', 'Outer', and the 'Generalised' rule. However, GAs were originally designed for unconstrained problems. So constraints like the SS design guidelines are indirectly enforced by penalising fitness scores of an infeasible solution. Nevertheless, penalisation affects population diversity, making a GA converge towards sub-optimal solutions. Hence, to better handle constraints, Irissari et al.[34] introduced stacking sequence tables (SST), where each column in a table represents a unique laminate for different layer counts in a blended structure. SSTs are

[4] Metaheuristics inspired from metallurgical annealing [64] or intelligence of bird swarm networks [65]
[5] Detailed explanation about commonly used selection and replacement operators can be referred from [45, 62]

continuously optimised by a GA, and as an alternative to penalisation, solution repair procedures were applied to the SSTs to conveniently incorporate the complete list of empirical guidelines (in section A.3). As such, better design space exploration was achieved without significantly increasing the computation cost. For completeness, the use of GA in other fibre stacking methods is stated as follows: a set of SS to be present throughout the structure were independently optimised using a GA, after which CA is used to design a 'relaxed generalised' SFVS laminates [32], or fibre-paths can be generated to design a steered fibre VS laminates [18].

To enhance the performance of GAs, the following strategies can be followed: improvement can be sought in solution repair procedures [34, 67]; the search process can be enriched with structural responses, which is approximated and predicted using a kriging model [32, 68, 69], or a neural network [70], or multi-point approximations [34, 35, 71]. However, GAs become more computationally expensive when designing laminates with Non-Conventional Orientations. As design space enlarges with more allowable ply orientations, a bigger initial population is required to maintain population diversity. However, this translates to more computational evaluations and operations. Hence, GAs become a less viable option to handle the inverse problem for laminates with Non-Conventional orientations efficiently.

3.2.3. Logic-based Methods

In the early years, iterative procedures worked such that a SS was built by sequentially optimising the orientations of each layer and adding more layers if necessary (for an objective like minimising compliance) [72]. However, such layerwise optimisations (LO) did not account for the fact that adding plies on top of an existing laminate affects their through-thickness load distribution, consequently making the orientations of previously inserted layers sub-optimal. Narita et al.[73, 74] hence used LO in a bi-level design context (section 2.1) and made two crucial changes to the process: the number of layers was fixed based on designed laminate thickness, and starting from the laminate surface the best orientation for each layer is chosen. This is done based on how the chosen angle brings the LPs of the partially constructed SS close to the designed LPs.

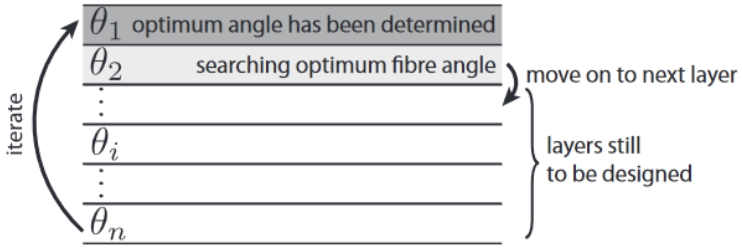

Figure 3.3: LO with fixed number of layers n and LP targets (Figure Courtesy:[62])

This simple 1-D enumeration process makes it less scalable with increasing layers and/or allowable ply orientations. Moreover, searching through design space based on locally optimum choices (greedy approach) need not necessarily provide optimum results. On this note, the fractal branch and bound(FBB) method was developed [75, 76, 77], where the LO problem was performed in a decision tree paradigm as illustrated in Figure 3.4.

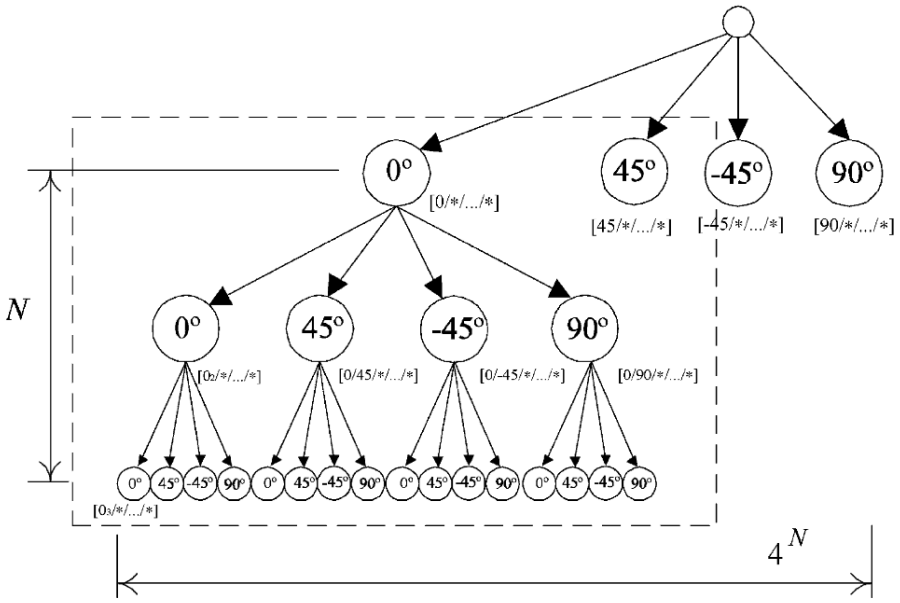

Figure 3.4: LO performed in a Decision Tree paradigm (N layers of SS with Conventional orientations)(Figure Courtesy:[75])

These studies showed how a decided ply orientation at each tree level influences the realisable LP space and shows their fractal nature. For brevity, the fractal patterns made by LPs of a 6-layer SS are shown in Figure A.5. Capitalising on the fractal nature, the FBB method allowed for navigating a decision tree in an informed manner and obtain globally optimum solution(s) for a known set of LPs and a number of layers. Here, complete design space enumeration is avoided by pruning branches of partial SS, which would violate empirical guidelines, or the realisable LP space of a branch does not contain the target LP[6]. However, with increasing dimensionality, the evaluations made for each nodal decision became expensive and slowed the search process. Therefore, Liu et al.[78] used a greedy search procedure with a simple cost function (Equation 3.4) to make gains in computational speed at the cost of optimality.

$$F = \sum_{1}^{12} |V_{Design} - V_{Target}| \tag{3.4}$$

This procedure was also extended for retrieving a set of blended SS [79], which was further enhanced with a parallel search approach, where optimisation information between a decision tree and GA is shared [80]. However, their studies were limited to conventional orientations, and a greedy approach need not assure optimal results. The decision tree approach was then on this front by Fedon et al. [81], who implemented a beam search procedure. This improved the exploration capabilities within the decision tree, and their implementation showed a relatively higher processing speed. Here, an SS design of 300 layers was performed within a minute, with a F error of the order 1E-2. However, the method does lose effectiveness with increasing allowable ply orientations (Non-Conventional Orientations like the set 15° multiples or 5° multiples) or while designing blended SS when compared to the SST method of Irissari et al.[34].

[6]Relations required to completely predict these patterns and shrunk LP spaces for a partial SS can be referred from [77].

4

Signal Decomposition and its Similarity to the Inverse Problem

> "If you keep rephrasing the question, it gradually becomes the answer."
>
> *Robert Breault*

The shortcomings faced while converting LPs to SS are termed the inverse problem in the literature. Procedures involving a decision tree [81] or a GA [45] are commonly used to handle this stage of the design process (Figure 2.13). However, it can be inferred from chapter 3 that they are not scalable for practical applications while considering design with non-conventional orientations. One commonality among these two procedures is that their functioning is problem-independent. To explore a design space, a GA uses evolution-inspired heuristics, and the decision tree uses a greedy search procedure. Although they allow for simpler implementations in a computer, the information contained within LPs is not appropriately utilised in the process. To explore this notion further, the LPs were analysed from a purely numeric aspect (by revisiting Equation 2.2):

$$V^{\{A,B,D\}}_{[1,2,3,4]} = \underbrace{\frac{1}{\left\{N, \frac{N^2}{2}, \frac{N^3}{4}\right\}}}_{\text{Normalisation Term}} \sum_{k=1}^{N} \underbrace{\left\{1, \left(\frac{N}{2}-k+1\right)^2 - \left(\frac{N}{2}-k\right)^2, \left(\frac{N}{2}-k+1\right)^3 - \left(\frac{N}{2}-k\right)^3\right\}}_{\text{Weight}} \underbrace{[\cos 2\theta_k, \sin 2\theta_k, \cos 4\theta_k, \sin 4\theta_k]}_{\text{Trigonometric Function}}$$

When termed as such, the LPs are a weighted sum of sines or cosines (sinusoids) of angles within a SS. Hence, the objective of the inverse problem could be rephrased as "to represent a set of LPs as a sum of sines or cosines", such that an SS can be inferred from it. Upon doing so, the problem had a striking similarity to a signal processing procedure known as frequency decomposition.

Inverse problem: represent a particular value (LPs) as a sum of sine (or) cosines.

Frequency decomposition: represent a signal as a sum of sine (and/or) cosine waves.

In practice, frequency decomposition of signals is efficiently performed using the Fast Fourier Transforms (FFT) [82]. Hence, by converting the inverse problem into an equivalent signal processing problem, the efficient FFT algorithm becomes available for use in the design of laminated composites. Nonetheless, before exploring this possibility, a literature study was conducted to learn how FFTs are implemented in signal processing problems. The learnings from this exercise are documented in the following sections.

4.1. Fast Fourier Transform

Developed by Joseph Fourier in the early 19th century, the Fourier Transform is a famous mathematical technique to analyse a signal for its frequency components [82]. This is visually explained in Figure 4.1.

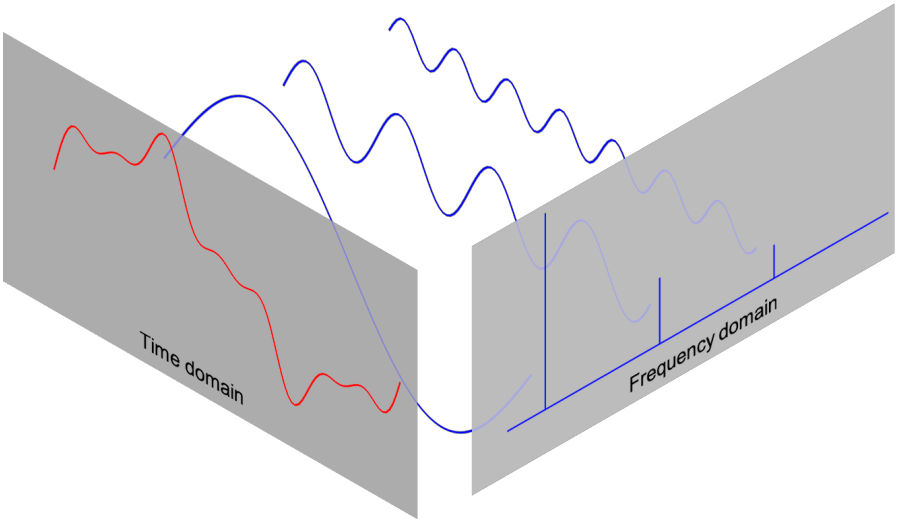

Figure 4.1: Working of the Fourier Transform (left to right) (Figure Courtesy:[83])

Hence, Fourier Transforms allow a function/signal represented in the time domain to be transformed into the frequency domain. To mathematically achieve this, the following operation is performed:

$$F(\omega) = \int_{-\infty}^{\infty} f(T)\, e^{-i\omega T}\, dT \tag{4.1}$$

Here, $F(\omega)$ is the frequency domain representation of a function whose time domain representation is $f(T)$. Moreover, ω is a frequency value, and T is time. The integrand seen here is a product of the original function $f(T)$ and a sinusoidal wave of frequency ω. When integrated over a time range ($-\infty$ to $+\infty$ in general), one obtains the overlapping area between $f(T)$ and the sinusoid of frequency ω. This overlapping area represents a sinusoidal frequency's contribution (amplitude) inside $f(T)$. As such, the Fourier transforms can reveal the frequency constituents of a given signal and their respective amplitudes. In other words, the signal is decomposed into a sum of sinusoidal waves. Here, the sinusoids are represented with the Euler's number e, upon using the elegant Euler's formula:

$$e^{i\omega} = \cos(\omega) + i\sin(\omega) \tag{4.2}$$

Upon using Euler's formula, the real part of the Fourier transform solution would correspond to cosine functions, and the imaginary part would correspond to sine functions. Sine and cosine waveforms look similar but are offset in time, as shown in Figure 4.2.

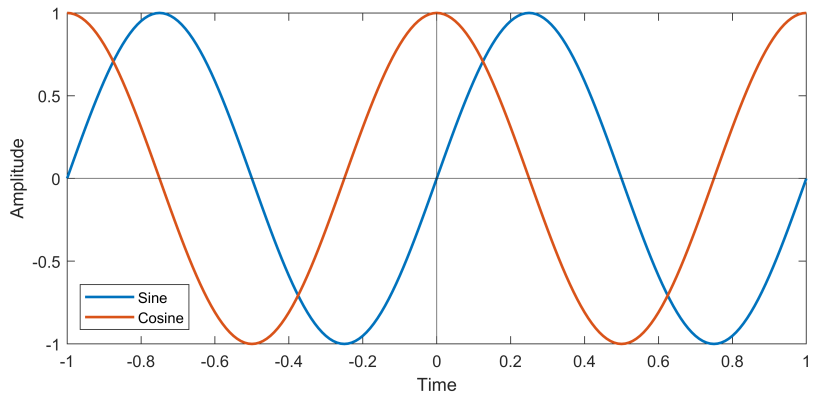

Figure 4.2: The Sinusoidal Function Family

This offset is commonly known as a phase difference. Hence, the Fourier transform provides information about a signal's frequency constituents, their respective amplitudes, and their phase differences. As

such, this transformation has found uses in various fields of signal processing, image processing, and audio analysis [82].

In practice, signals are often represented as discrete points and not a continuous function. Hence, discrete Fourier transforms (DFT) are used, which assume the form shown here:

$$X[k] = \sum_{n=0}^{\mathcal{N}-1} x[n] e^{-i(\frac{2\pi}{\mathcal{N}})kn} \tag{4.3}$$

Here, x is a list of $\mathcal{N}$ discrete points in a signal, $X[k]$ represents the amplitude and phase shift associated with $\mathcal{N}$ frequencies from 0, while k is an index variable for frequency. These discrete points in the time domain are also called samples of a signal. Hence, the DFT formula converts $\mathcal{N}$ time domain samples into $\mathcal{N}$ frequency-domain samples. These $\mathcal{N}$ outputs are called DFT coefficients, through which one obtains amplitude and phase shift information. Each of these $\mathcal{N}$ coefficients is part of a numerical array known as the frequency bins, whose individual elements correspond to a frequency value. Moreover, these bins are a uniformly spaced set of frequencies between 0 and the highest frequency one wants to detect from a signal. Hence, $\mathcal{N}$ must be appropriately decided such that the number of frequency bins generated contains the desired frequency resolution sought after.

For a signal with $\mathcal{N}$ samples, computing their DFT coefficients (using Equation 4.3) will require $\mathcal{N}^2$ complex number multiplications and $\mathcal{N}(\mathcal{N}-1)$ complex number additions. In computer science, the consumption of computational resources like time and memory is measured using computational complexity notations. As such, the DFT for $\mathcal{N}$ samples have a $O(\mathcal{N}^2)$ complexity. This means that the run-time of this procedure will quadratically depend on the $\mathcal{N}$. For applications such as seismic monitoring, to detect natural and unnatural events (for example, earthquakes and explosions, respectively), DFT must be performed for many samples in real-time [84]. During these cases, the complexity becomes a practical computational limitation. This led to the development of the Fast Fourier Transform (FFT) in the 1960s, which, even today, is considered the most impost algorithm of all time [85]. Capitalising on inherent symmetries offered by sinusoids, the FFT algorithm performed a DFT at a complexity of $O(\mathcal{N}log_2(\mathcal{N}))$. Hence, the FFT algorithm is used to compute DFT coefficients in all modern coding platforms, such as MATLAB.

4.2. Theoretical Background

The introduction of the FFT algorithm significantly reduced computation time, rendering DFTs more practical. Due to their accuracy and efficiency, FFTs have become an indispensable tool for engineers across various disciplines. However, further study was conducted to learn the characteristics of periodic functions (such as sinusoids) and the inputs required for the FFT to ensure reliable implementation.

4.2.1. Periodic Functions

FFT can decompose a signal into sinusoidal functions. Such functions are also termed periodic, as they repeat themselves throughout a time domain. These sinusoids can be mathematically represented as follows:

$$\underbrace{A}_{\text{Amplitude}} \sin(\overbrace{\omega}^{\text{Frequency}} T + \underbrace{\phi}_{\text{Phase Difference}}) \tag{4.4}$$

For a sinusoid (sine in the case shown in Equation 4.4), it can be understood that frequency ω and the phase difference ϕ are their arguments, and amplitude is the value scaling them. However, their behaviour varies when a signal is a combination of many such sines or cosines. Multiple entities can characterise them: the time the signal repeats itself (periodicity) and the extreme values they can have [86]. These entities depend on two factors:

1. The frequencies present within a signal. They influence the rate at which a signal repeats itself
2. The amplitudes of these frequencies scale up/down the peaks within a period.

For a signal composed of periodic functions with multiple unique frequencies (or a harmonic signal), its periodicity can be numerically quantified using the following relation [87]:

$$\text{Periodicity} = \frac{360}{\text{Fundamental Frequency}} \tag{4.5}$$

$$\text{Fundamental Frequency} = \text{Greatest Common Divisor of present frequencies}$$

As such, periodicity is determined by the fundamental frequency, the greatest common divisor of all the frequencies that ought to be present within them.

Another property of sinusoids that needs to be highlighted is their vertical symmetry about the origin. As seen in Figure 4.2, sine waves are anti-symmetric, while cosine waves are symmetric. This means that the value of the sine function is sensitive to the sign of their argument, while cosines are not.

$$\sin(-\omega) = -\sin(\omega)$$
$$\cos(-\omega) = \cos(\omega)$$

In mathematical terms, a sine is called an odd function, and a cosine is an even function.

For completeness, it has to be said that signals in the real world are rarely harmonic. However, performing FFTs over aperiodic signal samples gives a reasonable estimate of their constituent frequencies. This line of thought builds up to the limitation of the FFTs. Using the samples of a harmonic signal, FFT can help recreate the original signal with reasonable accuracy. This is because such signals always exist as a sum of sinusoids. Nevertheless, the same can never be guaranteed for aperiodic signals, as different signal parts can contain different frequencies. This limitation of FFT can be mathematically said to be the lack of temporal resolution. For example, an FFT can tell from a seismograph that an earthquake and an unnatural explosion have occurred. However, they cannot tell the sequence in which they occurred. For such problems, techniques like wavelet transforms are used [82]. Regardless, as temporal resolution increases, the frequency resolution decreases in wavelet transform output. This contrasting behaviour is termed the signal uncertainty principle[1].

4.2.2. Sampling Requirements

For FFTs, $\mathcal{N}$ discrete signal samples are provided as input. Consequently, the $\mathcal{N}$ value affects the FFT output and often gives rise to a phenomenon known as aliasing.

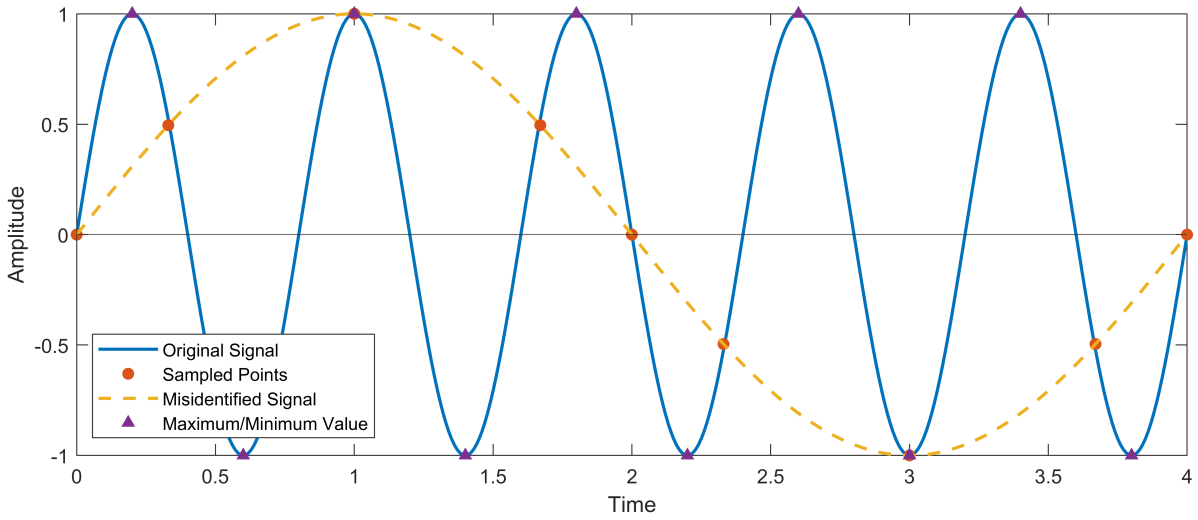

Figure 4.3: An aliased output signal

[1] Similar to Heisenberg Uncertainty principle from quantum mechanics [88]: one cannot know the position and speed of an atomic particle with the same accuracy

As shown in Figure 4.3, when a signal is poorly sampled (i.e., sampled points are too far apart), aliasing occurs, where the data points might end up representing a signal of a different frequency. To avoid this, a signal needs to be sampled at an appropriate rate. This can be quantified using the Nyquist-Shannon theorem [82]:

$$\text{Sampling Rate} \geq 2 * \text{Highest Angular Frequency in Signal} \tag{4.6}$$

The angular frequency of sinusoids is $\omega/2\pi$, and their units are rad/sec. The intuition behind this theorem is as follows: by sampling at a rate twice the highest frequency present, the signal's maximum and minimum peaks (indicated by the triangular markers in Figure 4.3) are sampled, and the information about the highest frequency present cannot be misinterpreted as a lower frequency. This assures that no loss of information occurs through aliasing. For applications outside frequency decomposition, a higher sampling rate might be necessary. Nonetheless, the exact value of $\mathcal{N}$ must be appropriately decided to generate frequency bins that contain the desired frequency resolution or, the desired frequencies to be detected. For a harmonic signal that ought to be a sum of sinusoids, this is usually achieved by ensuring that $\mathcal{N} - 1$ is a multiple of their periodicity [82]. Therefore, all the conditions that $\mathcal{N}$ needs to satisfy can be listed as following [82, 87]:

1. $\mathcal{N}$ samples must be appropriately spaced in time to satisfy the Nyquist-Shannon theorem.
2. $\mathcal{N}$ samples are uniformly-spaced in time.
3. $\mathcal{N} - 1$ is a non-zero multiple of the periodicity.

For an FFT, the $\mathcal{N}$ samples provided need to be uniformly spaced in time. However, a Non-Uniform FFT (NUFFT) can be used when this requirement cannot be satisfied. There are multiple ways to implement NUFFT, but one such implementation in MATLAB relies on interpolation to convert a non-uniformly spaced sample set into a uniform one [89]. While this approach eliminates aliasing by ensuring the right amount of uniformly spaced samples, it is worth noting that the interpolated samples may not precisely capture the signal's actual behaviour. As a result, this interpolation step can introduce slight discrepancies in the FFT output.

In summary, FFTs can use $\mathcal{N}$ time-domain samples of a signal and present the amplitudes of different frequencies within them. The exact value of $\mathcal{N}$ and the rate at which they are spaced apart in time can be precisely described for a harmonic signal whose constituent frequencies are known. With this understanding in mind, the notion of using FFTs in laminate design can be explored. To convert LPs into SS using FFTs, the LPs need to be parameterised in the time domain. This transforms the inverse problem into an equivalent signal processing problem. The choices taken for temporal parameterisation will also affect their sampling requirements. However, before exploring these ideas (in chapter 6), the gaps found in literature and the research questions for this master's thesis will be formulated and stated (in chapter 5).

5

Research to handle the Inverse Problem with Fast Fourier Transforms

> "There are no big problems; there are just a lot of little problems."
>
> *Henry Ford*

The design of laminated composite structures has been discussed until now. Upon using a bi-level procedure, variable stiffness laminates can be effectively designed. However, in this procedure, certain shortcomings can be faced while trying to convert designed lamination parameters (LPs) into stacking sequences (SS). This is called the inverse problem, which, when occurred, one of the two steps are usually performed: at the expense of possible structural infeasibility, the SS of the same thickness with inexactly matching LPs are used, or at the expense of increased structural weight, more layers are added to allow achieving the minimum required stiffness. Both these outcomes are not practically favourable. Hence, a literature study was performed to study concurrent solutions for the inverse problem. By doing so, the knowledge gaps found in the existing body of literature were understood (in section 5.1), and the research questions for this master thesis were framed based on that (in section 5.2)

5.1. Research Gaps

Among the techniques described in section 3.1 for directly converting LPs into an SS, only the polynomial homotopy continuation method considered all 12 LPs in design and assured providing all real solutions to a given problem. Theoretically, they can solve non-square systems (any number of layers for 12 LP targets). However, their ease of use and computational efficiency with increasing dimensionality (increasing N and allowable ply orientations in design) is questionable. Among the iterative methods described in section 3.2, genetic algorithms (GAs) were the most effective in exploring the non-convex SS design space (relative to a gradient-driven search). However, with growing dimensionality, they become computationally very expensive and will likely get stuck in local minima. Upon representing SS design in a decision tree paradigm, faster conversion of LPs to SS was possible when unfavourable solution branches were pruned to reduce the number of evaluations. These techniques were practically scalable with increasing layers, but their solution accuracy decreased with an increasing number of allowable ply orientations (like the set of 15° multiples, or, $[\Delta 15^{\circ}] = [0, \pm 15, \pm 30, \pm 45, \pm 60, \pm 75, 90]$). As such, a research gap was identified in the literature: ***currently used techniques to handle the inverse problem tend to lose their effectiveness and become computationally expensive when designing with ply orientations beyond the conventional set of*** $[0, \pm 45, 90]$ (or, $[\Delta 45^{\circ}]$). This gap provided the impetus to research and develop an efficient technique to design laminates with a set of non-conventional orientations (like $[\Delta 15^{\circ}]$).

Furthermore, while analysing GAs [45] and decision tree-based techniques [81], it was understood that their functioning is problem-independent. This made them explore LP space in a less informed manner

relative to techniques such as the fractal branch and bound [75] that use unique properties offered by LPs. To entertain this notion further, the LP formulations were analysed from an entirely numeric aspect. When LPs are seen as a weighted sum of sines or cosines (of the angles in a SS), the inverse problem's objective can be rephrased as "to decompose the LP values into sums of sines/cosines of many angles". The objective was now very similar to the Fast Fourier Transforms (FFT), which decomposes a signal into a sum of sinusoidal signals of different frequencies. As of 11/2023, to the author's knowledge, ***the notion of handling the inverse problem using FFT-based methods is yet to be explored in literature***. Moreover, the concepts presented in chapter 4 clarified that an FFT-based method could be used for such tasks if LPs can be parameterised in the time domain (as a signal). So, through this observation, another research gap was found in the existing literature.

5.2. Research Questions

Based on the research gap observed and inferences made, it was decided that the objective of the master thesis was to develop an FFT-based method to handle the inverse problem and evaluate its efficacy. With this in mind, the following research question and sub-questions have been formulated:

$$What\ is\ a\ computationally\ efficient\ method\ to\ convert\ Lamination\ Parameters\ into\ a\ Stacking\ Sequence\ of\ a\ given\ number\ of\ layers\ with\ Non\text{-}Conventional\ Orientations?$$

I. How can Fast Fourier Transforms be used to handle the Inverse Problem?
    i. How can the Inverse problem be parameterised as a signal processing problem?
    ii. What are the consequences of using a time-domain-based parameterisation?
II. What steps should be followed for converting Lamination Parameters to Stacking Sequence?
III. Considering both result quality and computational effort, what is a good performance metric for evaluating this conversion method with others?

Part II

Framework developed to handle the Inverse Problem

6

Parameterising Laminated Composites in Time-Domain

"Every decision for something is a decision against something else"

Jonas Kahnwald,
Dark (2017), Netflix

From the literature study, it was understood that the inputs of FFTs need to be time-domain samples of a signal. Thus, to use FFTs for converting LPs to SS, it is desirable to have LPs in a signal format. As there are three different types of stiffnesses and two different types of sinusoids within LPs, it is mathematically challenging to represent all of them in the same signal. Hence, multiple signals were used to represent a set of 12 LPs. This chapter, as such, will explain the following: how LPs were parameterised as a signal (in section 6.1), discuss the achievable outcome from FFTs (in section 6.2), and then show how the parameterisation influences the sampling requirements (in section 6.3).

6.1. Laminate Signals

In order to perform FFTs on LPs and obtain information about an SS, it is crucial to parameterise a signal that relates both of them. As seen from chapter 2, 12 LPs can be computed for a known SS using only one known relation (in Equation 2.2). Hence, they are revisited below and analysed to see if they could be used to parameterise a signal consisting of LPs:

$$V_{[1,2,3,4]}^{\{A,B,D\}} = \underbrace{\frac{1}{\left\{N, \frac{N^2}{2}, \frac{N^3}{4}\right\}}}_{\text{Normalisation Term}} \sum_{k=1}^{N} \underbrace{\left\{1, \left(\frac{N}{2}-k+1\right)^2 - \left(\frac{N}{2}-k\right)^2, \left(\frac{N}{2}-k+1\right)^3 - \left(\frac{N}{2}-k\right)^3\right\}}_{\text{Weight}} \underbrace{[\cos 2\theta_k, \sin 2\theta_k, \cos 4\theta_k, \sin 4\theta_k]}_{\text{Trigonometric Function}}$$

Even though all LPs are mathematically correlated, they are independently defined. So, a set of 12 LPs has to be represented using multiple signals. To achieve this, a fictitious time variable T can be incorporated into the arguments of the LP's sinusoids. Doing so would convert a sum of sinusoids into a sum of sinusoid signals. Moreover, the two different arguments within an LP's sinusoid are 2θ and 4θ, where one is a factor of the other. Hence, when a sum of sinusoidal signals have an argument of 2, they can numerically equal two LP values (at $T = 1$ and 2, respectively). As such, 12 LPs can be temporally represented using six laminate signals $L_{[1,2]}^{\{A,B,D\}}$ as shown here:

$$L_{[1,2]}^{\{A,B,D\}}(T) = \underbrace{\frac{1}{\left\{N, \frac{N^2}{2}, \frac{N^3}{4}\right\}}}_{\text{Normalisation Term}} \sum_{k=1}^{N} \underbrace{\left\{1, \left(\frac{N}{2}-k+1\right)^2 - \left(\frac{N}{2}-k\right)^2, \left(\frac{N}{2}-k+1\right)^3 - \left(\frac{N}{2}-k\right)^3\right\}}_{\text{Amplitude}} \underbrace{[\cos 2\theta_k T, \sin 2\theta_k T]}_{\text{Frequency}} \quad (6.1)$$

As seen in the literature review (chapter 4), the argument of a sinusoid is a combination of frequency, time, and the phase difference ($\omega T + \phi$), and the quantity multiplying a sinusoid is their amplitude.

Accordingly, the frequency ω corresponds with twice the ply orientation (2θ), and their corresponding amplitudes are the sum of their weighting terms (Sum of Weights). These weights are the quantities depicted in Equation 2.2, which relates LPs to SS. For In-Plane LPs, all layers in an SS are equally weighed by 1. For Coupled and Out-of-Plane LPs, the layers within an SS are assigned weights that follow a quadratic and cubic relationship, respectively, with respect to their position k.

For completeness, it will be mentioned here that the phase difference ϕ carries no meaning in terms of laminated composites. To summarise, the chosen parameterisation[1] can be summed up in the following table:

Table 6.1: Equivalent Terminologies within the chosen parameterisation

Digital Signals	Laminated Composites
Laminate Signals	Lamination Parameters
Frequency	$(2*)$Ply Orientation
Amplitude	Sum of Weights
Phase Difference	-

Therefore, L is the time-domain equivalent for the LPs. The information regarding the Coupled LPs (for B) is ignored from here onwards, as this thesis limits itself to the design of symmetric laminates[2]. So, the nullification of B implies that four different laminate signals exist ($L_{[1,2]}^{\{A,D\}}$): L_1^A, L_1^D, L_2^A, and L_2^D. Each of these signals consists of information about certain LPs. For completeness, they are tabulated as shown here:

Table 6.2: Laminate Signal $L_{[1,2]}^{\{A,D\}}$ and their constituent LPs

Laminate Signal ($L_{[1,2]}^{\{A,D\}}$)	Corresponding LPs ($V_{[1,2,3,4]}^{\{A,D\}}$)
L_1^A	$V_{1,3}^A$
L_1^D	$V_{1,3}^D$
L_2^A	$V_{2,4}^A$
L_2^D	$V_{2,4}^D$

Therefore, four laminate signals ($L_{[1,2]}^{\{A,D\}}$) can be used to represent eight LPs ($V_{[1,2,3,4]}^{\{A,D\}}$). Based on a signal's constituent LPs, the following classification can be made: L_1 signals contain cosine-based LPs $V_{1,3}^{\{A,D\}}$, while L_2 signals are made of the sine-based LPs $V_{2,4}^{\{A,D\}}$.

Regardless, FFTs may have to be performed on these four signals to obtain information about the SS corresponding to these LPs. To understand what can be obtained from these FFTs, the decided signal parameterisation is analysed further in the upcoming section.

6.2. Practical Interpretation of Fast Fourier Transform Output

It is known that FFTs can decompose a signal into sinusoids of different frequencies. By doing so, one could interpret the frequencies present in a signal and their respective amplitudes. For the chosen parameterisation (Table 6.1), the frequencies present in a laminate signal correspond to the ply orientation, and their amplitude corresponds to their Sum of weights. Hence, the FFTs on a laminate signal will provide the Sum of weights for every unique ply orientation in an SS related to them.

As explained earlier, there are four laminate signals $L_{[1,2]}^{\{A,D\}}$. Depending on the type of stiffness matrix (A or D), two different Sum of weights can be obtained. Furthermore, depending on the type of sinusoid present in the signal (1 or 2), the Sum of weights can either correspond to $|\theta|$ or off-axis θ's [3]. This latter distinction arises from the properties of sine and cosine functions, where sine functions are odd and

[1] For brevity, the alternate ideas examined for parameterisation are briefly explained in the Appendix (section B.1).

[2] The coupled LPs $V_{1,2,3,4}^B$ of symmetric laminates are always zero.

[3] Off-axis θ's are the ply orientations apart from 0 and 90.

sensitive to the sign of their arguments. In contrast, cosine functions are even and insensitive to the argument's sign.

Since cosine-based LPs ($V_{[1,3]}^{\{A,D\}}$) scale with $|\theta|$, their signal equivalents ($L_1^{\{A,D\}}$) provide the Sum of weights for all $|\theta|$. On the other hand, sine-based LPs ($V_{[2,4]}^{\{A,D\}}$) scale up only with off-axis orientations because their values are null for 0° and 90° ($\sin(2\theta) = \sin(4\theta) = 0$, for $\theta = [0^\circ, 90^\circ]$). Hence, their signal equivalents ($L_2^{\{A,D\}}$) provide the Sum of Weights for all off-axis θ's.

So, in summary, four different outputs can be obtained by performing an FFT on $L_{[1,2]}^{\{A,D\}}$, and they are tabulated as shown here:

Table 6.3: FFT Output (Sum of Weights) for four different laminate signals ($L_{[1,2]}^{\{A,D\}}$)

		FFT Output of $L_{[1,2]}^{\{A,D\}}$		
		Sum of Weights	**1**	**2**
			Cosine-Based ($V_{1,3}$)	**Sine-Based ($V_{2,4}$)**
A	**In-Plane**	$\sum_{k=1}^{N}(1)$	Sum of Weights for every $\|\theta\|$ in a SS	Sum of Weights for every off-axis θ in a SS
D	**Out-of-Plane**	$\sum_{k=1}^{N}\left(\frac{N}{2}-k+1\right)^3-\left(\frac{N}{2}-k\right)^3$		

Before discussing how to perform the FFT of these signals, it was crucial to understand how these Sum of Weights practically correspond to an SS. Therefore, these Sum of weights were numerically analysed. The observations from this analysis are now presented in the following two subsections.

6.2.1. In-Plane Sum of Weights

The laminate signals consisting of the In-Plane LPs are L_1^A and L_2^A. As inferred from Table 6.3, by performing FFT on them, one obtains the In-Plane Sum of weights corresponding to $|\theta|$ and the off-axis θ, respectively. To understand what these sum of weights practically correspond to, they were numerically analysed with an example symmetric SS $[-45, +45, 90, 90, 0, 0]_S$.

For In-Plane LPs, every layer in a SS is equally weighed by the value 1. Hence, the In-Plane Sum of weights for an SS can be calculated by counting the number of times a $|\theta|$ or off-axis θ appear in them:

Table 6.4: In-Plane Sum of Weights for the SS: $[-45, +45, 90, 90, 0, 0]_S$

		FFT Output of $L_{[1,2]}^A$	
		1	**2**
A	**In-Plane**	$[0_2, 45_2, 90_2]$	$[-45_1, +45_1]$

In this table, the base numbers correspond to a ply orientation in the SS, and the bottom exponent is their corresponding In-Plane Sum of weights. Based on all these values, the following observations were made:

1. The FFT of L_1^A provides the no. of plies belonging to all $|\theta|$ present in the SS (0°, 45°, and 90°).
2. The FFT of L_2^A provides the no. of plies belonging to the off-axis θ's present in the SS ($+45^\circ$, and -45°).

Therefore, by performing FFT on the In-Plane LPs $V_{[1,2,3,4]}^A$ (in the form of $L_{[1,2]}^A$), the number of plies belonging to every θ can be obtained. From here on, this output is referred to as a laminate's fibre angle distribution (FAD). However, to design a SS, the plies within a FAD need to be assigned a position (k) within a N-layer laminate. As seen in Table 6.3, the Out-of-plane sum of weights contains information about k. Hence, they are analysed in the upcoming subsection.

6.2.2. Out-of-Plane Sum of Weights

The laminate signals consisting of the Out-of-Plane LPs are L_1^D and L_2^D. Their FFT outputs are the Out-of-Plane Sum of weights for all $|\theta|$ and θ, respectively. Similar to the previous subsection, to know more about these outputs, they are analysed using the same example case. As a first step, one must know the Out-of-Plane weights corresponding to every position k in a laminate. These values can be computed using the cubic weight relation shown in Table 6.3.

Table 6.5: Position dependant Out-of-Plane weights for a 12-layer symmetric SS

Position (k)	1	2	3	4	5	6
Cubic Weight	91	61	37	19	7	1

The weights are only shown for the symmetric half of the SS, as their values are equal across the midplane. Using these values, the Sum of weights corresponding to all unique $|\theta|$ and θ within the SS are now computed. This is explained in the following table:

Table 6.6: Relating Out-of-Plane Sum of Weights to a SS: $[-45, 45, 90, 90, 0, 0]_S$

Position (k)	1	2	3	4	5	6
SS	-45	45	90	90	0	0

Orientations Present $(^\circ)$	-45	45	0	90
Corresponding Positions $(k'\mathbf{s})$	1	2	5,6	3,4
Corresponding Weights	91	61	7,1	37,19
Sum of Weights	91	61	8	56

From the given SS, the unique orientations present are first identified. The subsequent row then presents their laminate positions k. By associating the weights that correspond with these positions, the Out-of-Plane Sum of Weights for each orientation can then be obtained for $|\theta|$ and θ:

Table 6.7: Out-of-Plane Sum of Weights for the SS: $[-45, +45, 90, 90, 0, 0]_S$

		FFT Output of $L^D_{[1,2]}$	
		1	**2**
D	**Out-of-Plane**	$[0_8, 45_{152}, 90_{56}]$	$[-45_{91}, +45_{61}]$

To summarise, these quantities can be obtained by performing FFT on the Out-of-Plane LPs $V^D_{[1,2,3,4]}$ (in the form of $L^D_{[1,2]}$). However, unlike the In-Plane Sum of Weights (in Table 6.4), the Out-of-Plane sum of weights lacks physical intuition. This is because the Out-of-Plane Sum of Weights are aggregate information about multiple differently weighed k's corresponding to a unique ply orientation. Hence, they are not easily perceivable in the context of an SS.

6.2.3. Need for a Hierarchical Design Framework

The previous two subsections elucidate what can be practically obtained by performing an FFT on the In-Plane and Out-of-Plane LPs. They are listed as follows:

1. The In-Plane LPs $V^A_{[1,2,3,4]}$ can be represented as signals using $L^A_{[1,2]}$. By performing an FFT on those signals, a FAD can be obtained. They describe the no. of plies that belong to each unique orientation in an SS.
2. The Out-of-Plane LPs $V^D_{[1,2,3,4]}$ can be represented as signals using $L^D_{[1,2]}$. By performing an FFT on those signals, the Sum of position-dependant weights associated with all orientations in an SS can be obtained.

When studied separately, these outputs do not immediately correlate a set of LPs to an SS. But, when studied together, one has more information to design an SS that corresponds to a set of $V^{\{A,D\}}_{[1,2,3,4]}$. Hence, a step-by-step procedure was necessary to perform such a design. First, the FAD will have to be

designed using In-Plane LPs, and then the SS will be designed using the FAD and the Out-of-Plane LPs. Thus, the SS design framework proposed in this thesis will have a hierarchical nature:

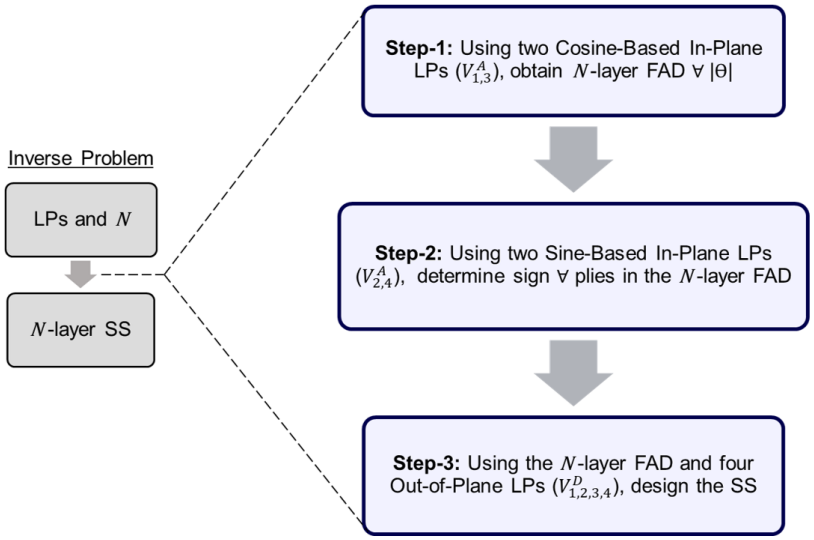

Figure 6.1: Inverse Problem (depicted on the left) partitioned into a step-by-step Hierarchical approach (depicted on the right)

It is known that the $V^A_{2,4}$ LPs are non-zero only for an unbalanced FAD. Hence, the second step will be considered only for unbalanced design, while being ignored for balanced design. Nevertheless, to obtain reliable outputs from FFT, it is essential to discuss the signal sampling requirements for the chosen parameterisation. The subsequent section elaborates upon this.

6.3. Sampling Requirements for chosen parameterisation

A laminate signal must be sampled appropriately to avoid aliasing. This ensures that the aforementioned outputs from FFT can be used reliably. The Nyquist-Shannon theorem is followed (from Equation 4.6) to achieve the same [82]. For the parameterisation shown above (in Table 6.1), frequency corresponds with 2θ, and $\theta \in (-90, 90]$. Hence, the highest frequency is $2 * 90^\circ$ or $\pi\ rad$. As such, the sampling rate in fictitious time T can be quantified as follows:

$$\text{Sampling Rate} \geq 2 * \text{Highest Angular Frequency in Signal}$$

$$\Rightarrow \text{Sampling Rate} \geq 2 * \frac{max(\omega)}{2\pi} \left[\because \text{Angular Frequency} = \frac{\omega}{2\pi}\ rad/s \text{ for sinusoids}\right]$$

$$\Rightarrow \text{Sampling Rate} \geq 2 * \frac{\pi}{2\pi}$$

$$\Rightarrow \text{Sampling Rate} \geq 1$$

This implies that a laminate signal L needs to be sampled at least once a second. However, the precise quantity of these samples ($\mathcal{N}$) is then determined based on another criterion [82]. The $\mathcal{N}$ must be a multiple of the periodicity.

As mentioned in the literature review (in section 4.1), the FFT of $\mathcal{N}$ samples provides an output as an array of DFT coefficients. Each array element is called a frequency bin as they are associated with a frequency value and contain their corresponding amplitude information (in the form of a DFT coefficient). These bins correspond to a uniformly spaced set of frequencies between 0° and the highest frequency we can detect from the signal (90° here). So by ensuring $\mathcal{N}-1$ to be a multiple of the signal's periodicity, the number of bins will be spaced such that the desired frequencies are obtained. For example, if a laminate is to be designed with four orientations $|\theta| \in [15^\circ, 45^\circ, 60^\circ, 90^\circ]$, their $\mathcal{N}$ can be calculated as follows. The periodicity is a function of the signal's fundamental frequency (revisiting Equation 4.5):

$$\text{Periodicity} = \frac{360}{\text{Fundamental Frequency}}$$

$$\Rightarrow \text{Periodicity} = \frac{360}{\text{Greatest Common Divisor}(2 * [15^\circ, 45^\circ, 60^\circ, 90^\circ])}$$
$$\Rightarrow \text{Periodicity} = \frac{360}{30}$$
$$\Rightarrow \text{Periodicity} = 12$$

Hence, the periodicity of the design case in this example is 12. So by using $\mathcal{N} = 13$, the frequency bins generated by them correspond to $[0^\circ, 7.5^\circ, 15^\circ, 22.5^\circ, 30^\circ, 37.5^\circ, 45^\circ, 52.5^\circ, 60^\circ, 67.5^\circ, 75^\circ, 82.5^\circ, 90^\circ]$. They contain the ply orientation information we desire for this example case ($|\theta| \in [15^\circ, 45^\circ, 60^\circ, 90^\circ]$), and $13 - 1$ is a multiple of the periodicity 12. Therefore, by sampling a laminate 13 times every second (i.e., $T = [0, 1, 2, 3, ..., 10, 11, 12]$), the sampling criterion for the given design case can be satisfied, and their FFT output is reliable to use.

It can now be understood that $\mathcal{N}$ needs to be precisely defined depending on the frequencies inside a signal. In terms of the laminate signal parameterisation, it meant that one needs to know beforehand which ply orientations are required to design the laminate. Moreover, as the number of ply orientations to be designed with increases (like ply angle multiples of 1° or $[\Delta 1^\circ]$), the periodicity interval of the signal, and consequently, $\mathcal{N}$, increases. So, at this stage, it was decided that this thesis would limit itself to $[\Delta 15^\circ]$ ply orientations to design laminate. As the aforementioned example case used four orientations from $[\Delta 15^\circ]$, the laminate signals for them ought to possess the same fundamental frequency. Hence, $\mathcal{N} = 13$ with a sampling rate of 1 can be used for the design of laminates with $[\Delta 15^\circ]$. The consequent chapter explains how 13 samples are described using the known set of LPs.

Overview of the following chapters

As shown in Figure 6.1, a hierarchical SS design procedure was proposed in this thesis. Consequently, the layout of the remaining Part-II of this report is structured as follows: chapter 7 describes the design of Symmetric-Balanced FAD using $V^A_{1,3}$, chapter 8 describes the design of Symmetric-Unbalanced FAD by accounting for $V^A_{2,4}$, and chapter 9 describes SS design using a known FAD and $V^D_{1,2,3,4}$.

While implementing the concepts presented, it became apparent that performing FFTs on the sine-based signals ($L_2^{A,D}$) and reliably obtaining outputs from L_1^D was not a viable task. Consequently, FFTs could only be used in step-1 of the hierarchical framework (on L_1^A). These limitations will be detailed in the respective chapters, and alternative methods for carrying out steps-2 and 3 will be introduced. However, due to the time constraints of this thesis, the alternate methodology drafted for step-3 was not implemented. Thus, this thesis primarily centres on the FAD design procedure (steps-1 and 2). Part-III of this report exclusively demonstrates the effectiveness of the implementations for designing Symmetric-Balanced and Symmetric-Unbalanced FADs.

In summary, all assumptions and objectives stated in this chapter can be encapsulated as follows:

This thesis will demonstrate the effectiveness of using a Hierarchical framework to design Symmetric-Balanced and Symmetric-Unbalanced FADs, with Non-Conventional Orientations [$\Delta 15^\circ = 0, \pm 15, \pm 30, \pm 45, \pm 60, \pm 75, 90$***]*** .

7

In-Plane Stiffness Design of Symmetric-Balanced Laminates

"The mathematical sciences particularly exhibit order, symmetry, and limitation; and these are the greatest forms of the beautiful."

Aristotle

To handle the inverse problem using FFTs, the LPs were decided to be represented as a periodic signal composed of sinusoids (in Equation 6.1). Moreover, it was understood that one set of LPs needs to be represented using multiple signals. By performing FFTs on all such signals, it is possible to obtain different outputs that can be used to design an SS. Hence, the SS design procedure is decided to be handled hierarchically. As such, the first step of this design framework was the following:

Step-1: Using two Cosine-Based In-Plane LPs ($V_{1,3}^A$), obtain N-layer FAD $\forall\ |\theta|$

By performing FFT of $V_{1,3}^A$ through L_1^A, an N-layer FAD $\forall\ |\theta|$ can be obtained. This chapter will elucidate how $\mathcal{N}$ samples of L_1^A are generated. Due to the multi-modal nature of the inverse problem, different laminates can share the same LPs. Consequently, multiple different L_1^A can correspond to the same $V_{1,3}^A$. Therefore, this chapter analyses the behaviour of different L_1^A that correspond to the same LPs and parameterise their behaviour in terms of the LPs (as explained in section 7.1). This allowed describing samples of multiple different L_1^A and, consequently, generate multiple different FADs for the same $V_{1,3}^A$. Additionally, this chapter also explains the necessary post-processing steps that ensure the FAD only has integer ply counts and a balanced output can be interpreted from it (in section 7.2). Since this thesis only considers the design of symmetric laminates, N from here onwards refers to the total number of layers in the symmetric half.

7.1. Generating Samples of Laminate Signals with $V_{1,3}^A$

For the design of FADs with $[\Delta 15^\circ]$, the findings from the previous chapter (in section 6.3) stated that the FFTs require $\mathcal{N} = 13$ samples of L_1^A, and they need to be sampled every second. This implies that the value of L_1^A needs to be provided to the FFT from $T = [0, 1, 2, ..., 12]$. It was already shown that the value of any laminate signal at $T = [1, 2]$ are their constituent LPs. Moreover, when $T = 0$, the cosines have a null argument and a value of 1. Hence, by simple substitution, the value of L_1^A can be known for $T = [0, 1, 2]$:

Table 7.1: Values of L_1^A in the initial time-stamps $T = [0, 1, 2]$

	$T=0$	$T=1$	$T=2$
$L_1^A(T)$	1	V_1^A	V_3^A

However, describing samples of a L_{A1} beyond the first few trivial timestamps ($T = [0, 1, 2)$ is challenging due to the multi-modal nature of the Inverse Problem: a set of LPs can correspond to more than one SS. This can be observed for a simple quasi-isotropic (QI) case[1]:

Table 7.2: Multiple Symmetric FADs ($\forall\ |\theta|$) corresponding to one set of $V_{1,3}^A$ LPs (QI Case)

V_1^A	V_3^A	**12-layer Symmetric FAD ($\forall\ \|\theta\|$)**
0	**0**	$[0_3, 45_6, 90_3]_S$
		$[0_4, 60_8]_S$
		$[0, 15_2, 30_2, 45_2, 60_2, 75_2, 90]_S$

Here, it can be seen that different FADs are each made up of different sets of ply orientations and their respective ply counts. So, even though they correspond to the same LP values, their signal equivalents must have different fundamental frequencies and, consequently, different behaviour. This can be visualised by plotting the signal form of these FADs, using the L_1^A signal definition (Equation 6.1). As such, the QI FADs can be viewed in the signal form as shown here:

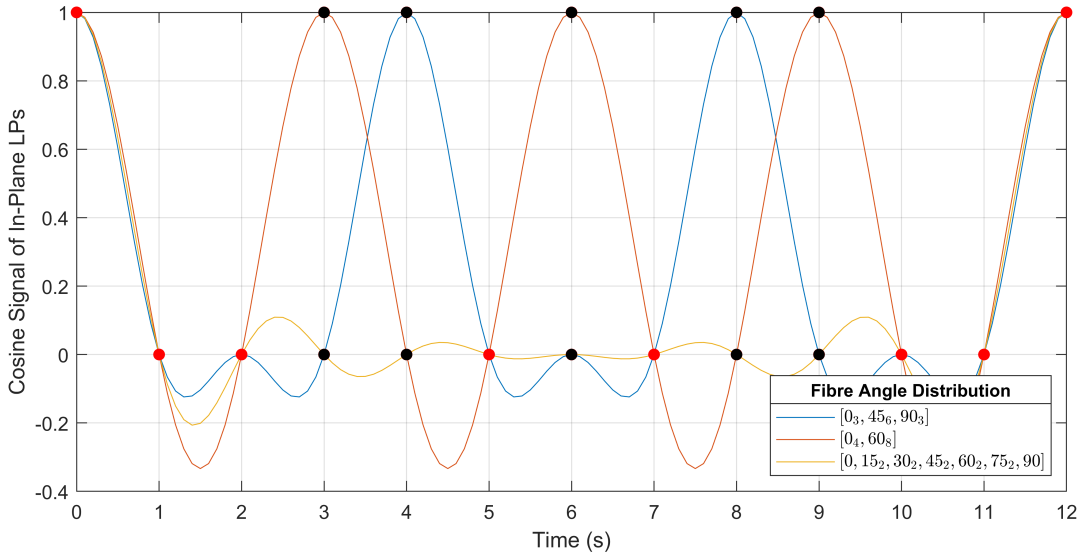

Figure 7.1: L_1^A of QI FADs. Sampled points with identical values are marked red, and non-identical values are marked black

As such, the multi-modality of LPs also exists in the signal parameterisation. At the time $T = 0, 1, 2$, all these signals equal unity and $V_{1,3}^A$, respectively (as seen in Table 7.1). Beyond $T = 2$, the values of the samples can be seen to assume different values, albeit coinciding in certain timestamps. Each of the three signals constitutes a FAD with multiples of different θ's: $[\Delta 45^\circ]$,$[\Delta 60^\circ]$, and $[\Delta 15^\circ]$. So, by learning how the values of these signals vary, it is possible to describe samples of different laminate signals corresponding to the same $V_{1,3}^A$. Consequently, it allows the design of multiple FADs, each with a unique set of ply orientations. This is an important notion to consider, as only one set of finite ply orientations cannot achieve every feasible combination of $V_{1,3}^A$. As seen in Miki's diagram from the literature study (Figure 3.1), laminates made with the conventional orientations ($\theta \in [0, \pm 45, 90]$) can never achieve LPs outside a triangular design domain. Hence, by having the capability to design with multiple sets of ply orientations, a larger part of the feasible In-Plane LP Space can be matched exactly with an FAD. To achieve this, more attention was paid to understanding how these sample values vary at time $T > 2$ and make different signal samples for the same $V_{1,3}^A$.

To reinstate, three signals were plotted in Figure 7.1, each corresponding to a unique FAD. These FADs were made of multiples of different θ's, and each can be seen to repeat themselves at different periodic intervals (different periodicity behaviours). These traits correspond with the findings presented in chapter 4, that the set of frequencies present within a periodic signal influence the rate at which

[1] Quasi-Isotropy implies equal stiffness across In-Plane direction for a laminate. In-Plane LPs of such laminates are zero

they repeat themselves. In particular, by knowing the set of frequencies that are present in a signal, their fundamental frequency (greatest common divisor of frequencies) can be computed to predict their periodicity (restating Equation 4.5):

$$\text{Periodicity} = \frac{360}{\text{Fundamental Frequency}}$$

For FADs made with different sets of ply orientations, their signal periodicity varies, as shown here:

Table 7.3: Periodicity values of Laminate Signals containing different sets of ply orientations $[\Delta\theta]$

Set of Ply Orientations	Fundamental Frequency	Period
$[\Delta 60°] = [0, \pm 60]$	120	**3**
$[\Delta 45°] = [0, \pm 45, 90]$	90	**4**
$[\Delta 30°] = [0, \pm 30, \pm 60, 90]$	60	**6**
$[\Delta 15°] = [0, \pm 15, \pm 30, \pm 45, \pm 60, \pm 75, 90]$	30	**12**

It can be observed that these periodicity values also correspond with the signal behaviour in Figure 7.1. Hence, the periodic nature can be capitalised further to describe the value of the signal at many timestamps. As seen in Table 7.3, laminate signals of $[\Delta 60^\circ]$ FADs have a periodicity value of 3. This implies that the signal values at the first three timestamps ($T = [0, 1, 2]$) keep repeating throughout time as a forever pattern. From here onwards, repetitions such as these are called a 'signal pattern'. As such, the signal pattern for laminates made of $[\Delta 60^\circ]$ can be described as follows:

Table 7.4: Signal Pattern for laminates made of $[\Delta 60^\circ]$ orientations

Angle Increments	$T = 0$	$T = 1$	$T = 2$	$T = 3$	$T > 3$
$[\Delta 60°]$	1	V_1^A	V_3^A	1	repeated

Therefore, the strategy moving forward was to identify signal patterns such that they can be used to generate any desired $\mathcal{N}$ number of samples. By performing FFTs on the samples described using the signal pattern shown here, FAD can be designed using $[\Delta 60^\circ]$ orientations. Similarly, to interpret a signal pattern for $[\Delta 45^\circ]$, their signal from Figure 7.1 was analysed again. It was observed that signals with even-numbered periods possess vertical symmetry. In other words, a periodic pattern mirrored itself about its centre. In the case of $[\Delta 45^\circ]$, this symmetry was observed about the second timestamp ($T = 2$). By utilising this geometric property, their signal pattern was described as follows:

Table 7.5: Signal Pattern for laminates made of $[\Delta 45^\circ]$ orientations

Angle Increments	$T = 0$	$T = 1$	$T = 2$	$T = 3$	$T = 4$	$T > 4$
$[\Delta 45°]$	1	V_1^A	V_3^A	V_1^A	1	repeated

Geometric properties such as periodicity and symmetries helped describe signal patterns for $[\Delta 60^\circ]$ and $[\Delta 45^\circ]$ orientations. However, they are not sufficient to describe signals with $[\Delta 15^\circ]$, which was chosen to be the objective of this study. As seen in Table 7.3, the periodicity values of a set with smaller angle increments like $[\Delta 30^\circ]$ and $[\Delta 15^\circ]$ are 6 and 12 respectively. Because of that, the signal patterns for those angle increments cannot be described entirely with the first three known signal values. Hence, this situation was handled with two different approaches. One would be to describe the signal behaviour for a known number of ply orientations, while the other would be to observe repeating behaviours of different FAD signals and then approximating these patterns by parameterising them in terms of LPs. Hence, these two approaches yielded the 'Exact' and 'Approximate' signal patterns, respectively. The following subsections will focus on how these patterns are formulated/identified. By generating a pool of signal patterns with them, the FFT-based method can work with a diverse set of ply orientations, providing a diverse pool of solutions.

7.1.1. Exact Signal Patterns

From Equation 6.1, the mathematical form of the signal L_1^A can be written as:

$$L_1^A(T) = \frac{1}{N}\sum_{k=1}^{N}[\cos 2\theta_k T] \tag{7.1}$$

As seen in Table 7.1, the value of $L_1^A(T)$ at the initial three timestamps is equal to unity and $V_{1,3}^A$, respectively. Hence, L_1^A at all $T > 2$ was decided to be described as a linear combination of the known quantities $L_1^A(T = 0, 1, 2)$:

$$\begin{gathered} L_1^A(T) = a_T\left(L_{1,3}^A(T=0)\right) + b_T\left(L_{1,3}^A(T=1)\right) + c_T\left(L_{1,3}^A(T=2)\right) \\ (or) \\ L_1^A(T) = a_T + b_T V_1^A + c_T V_3^A \end{gathered} \tag{7.2}$$

The signal value can be calculated when the values of a b and c are known for a given timestamp T. Hence, for a given T, a b and c are the three unknowns to be found. To know their values, a system of equations was created by equating Equation 7.1 and 7.2:

$$\begin{aligned} &\frac{1}{N}\sum_{k=1}^{N}[\cos 2\theta_k T] = a_T\left(L_1^A(T=0)\right) + b_T\left(L_1^A(T=1)\right) + c_T\left(L_1^A(T=2)\right) \\ \Rightarrow &\frac{1}{N}\sum_{k=1}^{N}[\cos 2\theta_k T] = a_T\left(\frac{1}{N}\sum_{k=1}^{N}[\cos 2\theta_k * 0]\right) + b_T\left(\frac{1}{N}\sum_{k=1}^{N}[\cos 2\theta_k * 1]\right) + c_T\left(\frac{1}{N}\sum_{k=1}^{N}[\cos 2\theta_k * 2]\right) \end{aligned}$$

The summation rule adds the contribution of all N plies in the symmetric half of the FAD. For convenience, they are now replaced as a sum of p different ply orientations and their respective volume fractions ν (the fraction of plies belonging to a certain orientation). For example, in a 20-layer FAD, if 5 plies have the orientation 45°, the volume fraction ν of 45° is 0.25 ($\because$, $5/20$=0.25).

$$\begin{aligned} \Rightarrow \begin{bmatrix} \nu_1 & \nu_2 & \cdots & \nu_p \end{bmatrix} \begin{bmatrix} \cos(2\theta_1 T) \\ \cos(2\theta_2 T) \\ \vdots \\ \cos(2\theta_p T) \end{bmatrix} = \quad & a_T\left(\begin{bmatrix} \nu_1 & \nu_2 & \cdots & \nu_p \end{bmatrix} \begin{bmatrix} \cos(2\theta_1 * 0) \\ \cos(2\theta_2 * 0) \\ \vdots \\ \cos(2\theta_p * 0) \end{bmatrix}\right) \\ & + b_T\left(\begin{bmatrix} \nu_1 & \nu_2 & \cdots & \nu_p \end{bmatrix} \begin{bmatrix} \cos(2\theta_1 * 1) \\ \cos(2\theta_2 * 1) \\ \vdots \\ \cos(2\theta_p * 1) \end{bmatrix}\right) \\ & + c_T\left(\begin{bmatrix} \nu_1 & \nu_2 & \cdots & \nu_p \end{bmatrix} \begin{bmatrix} \cos(2\theta_1 * 2) \\ \cos(2\theta_2 * 2) \\ \vdots \\ \cos(2\theta_p * 2) \end{bmatrix}\right) \end{aligned}$$

$$\Rightarrow \begin{bmatrix} \cos(2\theta_1 T) \\ \cos(2\theta_2 T) \\ \vdots \\ \cos(2\theta_p T) \end{bmatrix} = a_T\left(\begin{bmatrix} \cos(2\theta_1 * 0) \\ \cos(2\theta_2 * 0) \\ \vdots \\ \cos(2\theta_p * 0) \end{bmatrix}\right) + b_T\left(\begin{bmatrix} \cos(2\theta_1 * 1) \\ \cos(2\theta_2 * 1) \\ \vdots \\ \cos(2\theta_p * 1) \end{bmatrix}\right) + c_T\left(\begin{bmatrix} \cos(2\theta_1 * 2) \\ \cos(2\theta_2 * 2) \\ \vdots \\ \cos(2\theta_p * 2) \end{bmatrix}\right)$$

$$\Rightarrow \begin{bmatrix} \cos(2\theta_1 T) \\ \cos(2\theta_2 T) \\ \vdots \\ \cos(2\theta_p T) \end{bmatrix} = \begin{bmatrix} 1 & \cos(2\theta_1) & \cos(4\theta_1) \\ 1 & \cos(2\theta_2) & \cos(4\theta_2) \\ \vdots & \vdots & \vdots \\ 1 & \cos(2\theta_p) & \cos(4\theta_p) \end{bmatrix} \begin{bmatrix} a_T \\ b_T \\ c_T \end{bmatrix}$$

$$\Rightarrow \begin{bmatrix} a_T \\ b_T \\ c_T \end{bmatrix} = \begin{bmatrix} 1 & \cos(2\theta_1) & \cos(4\theta_1) \\ 1 & \cos(2\theta_2) & \cos(4\theta_2) \\ \vdots & \vdots & \vdots \\ 1 & \cos(2\theta_p) & \cos(4\theta_p) \end{bmatrix}^{-1} \begin{bmatrix} \cos(2\theta_1 T) \\ \cos(2\theta_2 T) \\ \vdots \\ \cos(2\theta_p T) \end{bmatrix}$$

To solve this system of equations, the dimensions across both ends should match. Hence, $p = 3$:

$$\Rightarrow \begin{bmatrix} a_T \\ b_T \\ c_T \end{bmatrix} = \begin{bmatrix} 1 & \cos(2\theta_1) & \cos(4\theta_1) \\ 1 & \cos(2\theta_2) & \cos(4\theta_2) \\ 1 & \cos(2\theta_3) & \cos(4\theta_3) \end{bmatrix}^{-1} \begin{bmatrix} \cos(2\theta_1 T) \\ \cos(2\theta_2 T) \\ \cos(2\theta_3 T) \end{bmatrix} \tag{7.3}$$

Thus, using Equation 7.3, the value of the signal (Equation 7.2) can be exactly calculated for any timestamp T, upon assuming a set of three-ply orientations. As such, an 'Exact' signal pattern can be formulated. For example, when a FAD is to be designed with the orientations $[0^\circ, 15^\circ, 30^\circ]$, an exact can be formulated as follows:

Table 7.6: Exact signal pattern for laminates made of $[0^\circ, 15^\circ, 30^\circ]$ orientations

Orientations	$T=0$	$T=1$	$T=2$	$T=3$	$T=4$	$T=5$	$T=6$
$[0°, 15°, 30°]$	1	V_1^A	V_3^A	$6.46 - 10.19V_1^A + 4.73V_3^A$	$20.39 - 30.58V_1^A + 11.19V_3^A$	$35.32 - 51.98V_1^A + 17.66V_3^A$	$41.78 - 61.17V_1^A + 20.39V_3^A$

The signal pattern is described only till $T = 6$ since a period within cosine signals was found to have vertical symmetry. Thus, the values repeat themselves about $T = 6$ till the period ends (at $T = 12$). When angle increments of $[\Delta 15^\circ]$ are chosen as design variables for the FAD, a set of three orientations can be chosen in ${}^7C_3$ ways ($\because$, seven unique orientations exist within $[\Delta 15^\circ]$). This computes a total of 35 exact signal patterns. For brevity, they are presented in the Appendix (in Table B.2).

7.1.2. Approximate Signal Patterns

Using the procedure mentioned in the previous sub-section, making signal patterns for designing a FAD with more than three orientations was not mathematically possible. This is because the L_1^A signal was described as a function of three known quantities ($L_1^A(T = 0, 1, 2)$). To circumvent this limitation, a signal pattern can be constructed by fixing the contribution of specific ply orientations (proportion of plies belonging to certain θ's) while still designing the contribution of three orientations. Doing this allows a FAD to be designed with more than three orientations.

By arbitrarily assuming the contribution of certain orientations, infinitely many possible signal patterns can be conceived. However, the signal representation of the FAD allows us to handle this situation with ease. It provides a visual medium to examine FADs through their L_1^A signals. Consequently, the L_1^A of FADs with more than three-ply orientations are analysed. First, the repeated patterns within them are manually identified and then approximated in terms of the three known quantities (unity and the $V_{1,3}^A$ LPs). This differs from the previous approach (involving Exact Patterns) since FADs are used as a basis to create patterns rather than selecting three-ply orientations. Here, the contribution of certain orientations is involuntarily fixed, while the others vary with the known quantities. Therefore, by approximating visually identified patterns in terms of LPs, several 'Approximate' patterns for the FAD with $[\Delta 15^\circ]$ were made during this thesis work. This chapter will explain how these patterns can be identified and used later for designing a Symmetric-Balanced FAD.

The process in which these patterns are created will be explained using an example similar to the previously used QI case. A combination $V_{1,3}^A = [0.17, -0.1]$ was randomly chosen from the feasible In-Plane LP space. Using an open-source GA known as OptiBLESS([90])[2], multiple FADs that correspond to this $V_{1,3}^A$ combination were designed with $[\Delta 15^\circ]$. The L_1^A signal of these FADs was then plotted.

[2]The parameters used to operate OptiBLESS can be referred from the Appendix (in section B.2).

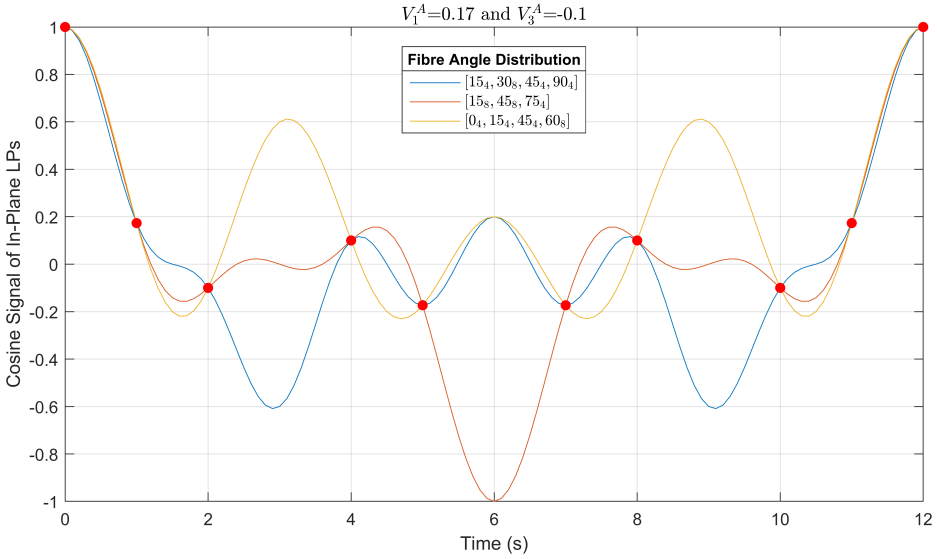

Figure 7.2: Cosine-Based In-Plane Signals of FADs corresponding to $V_{1,3}^A = [0.17, -0.1]$. Sampled Points with equal values across all the FADs are marked in red.

Here, the signals of three unique FADs can be observed. The signal values at timestamps $T = 4$ and 5 are equal, while a variation can be observed at timestamps $T = 3$ and 6. Nevertheless, these common and uncommon points (at $T > 2$) were manually approximated as a function of the known LPs. From a visual perspective, the sample values at $T = 4$ and 5 appeared as a negative of V_3^A and V_1^A, respectively. However, the sample value at $T = 3$ and 6 can be parameterised in at least three or two different ways, respectively. This is tabulated as shown below:

Table 7.7: Approximate Signal Pattern(s) corresponding to the $V_{1,3}^A = [0.17, -0.1]$

$T=0$	$T=1$	$T=2$	$T=3$	$T=4$	$T=5$	$T=6$
1	V_1^A	V_3^A	0	$-V_3^A$	$-V_1^A$	$-2V_3^A$
			$6V_3^A$			$10V_1^A$
			$-6V_1^A$			

As such, this visual pattern-finding exercise for one point in the LP space ($V_{1,3}^A = [0.17, -0.1]$) yielded six different approximate signal patterns ($3 * 2$ permutations). The uncommon points ($T = 3$ and 6) can also be left unsampled (timestamps labelled as 'X' in Table 7.8).

Table 7.8: Non-Uniform Approximate Signal Pattern corresponding to the $V_{1,3}^A = [0.17, -0.1]$; Unsampled timestamps are marked with an 'X'

$T=0$	$T=1$	$T=2$	$T=3$	$T=4$	$T=5$	$T=6$
1	V_1^A	V_3^A	X	$-V_3^A$	$-V_1^A$	X

This makes a non-uniform signal pattern. The FFT on samples derived from such patterns was performed using MATLAB's NUFFT implementation. Initially, the values of a non-uniform set of samples and their respective timestamps are generated with a non-uniform pattern. When provided to NUFFT, additional samples are generated by interpolation. These additional samples are added to the initially provided set to make it uniform. After this, a regular FFT is performed.

These approximations are based on a randomly sampled $V_{1,3}^A$ combination. To verify the efficacy of these approximations, they were checked with LP combinations local to the randomly sampled point. Two locally close combinations of $V_{1,3}^A$ can be made by perturbing ply counts of a known FAD from the above-mentioned example (Figure 7.2). This is explained with the FAD $[15_4, 30_8, 45_4, 90_4]$, in the following table:

Table 7.9: Generate locally nearby $V_{1,3}^A$ combinations by perturbing a known FAD

V_1^A	V_3^A	**FAD** $(\forall\|\theta\|)$	**Source**
0.1732	-0.1	$[15_4, 30_8, 45_4, 90_4]$	Known entity from Figure 7.2
0.1482	-0.125	$[15_4, 30_7, 45_5, 90_4]$	Obtained by perturbing ply counts of 30 and 45
0.1915	-0.05	$[15_5, 30_7, 45_4, 90_4]$	Obtained by perturbing ply counts of 15 and 30

Plotting the L_1^A values for these three FADs reveals their consistent behaviour (same pattern):

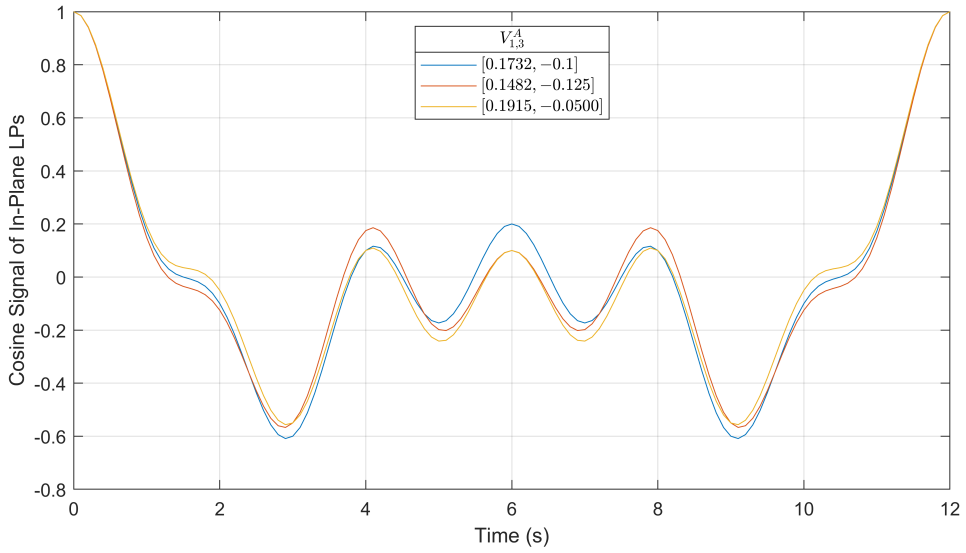

Figure 7.3: Different FADs that can be described using the same Approximate Pattern

Hence, the same signal pattern is observed to be present locally in LP space (near $V_{1,3}^A = [0.17, -0.1]$). Nevertheless, by using this plot, the accuracy of an approximate pattern can be tested to see if it can recreate the same sample values when the perturbed LP combinations are provided.

In summary, one can infer that by approximating the behaviour of L_1^A in terms of $V_{1,3}^A$, an approximate signal pattern locally valid in the LP space can be made. Similar to the Exact Patterns, this localised validity is because one requires different sets of ply orientations to match distinct regions of the LP space. As the ply orientations change, so does the behaviour of L_1^A, resulting in differing patterns. Consequently, this visual pattern-finding exercise must be repeated at different parts of the LP space. While the number of exact patterns for $[\Delta 15^\circ]$ remains 35, the total number of approximate patterns needs to be decided such that they are limited in amount, but still capable of designing FADs for LP values from all over the $V_{1,3}^A$ space. So for brevity, the complete pool of signal patterns will be optimised to be limited and efficient in chapter 10. Meanwhile, this chapter will focus on using an identified pattern to design a Symmetric-Balanced Laminate.

7.2. Examining Fourier Transform Output: Insights and Requisite Post-processing

Signal patterns can be created using the techniques explained in the previous section. Using these patterns, the FFT can be provided with the samples of the laminate signal L_1^A for every second in T. The amplitude of every frequency in L_1^A corresponds to a FAD ($\forall\ |\theta|$). However, it can be noticed that the signal patterns are constructed only using the LPs and not N. This is simply because the LPs are normalised with respect to them. Therefore, a N-layer Symmetric FAD needs to be interpreted from the FFT output. The typical way to represent this output is using a frequency spectrum. This output format and their requisite post-processing will be explained using an example case: target LPs $V_{1,3}^A = [0.5232, 0.1500]$, and $N = 20$. These LPs were calculated from a real Symmetric-Balanced FAD: $[0_4, +15_3, -15_3, +30_3, -30_3, +45, -45, +75, -75]_S$. The samples of L_1^A here will be generated

using the non-uniform approximate pattern (shown in Table 7.8). Since they are non-uniform, they can only generate $\mathcal{N} = 10$ non-uniform samples. To handle such cases, the NUFFT implementation of MATLAB can be used, which automatically interpolates more values to the sample set such that they are uniform in time. The FFT results from using this signal pattern can then be represented by the following spectrum :

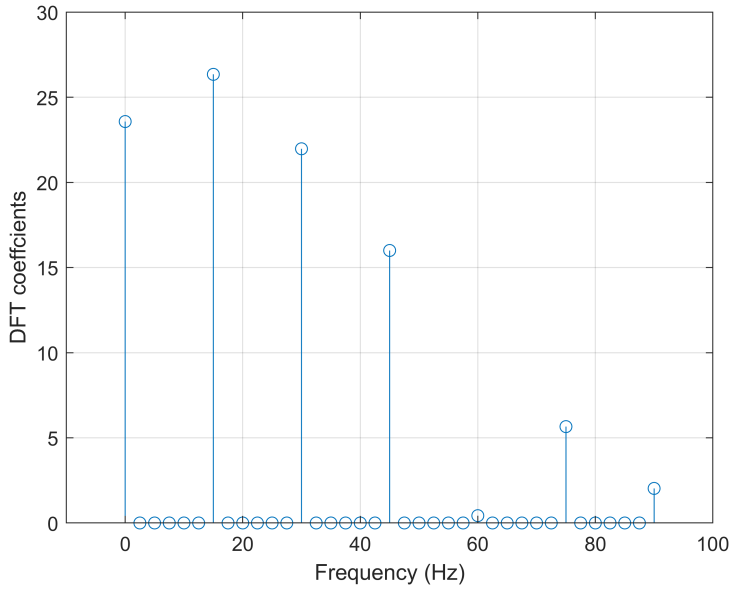

Figure 7.4: Frequency spectrum of L_1^A ($V_{1,3}^A = [0.5232, 0.1500]$)

DFT coefficients represent the amplitude information corresponding to all the frequencies[3]. To relate this spectrum to a 20-layer FAD ($\forall\ |\theta|$), they were normalised with respect to N.

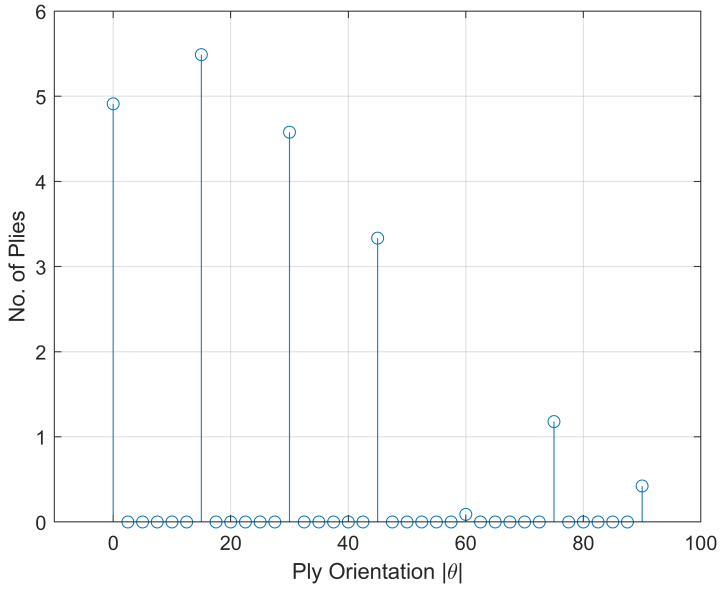

Figure 7.5: Normalised Frequency spectrum of L_1^A ($V_{1,3}^A = [0.5232, 0.1500]$ and $N = 20$)

[3]For completeness, it is mentioned here that only the positive and real components of the DFT coefficients are used to make the frequency spectrum. This is because imaginary and negative DFT correlations do not mean anything in the laminate signal parameterisation followed in this thesis (can be referred from Table 6.1).

Using this normalised spectrum, the following FAD ($\forall|\theta|$) can be tabulated:

Table 7.10: FAD ($\forall\ |\theta|$) obtained from L_1^A ($V_{1,3}^A = [0.5232, 0.1500]$ and $N = 20$)

Ply Orientation (°)	0	15	30	45	60	75	90
Ply Count	4.91067	5.488	4.57733	3.33333	0.08933	1.17866	0.422667

The ply counts shown here add up to $N = 20$, and the relevant LPs compute to $V_{1,3}^A = [0.53, 0.15]$. However, a FAD with non-integer ply counts is practically meaningless. Moreover, to design a balanced FAD, the ply counts of an off-axis θ must be equally split between $+\theta$ and $-\theta$. Hence, in the table above, the ply counts with off-axis ply orientation must be an even integer. Therefore, post-processing the FFT output was necessary to achieve a feasible outcome.

As the problem at hand involves converting non-integer values into an integer while ensuring off-axis ply counts are even, a rounding procedure was developed. This procedure involved rounding down the ply counts within the obtained FAD to even numbers. Upon this step, they can be rounded up again to be integers, and the off-axis $|\theta|$'s are balanced. This will be explained step-by-step with the FAD shown in Table 7.10. To begin with, the ply counts of odd non-integer numbers are decomposed into their even, odd and fractional components.

Table 7.11: Analysing a non-integer FAD ($\forall|\theta|$) obtained from L_1^A ($V_{1,3}^A = [0.5232, 0.1500]$ and $N = 20$)

								Sum
Ply Count	$0°$ =4.91067	$15°$ =5.488	$30°$ =4.57733	$45°$ =3.33333	$60°$ =0.08933	$75°$ =1.17866	$90°$ = 0.422667	20
Even Integer	4	4	4	2	0	0	0	14
Odd Integer	0	1	0	1	0	1	0	3
Fraction	0.91067	0.488	0.57733	0.33333	0.08933	0.17866	0.422667	3

As seen here, the even ply counts add up to 14. Hence, to obtain a 20 layered balanced FAD with integer ply counts, 6 more plies need to be added. This was achieved by rounding up the ply counts such that the off-axis counts were even numbers. In this case, such a rounding step can be performed 112 different ways [4]. So, this yields 112 different interpretations of a FAD. The best FAD out of them was chosen by observing their closeness to the target LPs. A distance measure like the 'Euclidean Distance' or 'L2-norm' was used to compute the same:

$$\varepsilon = \sqrt{\sum_{1}^{d}(|V_{Design}^A - V_{Target}^A|)^2} \tag{7.4}$$

As the entities of interest here are the two LPs $V_{1,3}^A$, the upper limit of this sum is $d = 2$. The V_{Design} would be the LPs corresponding to a rounded FAD, while V_{Target} is the target case. In this example, out of 112 FADs, the following solution had the lowest mismatch with the target LPs:

Table 7.12: Symmetric-Balanced FAD ($\forall|\theta|$) obtained from L_1^A ($V_{1,3}^A = [0.5232, 0.1500]$ and $N = 20$) using an Approximate Pattern

Ply Orientations (°)	0	15	30	45	60	75	90
Ply Count	4	6	6	2	0	2	0
Mismatch Error ε	0						

By equally splitting the ply counts of an off-axis $|\theta|$ between $+\theta$ and $-\theta$, the FAD ($\forall\ |\theta|$) can be inferred as a Symmetric-Balanced FAD: $[0_4, +15_3, -15_3, +30_3, -30_3, +45, -45, +75, -75]_S$. As such, the procedure explained in this section can be used to design a Symmetric-Balanced FAD for a given $V_{1,3}^A$ and N, using the non-uniform approximate pattern shown in Table 7.8.

[4] In this case, 6 plies are to be added, and there are seven-ply orientations. Hence, this combinatoric was obtained by generating all possible ways 6 values can be chosen from the set of seven orientations. And then 112 combinations remained when the instances with odd-number off-axis orientations were removed.

Regardless, this pattern will not help convert any given $V_{1,3}^{A}$ combination into an N-layer Symmetric-Balanced FAD. As explained earlier, any identified pattern will be valid only to a localised region in the LP space. This can be observed when repeating this procedure for another case: target LPs $V_{1,3}^{A} = [0.80, 0.60]$ and $N = 20$. These LPs are randomly sampled and far away from the previous example case.

Table 7.13: Symmetric-Balanced FAD ($\forall|\theta|$) obtained from L_1^A ($V_{1,3}^{A} = [0.80, 0.60]$ and $N = 20$) using an Approximate Pattern

Ply Orientations (°)	0	45	75	90
Ply Count	4	12	2	2
Mismatch Error ε	0.215550			

As seen here, the mismatch error ε is significantly higher than in the previous case. Hence, a new pattern valid for this region needs to be made to improve the performance of the FFT-based method. When multiple patterns are present in the tool, the FAD design procedure will be repeated for all patterns, and the best solutions among them will be selected. More patterns can be made by following the procedure shown in subsection 7.1.1 and subsection 7.1.2.

However, as mentioned earlier, this chapter limits itself to pattern identification and designing a Symmetric-Balanced FAD. The total pool of signal patterns will be found and optimised later in chapter 10. Over there, the FFT-based method will be iteratively improved by creating and adding new Approximate patterns. This will be performed such that the method guarantees the conversion of almost any feasible set of $V_{1,3}^{A}$ into a FAD using $[\Delta 15^{\circ}]$, all while using a limited number of patterns.

8

In-Plane Stiffness Design of Symmetric-Unbalanced Laminates

"We cannot solve our problems with the same thinking we used to create them."

Albert Einstein

From the FFT-based implementation explained in the previous chapter, the cosine-based In-Plane LPs ($V^A_{1,3}$) can be used to design a N-layer FAD $\forall$ $|\theta|$. By utilising the symmetries and patterns offered by the signal parameterisation of LPs, a (balanced) FAD could be designed with many different sets of ply orientations. This step was primarily powered by the FFTs, accompanied by some post-processing. However, these solutions were created independent of $V^A_{2,4}$. So, they cannot be used for the design of unbalanced FAD. For such a design, the ply count of a $|\theta|$ must be unequally split between $+\theta$ and $-\theta$. To perform this appropriately is the goal of step-2 in this proposed design framework.

Step-2: Using two Sine-Based In-Plane LPs ($V^A_{2,4}$), determine sign $\forall$ plies in the N-layer FAD

The In-Plane LPs $V^A_{2,4}$ are used for this particular step, as they consist of sine functions, whose values are sensitive to the sign of θ's. As such, this chapter will focus on designing an unbalanced N-layer FAD for a given target of $V^A_{2,4}$. Due to some inherent difficulties in handling sine-based entities (presented in section 8.1), the FFTs were not used for this purpose, the same way it was used with the $V^A_{1,3}$. Therefore, a different methodology was pursued to design Symmetric-Unbalanced FADs (in section 8.2).

8.1. Limitations on performing Fast Fourier Transform on $V^A_{2,4}$

By revisiting Equation 2.2, one could infer that the In-Plane LPs can consist of two different sinusoids:

$$V^A_{[1,2,3,4]} = \frac{1}{N}\sum_{k=1}^{N}[\cos 2\theta_k, \sin 2\theta_k, \cos 4\theta_k, \sin 4\theta_k]$$

The cosines are known to be even functions that are insensitive to the sign of their arguments. As such, $V^A_{1,3}$ helps designing a FAD for $|\theta|$. On the contrary, the sines are considered odd functions, sensitive to their arguments' sign. Hence, they theoretically contain the information on how many plies belonging to a θ need to be split between $+\theta$ and $-\theta$. Moreover, the $V^A_{2,4}$ only scales with the number of off-axis plies, as the value of the sine functions for 0° and 90° is null.

In the previous chapter (chapter 7), pre-observed signal patterns were made to aid the design of FAD. These patterns were obtained using two ways: the mathematically derived 'Exact Patterns' can design a FAD for three given $|\theta|$'s, and the visually derived 'Approximate Patterns' can design a FAD with more

than three $|\theta|$'s. However, these patterns cannot be reused when handling the Sine-based In-Plane LPs. As we know, one off-axis $|\theta|$ can correspond to $+\theta$ and $-\theta$. Since the sine functions inside $V_{2,4}^A$ are sensitive to the sign of their arguments, they correspond to double the number of entities relative to $V_{1,3}^A$. So, this constitutes a higher amount of unknowns, making it difficult, if not impossible, to mathematically derive exact signal patterns with $V_{2,4}^A$. This is because the known quantities in this case (N and $V_{2,4}^A$) will allow designing a FAD for three orientations (off-axis θ). For instance, these three orientations could be $[+\theta_1, -\theta_1, +\theta_2]$ or $[+\theta_1, -\theta_1, -\theta_2]$. This implies that the signal pattern made for three orientations cannot design a FAD with more than one off-axis $|\theta|$ value. Moreover, if signal patterns are to be visually identified, it would require the creation of a new and more exhaustive pool. Since these limitations do not favour the creation of a computationally efficient SS design procedure, FFTs were not used to handle $V_{2,4}$. Instead, a system of linear equations consisting of all known information was used. This will be explained in the subsequent section.

8.2. Designing Unbalanced Fibre Angle Distributions with a System of Linear Equations

At the second step of the SS design framework, the known information is the output from the first step (FAD $\forall$ $|\theta|$) and the Sine-based In-Plane LPs $V_{2,4}$. Within this FAD, the ply counts belonging to multiple $|\theta|$'s can be written as a sum of their positive and negative orientation counterparts ($+\theta$ and $-\theta$). As such, using the FAD and $V_{2,4}$, a system of equations[1] can be written:

$$\begin{cases} N_i = N_i^+ + N_i^- \\ V_{[2,4]}^A = \frac{1}{N} \sum_{i=1}^{n} N_i[\sin(2\theta_i),\ \sin(4\theta_i)] \end{cases}$$

Here, n represents the number of off-axis $|\theta|$'s in a FAD, N_i is their respective ply count, while N_i^+ and N_i^- are the ply counts of $+\theta_i$ and $-\theta_i$ respectively. To obtain solutions from any system of linear equations, the number of equations present must equal the number of unknown entities. Two equations can always be written using the LPs $V_{2,4}^A$, and an additional equation can be written for every off-axis θ_i. Hence, this arrangement can be used to design an unbalanced FAD with $n = 1$ and 2:

Table 8.1: System of Linear equations to design Unbalanced FAD with one or two off-axis ply orientations

Number of off-axis $\|\theta\|$ (n)	$n = 1$	$n = 2$
System of Linear Equations	$N_1 = N_1^+ + N_1^-$ $V_2^A = \frac{1}{N}\left(N_1^+ \sin(2\theta_1) + N_1^- \sin(-2\theta_1)\right)$	$N_1 = N_1^+ + N_1^-$ $N_2 = N_2^+ + N_2^-$ $V_2^A = \frac{1}{N}\left(N_1^+ \sin(2\theta_1) + N_1^- \sin(-2\theta_1) + N_2^+ \sin(2\theta_2) + N_2^- \sin(-2\theta_2)\right)$ $V_4^A = \frac{1}{N}\left(N_1^+ \sin(4\theta_1) + N_1^- \sin(-4\theta_1) + N_2^+ \sin(4\theta_2) + N_2^- \sin(-4\theta_2)\right)$

Using these systems of equations, one could solve for N_i^+ and N_i^-, while knowing the N_i and the LPs $V_{2,4}^A$. While this could only be performed for at most $n = 2$, the FAD provided by the FFTs in step-1 can potentially contain an $n > 2$. As established before, the mathematically derived 'Exact Patterns' can design a FAD for at most $n = 3$. Hence, efforts were made to ensure that an unbalanced FAD can be designed for the same case. When step-1 provides a FAD with $n = 3$, we know the values N_1, N_2, and N_3. So, by assuming the values of N_3^+ and N_3^-, a system of equations can be constructed to solve for N_1^+, N_1^-, N_2^+ and N_2^-. Such a system of equations will look as follows:

Table 8.2: System of Linear equations to design Unbalanced FAD with three off-axis ply orientations

Number of off-axis $\|\theta\|$ (n)	$n = 3$
System of Linear Equations	$N_1 = N_1^+ + N_1^-$ $N_2 = N_2^+ + N_2^-$ $V_2^A = \frac{1}{N}\left(N_1^+ \sin(2\theta_1) + N_1^- \sin(-2\theta_1) + N_2^+ \sin(2\theta_2) + N_2^- \sin(-2\theta_2) + N_3^+ \sin(2\theta_3) + N_3^- \sin(-2\theta_3)\right)$ $V_4^A = \frac{1}{N}\left(N_1^+ \sin(4\theta_1) + N_1^- \sin(-4\theta_1) + N_2^+ \sin(4\theta_2) + N_2^- \sin(-4\theta_2) + N_3^+ \sin(4\theta_3) + N_3^- \sin(-4\theta_3)\right)$

Here, the assumption of N_3^+ and N_3^- values was made systematically by generating different subset-sums of N_3. For example, if $N_3 = 6$, an unbalanced split can be achieved in 6 different ways:

[1] For the Inverse Problem of converting LPs to SS, the Out-of-Plane LPs are also known information at this design stage. However, they mathematically correspond with layer positions k, which are unknown quantities. Hence, they cannot be used in this System of Equations without increasing the amount of unknown entities.

Table 8.3: Different combinations by which an off-axis ply count ($N_3 = 6$) can be split in an unbalanced manner ($N_3^+ \neq N_3^-$)

$N_3 = 6$						
N_3^+	6	5	4	2	1	0
N_3^-	0	1	2	4	5	6

Hence, an N_3 can be split into N_3^+ and N_3^-, at least by N_3 different ways [2]. Consequently, multiple different interpretations of a FAD are generated. Similar to the procedure followed in section 7.2, when several interpretations of a FAD exist, the best solution among them is chosen based on their mismatch with the target LPs (L2-Norm or ε from Equation 7.4). As such, a FAD with $n = 3$ can be designed. For completeness, the closed-form solutions for the unbalanced ply counts upon solving the system of equations in Table 8.1 and Table 8.2 are shown here:

Table 8.4: Closed-form solutions for designing off-axis ply counts in an unbalanced FAD

Number of off-axis $\lvert\theta\rvert$ (n)	**Closed-form solutions for N_i^+ and N_i^-**
$n = 1$	$N_1^+ = \frac{N_1}{2} + \frac{NV_2^A}{2\sin(2\theta_1)}$ $N_1^- = \frac{N_1}{2} - \frac{NV_2^A}{2\sin(2\theta_1)}$
$n = 2$	$N_1^+ = \frac{N_1}{2} + \frac{N(V_2^A\sin(4\theta_2) - V_4^A\sin(2\theta_2))}{2(\sin(2\theta_1)\sin(4\theta_2) - \sin(4\theta_1)\sin(2\theta_2))}$ $N_1^- = \frac{N_1}{2} - \frac{N(V_2^A\sin(4\theta_2) - V_4^A\sin(2\theta_2))}{2(\sin(2\theta_1)\sin(4\theta_2) - \sin(4\theta_1)\sin(2\theta_2))}$ $N_2^+ = \frac{N_2}{2} - \frac{N(V_2^A\sin(4\theta_1) - V_4^A\sin(2\theta_1))}{2(\sin(2\theta_1)\sin(4\theta_2) - \sin(4\theta_1)\sin(2\theta_2))}$ $N_2^- = \frac{N_2}{2} + \frac{N(V_2^A\sin(4\theta_1) - V_4^A\sin(2\theta_1))}{2(\sin(2\theta_1)\sin(4\theta_2) - \sin(4\theta_1)\sin(2\theta_2))}$
$n = 3$ (for known values of N_3^+ and N_3^-)	$N_1^+ = \frac{N_1}{2} + \frac{N_3^+(\sin(4\theta_2)\sin(2\theta_3) - \sin(2\theta_2)\sin(4\theta_3)) + N_3^-(\sin(2\theta_2)\sin(4\theta_3) - \sin(4\theta_2)\sin(2\theta_3)) + N(V_4^A\sin(2\theta_2) - V_2^A\sin(4\theta_2))}{2(\sin(4\theta_1)\sin(2\theta_2) - \sin(2\theta_1)\sin(4\theta_2))}$ $N_1^- = \frac{N_1}{2} - \frac{N_3^+(\sin(4\theta_2)\sin(2\theta_3) - \sin(2\theta_2)\sin(4\theta_3)) + N_3^-(\sin(2\theta_2)\sin(4\theta_3) - \sin(4\theta_2)\sin(2\theta_3)) + N(V_4^A\sin(2\theta_2) - V_2^A\sin(4\theta_2))}{2(\sin(4\theta_1)\sin(2\theta_2) - \sin(2\theta_1)\sin(4\theta_2))}$ $N_2^+ = \frac{N_2}{2} - \frac{N_3^+(\sin(4\theta_1)\sin(2\theta_3) - \sin(2\theta_1)\sin(4\theta_3)) + N_3^-(\sin(2\theta_1)\sin(4\theta_3) - \sin(4\theta_1)\sin(2\theta_3)) + N(V_4^A\sin(2\theta_1) - V_2^A\sin(4\theta_1))}{2(\sin(4\theta_1)\sin(2\theta_2) - \sin(2\theta_1)\sin(4\theta_2))}$ $N_2^- = \frac{N_2}{2} + \frac{N_3^+(\sin(4\theta_1)\sin(2\theta_3) - \sin(2\theta_1)\sin(4\theta_3)) + N_3^-(\sin(2\theta_1)\sin(4\theta_3) - \sin(4\theta_1)\sin(2\theta_3)) + N(V_4^A\sin(2\theta_1) - V_2^A\sin(4\theta_1))}{2(\sin(4\theta_1)\sin(2\theta_2) - \sin(2\theta_1)\sin(4\theta_2))}$

For completeness, it is stated that when a FAD with $n > 3$ is received from step-1, the following was decided to be performed: an unbalanced split is calculated for three-ply counts, while the rest are rounded to be balanced. This allows the unbalancedness to be matched using three angles for a given $V_{2,4}^A$ target, while the other angles remain balanced and do not contribute to the value of $V_{2,4}^A$.

8.3. Examining Solutions: Insights and Requisite Post-processing

Similar to section 7.2, an example case will explain the design of unbalanced solutions. Here, the target LPs are $V_{1,2,3,4}^A = [0.4964, 0.2098, -0.2500, 0.3464]$ and $N = 20$. These LPs are calculated from a real Symmetric-Unbalanced FAD: $[-45_4, -15_3, +15_5, +30_6, +45_2]_S$. Initially, the FAD for $|\theta|$ will be obtained by performing FFTs on the $V_{1,3}$. Then, using the $V_{2,4}^A$ based closed-form relations, the ply counts of $|\theta|$ will be appropriately split between $+\theta$ and $-\theta$.

In this case, the $V_{1,3}^A = [0.4964, -0.2500]$. Among the set of 35 Exact signal patterns [3], the pattern made for the orientations $[15^\circ, 30^\circ, 45^\circ]$ provided the closest matching result for this $V_{1,3}^A$ combination. For brevity, the solution interpreted only from their frequency spectrum is presented and used:

Table 8.5: FAD obtained from L_1^A ($V_{1,3}^A = [0.4964, -0.2500]$ and $N = 20$)

Ply Orientations (°)	15	30	45
Ply Count	8.202222	5.39334	6.40444
Mismatch Error ε	0		

This solution shows that the ply counts present here are non-integer values. Hence, a rounding procedure analogous to the one presented in section 7.2 will be included in the following steps. Moving forward, it can be seen that this FAD has $n = 3$. Thus, N_i^+ and N_i^- of one orientation must be assumed

[2] If N_3 was an odd number, it could be split into $N_3 + 1$ different ways.

[3] 35 Exact Patterns derived for $[\Delta 15^\circ]$ can be referred from the Appendix (Table B.2).

to design an unbalanced FAD. Since the ply count of 30° was the lowest [4], their unbalanced split was decided to be assumed. Their ply count was hence labelled as N_3, and upon rounding them to the closest integer ($5.39334 \approx 5$), their unbalanced splits are obtained:

Table 8.6: Different combinations by which $N_3 = 5$ can be split in an unbalanced manner ($N_3^+ \neq N_3^-$)

$N_3 = 5$						
N_3^+	5	4	3	2	1	0
N_3^-	0	1	2	3	4	5

Consequently, the ply counts corresponding to 15° and 45° are labelled N_1 and N_2. Since N_3 can be split in six different ways, N_1 and N_2 can be split in 6 different ways. This was computed using the closed-form relations presented for $n = 3$ in Table 8.4. Among these six interpretations, the solution with the least mismatch with target $V_{2,4}^A$ was the following:

Table 8.7: Unbalanced (non-integer) FAD obtained from FFT and appropriate modification from a System of Linear Equations

Ply Orientations (°)	-45	-15	15	30	45
Ply Count	4.01923	2.60123	5.60099	5	2.38522
Mismatch Error ε	3E-3				

Thus, a FAD obtained from the FFT of $V_{1,3}^A$, has now been appropriately corrected to be unbalanced, using a system of linear equations. However, this solution contains non-integer ply counts, and due to the rounding of N_3 in the previous step, the FAD adds up to 19.6 and not 20. This complication with the total ply count not adding up to the desired number could have been avoided when the solution from Table 8.5 could have been rounded to an integer. However, the subsequent step with the System of Equations does not guarantee to provide an integer solution either, which would warrant another set of rounding. Hence, a rounding procedure was only implemented once to add enough plies to the system to ensure a desired value of N, and have integer ply counts. For this, the unbalanced FAD is first rounded down to the closest whole number:

Table 8.8: Analysing a non-integer Unbalanced FAD

Ply Count	$-45^\circ = 4.01923$	$-15^\circ = 2.60123$	$15^\circ = 5.60099$	$30^\circ = 5$	$45^\circ = 2.38522$	
Whole Number	4	2	5	5	2	Sum = 18
Fraction	0.01923	0.60123	0.60099	0	0.38522	

When rounded down to a whole number, the ply counts add up to 18. Thus, $20 - 18 = 2$ layers need to be added. To perform this, two out of the five-ply counts present in this FAD were planned to be rounded up. This can be performed in ten ways ($\because$, ${}^5C_2$). However, the best solution out of these ten interpretations needs to be chosen considering all the target LPs $V_{1,2,3,4}^A$. Hence, the summation within the distance measure (Equation 7.4) shall have an upper limit of $d = 4$. By computing their LP mismatch as such, the best interpretation was observed to be the one where the ply counts of -15° and $+30^\circ$ are rounded up. Thus, they were chosen as the closest-matching solution:

Table 8.9: Unbalanced FAD designed for $V_{1,2,3,4}^A = [0.4964, 0.2098, -0.2500, 0.3464]$ and $N = 20$

Ply Orientations (°)	-45	-15	15	30	45
Ply Count	4	3	5	6	2
Mismatch Error ε	0				

[4] A small number has a small amount of subset-sum combinations.

8.4. Overview of the Fibre-Angle Distribution Design in MATLAB

Currently, steps-1 and 2 of the proposed SS design framework have been discussed. Using the In-Plane LPs $V^A_{1,2,3,4}$, an N-layered balanced or unbalanced FAD can be designed. The design of both these outputs initially involved the use of the FFTs. However, different steps were performed to interpret a balanced or unbalanced solution from the FFT. Thus, steps-1 and 2 were implemented in a particular sequence in MATLAB, as shown in a flowchart (presented on the following page):

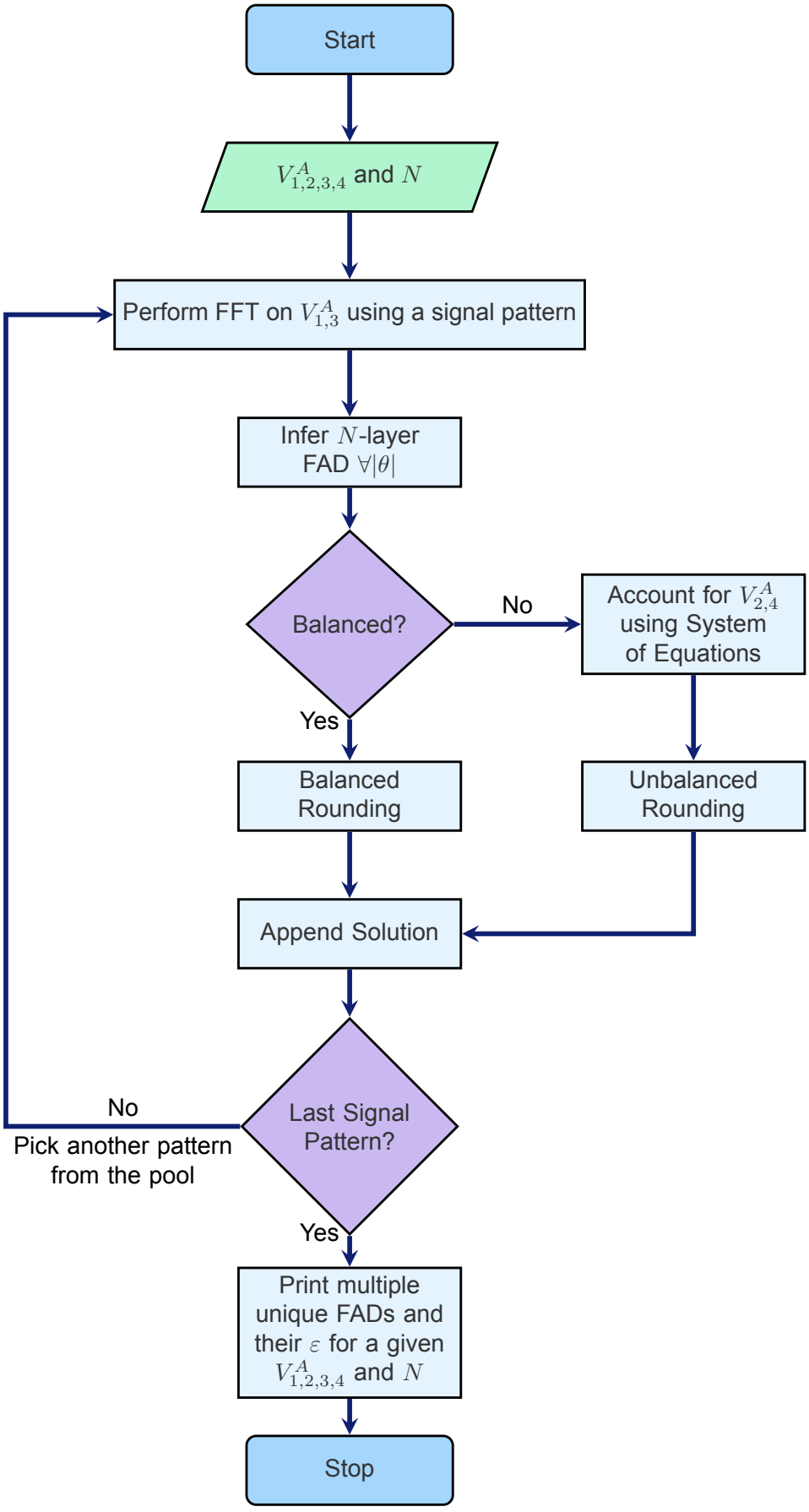

Figure 8.1: MATLAB implementation of the FAD design (Steps-1 and 2 of the Hierarchical Design Framework)

The MATLAB implementation accepts input parameters, namely the In-Plane LPs ($V^A_{1,2,3,4}$) and the number of symmetric layers N. Using a given signal pattern from the pool, the code generates samples of the L^A_1 signal (contains $V^A_{1,3}$). A FFT is performed on these signal samples to obtain the frequency spectrum of L^A_1. From this spectrum, a Symmetric FAD with N layers ($\forall|\theta|$), is inferred.

If the intended solution is to be balanced, the 'balanced rounding' procedure is performed. Here, the FAD obtained from the FFT is modified such that the ply counts of all off-axis $|\theta|$ are equally distributed between $+\theta$ and $-\theta$. Then, this distribution is rounded to ensure that all ply counts are integers and the off-axis orientations have even-numbered ply counts.

In cases where the solution is meant to be unbalanced, the contribution of $V^A_{2,4}$ has to be considered. Here, the FAD obtained from the FFT is modified such that the ply counts of all off-axis $|\theta|$ are unequally distributed between $+\theta$ and $-\theta$. This unequal distribution is determined using a System of Equations with the FAD from FFT and the $V^A_{2,4}$. Subsequently, the 'unbalanced rounding' procedure ensures all ply counts in the FAD to be integers.

Following the post-processing of solutions, for balanced or unbalanced requirements, the resulting solution is saved to a list. If more signal patterns exist in the pool of available patterns, they will be used to generate more solutions. This process is repeated until a solution is generated using all available patterns. Finally, the tool prints all the saved solutions.

This FAD design implementation was named 'LP2FAD', and it has been made available open-source in a GitHub repository at `https://github.com/rakshith-m1505/LP2FAD`.

9

In-Plane and Out-of-Plane Stiffness Design of Laminates

"You don't have to build everything you want today, just lay a brick"

James Clear

This thesis proposes using a hierarchical procedure to convert LPs into SS. Initially, a FAD was designed using the In-Plane LPs. As highlighted in the previous two chapters, the FFT primarily aided this design by providing the In-Plane Sum of weights (of $V^A_{1,3}$). This concluded the In-Plane Stiffness design of a laminate. As a next step, the SS must be defined for the Out-of-Plane Stiffness design of a laminate.

Step-3: Using two Sine-Based In-Plane LPs ($V^A_{2,4}$), determine sign $\forall$ plies in the N-layer FAD

To perform step-3 of this design framework, the known quantity of plies in the FADs must be arranged in a particular order within a laminate to match a set of Out-of-Plane LPs $V^D_{1,2,3,4}$. Analogous to the initial step, this process was ought to be aided by the Out-of-Plane Sum of weights. However, reliably obtaining them using FFTs was proven difficult. Hence, this chapter limits itself to explaining how step-3 was initially planned to be performed (in section 9.1) and outline difficulties faced in their implementation (in section 9.2). Although not implemented in this thesis due to time constraints, an alternate method to perform step-3 is recommended in section 9.3 for future studies to attempt converting a FAD into SS.

9.1. Designing Stacking Sequence using Out-of-Plane Sum of Weights

As seen from chapters 7 and 8, the In-Plane Sum of weights correspond to the number of plies belonging to every laminate orientation. However, the Out-of-Plane Sum of Weights were not perceivable practically. The previously used example of a symmetric SS (in Table 6.7) is now revisited to understand this:

Table 9.1: Out-of-Plane Sum of Weights for the SS: $[-45, 45, 90, 90, 0, 0]_S$

		FFT Output of $L^D_{1,2}$	
		1	**2**
D	**Out-of-Plane**	$[0_8, 45_{152}, 90_{56}]$	$[-45_{91}, +45_{61}]$

The above-mentioned Sum of Weights (Outputs) can be obtained if FFT is performed on the $V^D_{1,2,3,4}$ LPs using the signals $L^D_{1,2}$. As discussed in chapter 6, the Out-of-Plane Sum of weights contains aggregate information corresponding to multiple k values. Hence, a post-processing step is needed to break this Sum into subset values corresponding to the cubic weights of different layers. Such a post-processing step for a known FAD and Out-of-Plane weights is now explained with the same example:

Table 9.2: Relating subsets of the Out-of-Plane Sum of Weights to a laminate position (for the SS: $[-45, 45, 90, 90, 0, 0]_S$)

Position (k)	1	2	3	4	5	6
Cubic Weight	91	61	37	19	7	1

Orientations Present $(^\circ)$	-45	45	0		90	
No. of Plies	1	1	2		2	
Sum of Weights	91	61	8		56	
Subset Sum(s) of the Weight	91	61	7	1	37	19
k**'s corresponding to the weights**	1	2	5	6	3	4

The cubic weights corresponding to every position k in an SS can be calculated beforehand. Upon this step, the number of plies and the Out-of-Plane Weights corresponding to every unique orientation are segregated. Since there is only one ply of -45° and $+45^\circ$, their Out-of-Plane weight must only be associated with one k value each. Referring to the pre-calculated cubic weights, these k's can be identified as 1 and 2, respectively. However, the same is not valid for the 0° and 90° as they contain two plies each. Hence, their Sum of weight must be broken down such that they correspond to the cubic weight of two k's. As such, their k's can also be identified. To perform these subset-sum divisions, a branch and bound method can be used to iteratively assign k's to every ply in a FAD, such that their respective cubic weights add up to the desired Out-of-Plane weight. Nonetheless, the Out-of-Plane weights need to be known before discussing the working of such SS design procedures. Thus, the hierarchical design framework will now focus on performing FFTs on the $V_{1,3}^D$ LPs (in the form of L_1^D).

9.2. Difficulties obtaining Out of Plane Sum of Weights

In chapter 7, multiple signal patterns were used to describe different interpretations of the signal L_1^A. However, it is known that harmonic signals made with the same set of frequencies tend to behave similarly. Thus, a cosine signal pattern of L_1^A corresponding to a particular set of ply orientations must also be compatible with L_1^D corresponding to the same set of orientations. Hence, the previously found signal patterns can be reused by replacing $V_{1,3}^A$ with $V_{1,3}^D$. For the SS example used above, the orientations present are $[0^\circ, 45^\circ, 90^\circ]$, and their $V_{1,3}^D = [-0.2222, -0.4074]$. So, by using the signal pattern of $[\Delta 45^\circ]$, samples of L_1^D can be described. Upon performing an FFT on these samples, the following frequency spectrum was obtained:

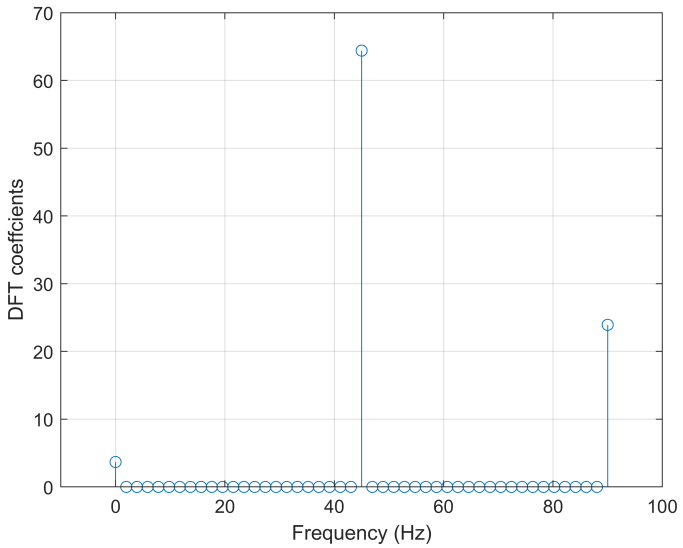

Figure 9.1: Frequency spectrum of L_1^D ($V_{1,3}^A = [-0.2222, -0.4074]$)

Similar to the FFT of the $V_{1,3}^A$, only the positive and real parts of the DFT coefficients are plotted for all

the frequencies. To relate this spectrum to a 12-layer symmetric SS, they had planned to be normalised with the quantity $0.5 * ((2N)^3/4)$, or, $\Rightarrow N^3$: This was based on the normalising term $N^3/4$ from the V^D LPs formulation (in Equation 2.2); the N within them had to be doubled to represent the total number of layers (from the symmetric layers), and the overall term is halved (with 0.5) as we are interested in the sum of weights only belonging to the symmetric half of the SS.

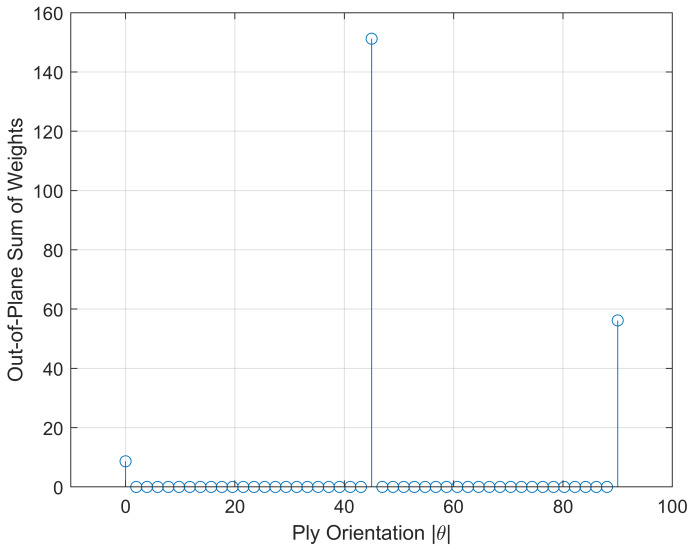

Figure 9.2: Normalised Frequency spectrum of L_1^D ($V_{1,3}^D = [-0.2222, -0.4074]$ for 6 symmetric layers)

As such, the Out-of-Plane weights for $|\theta|$ were obtained upon normalising the frequency spectrum.

Table 9.3: Out-of-Plane Sum of weights obtained from L_1^D ($V_{1,3}^D = [-0.2222, -0.4074]$)

Ply Orientation (°)	0	45	90
Sum of Weights	8.64102	151.19230	56.16666

Here, it can be observed that the Sum of Weight values are non-integers. This is similar to the situation encountered with the FAD. Over there, the infeasibility of this solution was repaired by rounding the ply counts to an integer value. However, the same rule cannot apply to the Out-of-Plane weights as their formulation is different:

$$\sum_{k=1}^{N} \left(\frac{N}{2} - k + 1\right)^3 - \left(\frac{N}{2} - k\right)^3$$

When $N = 1$, the value of this expression becomes 0.25. As such, it can be inferred that the Out-of-Plane (cubic) Sum of Weights is a multiple of 0.25. Nevertheless, rounding a given distribution of Out-of-Plane weights to the closest 0.25 need not guarantee that they correspond with an achievable value. For example, even when the distribution from Table 9.4 is rounded to the nearest multiples of 0.25 such that they add up to form the same value, they will still be far from the actual Sum of weights shown in Table 9.1.

Table 9.4: Out-of-Plane Sum of weights of the SS $[-45, 45, 90, 90, 0, 0]_S$, compared to the ones obtained from FFT of L_1^D

Ply Orientation (°)	0	45	90
Sum of Weights (actual)	8	152	56
Sum of Weights (from FFT)	8.64102	151.19230	56.16666

As a result, the Out-of-Plane weights could not be reliably obtained through FFTs, rendering them unsuitable for SS design.

9.3. Proposed Alternative to Convert Fibre Angle Distributions into a Stacking Sequence

As mentioned in the previous section, the FFT solutions from In-Plane LPs could be repaired using rounding procedures. This was because the FAD always needs to have an integer ply count. However, such an analogous rule could not be set up to repair the out-of-plane weights from FFT. Hence, there is no assurance that a distribution of out-of-plane weights obtained from FFT is practically realisable. Therefore, a more fool-proof approach is recommended for future studies regarding the conversion of FAD to SS. The literature review showed that a layerwise optimisation approach was implemented in a decision tree paradigm to convert LPs to SS. They performed well with increasing N, but their solution accuracy did fall behind with an increasing number of allowable θ's [81]. However, upon using a hierarchical SS design approach, the quantity of plies in each ply orientation is known through the FAD. Hence, decision trees can be better used to solve a combinatorial problem of arranging a FAD to match a given set of Out-of-Plane LPs. The hierarchical design procedure for an SS would be completed by accomplishing this step.

Part III

Validation and Results

10

Results and Discussion

"Nothing exists until it is measured."

Niels Bohr

Through this thesis, a novel FFT-based method was implemented to design laminates FAD efficiently. A series of benchmarking exercises were conducted to validate their performance and compare them with other tools in the literature. Initially, the implementation needs to be set up to design FADs with $[\Delta 15^\circ]$. The mathematically derived Exact Patterns can instantly be generated for any given $[\Delta\theta]$. However, the same cannot be said for the Approximate Patterns, as infinitely many may exist. Hence, the process by which they were iteratively found is explained in section 10.1. After setting up the pool of signal patterns, the FFT-based method's capability to design Symmetric-Balanced and Unbalanced FADs was thoroughly tested in section 10.2 and section 10.3, respectively. Upon obtaining these results, there was enough information to assess the benefits of handling the Inverse Problem using a Hierarchical approach and the benefits of using $[\Delta 15^\circ]$ over $[\Delta 45^\circ]$. The learnings from this discussion can be found in section 10.4. The research questions were answered by reflecting on these discussions and the findings made during this thesis. All findings in this thesis are the outcome of computations on a computer equipped with a standard Intel® Core™ i7 processor (2.6 GHz) and 8GB of RAM, specifications commonly encountered in office laptops.

10.1. Optimising set of Approximate Patterns to Design with $[\Delta 15^\circ]$

As seen in chapter 7, the signal representation of $V_{1,3}^A$ LPs offers many symmetries and patterns, which can be used to design FADs ($\forall\ |\theta|$). These patterns can be mathematically derived using the Exact Patterns approach as shown here (restating Equation 7.2 and 7.3):

$$L_1^A(T) = a_T + b_T V_1^A + c_T V_3^A$$

$$\begin{bmatrix} a_T \\ b_T \\ c_T \end{bmatrix} = \begin{bmatrix} 1 & \cos(2\theta_1) & \cos(4\theta_1) \\ 1 & \cos(2\theta_2) & \cos(4\theta_2) \\ 1 & \cos(2\theta_3) & \cos(4\theta_3) \end{bmatrix}^{-1} \begin{bmatrix} \cos(2\theta_1 T) \\ \cos(2\theta_2 T) \\ \cos(2\theta_3 T) \end{bmatrix}$$

Time-domain samples of L_1^A can be obtained for any given T and a set of three $|\theta|$'s. Since $[\Delta 15^\circ]$ contains seven different $|\theta|$'s, a set of 35 Exact Signal patterns($\cdot C_3$) can be mathematically derived. However, for the visually derived approximate patterns, infinitely many of them may exist. So, they were planned to be iteratively made and added to the FFT tool, as explained here:

1. When a Symmetric FAD of N layers cannot be designed to closely match a given $V_{1,3}^A$ target, a new approximate pattern belonging to that region of the LP space is strategically added into the pool. Hence, the implementation's capability to provide a closely matching solution throughout the feasible $V_{1,3}^A$ space was progressively improved.
2. Over time, many approximate patterns were removed from the pool, citing redundancy. This was judged based on the 'design domain' of a signal pattern: the regions of LP space where

an approximate signal pattern could provide accurate solutions. So, by regularly monitoring the design domains, redundant patterns were consistently recognised and removed. Moreover, it is time-efficient for the implementation to have a pool of signal patterns that is as small as possible.

One must know how the FFT-based method performs throughout the design space to enable such an iterative refinement. Hence, with every added approximate pattern, the FFT-based method was thoroughly tested with 2000+ feasible combinations of $V^A_{1,3}$. These LP combinations were obtained by uniformly sampling the feasible design space as shown here:

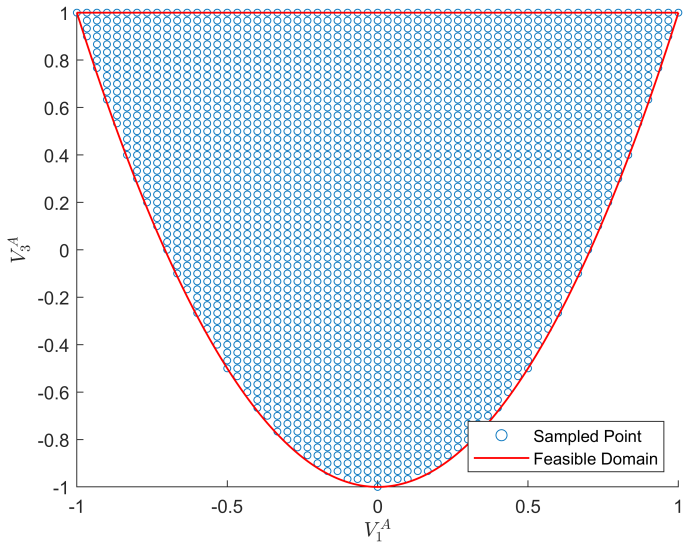

Figure 10.1: Uniformly Sampled Feasible $V^A_{1,3}$ Space

These targets were collectively known as a 2D-benchmark dataset as they contained several two dimensional targets to test the FFT-based method. This dataset can be accessed from the GitHub Repository of this thesis. As seen in chapter 7, a mismatch error can be incurred in the conversion. Thus, by plotting the ε associated with all these target points, the FAD design performance can be visualised across the LP space. Such plots will be addressed as 'Error Profiles' from here onwards. In chapter 7, a non-uniform Approximate Pattern was found (in Table 7.8). When this is the only pattern present in the pool, the error profile of the FFT-based method for $N = 20$ and 100 (or, $N = [20, 100]$) looks as follows:

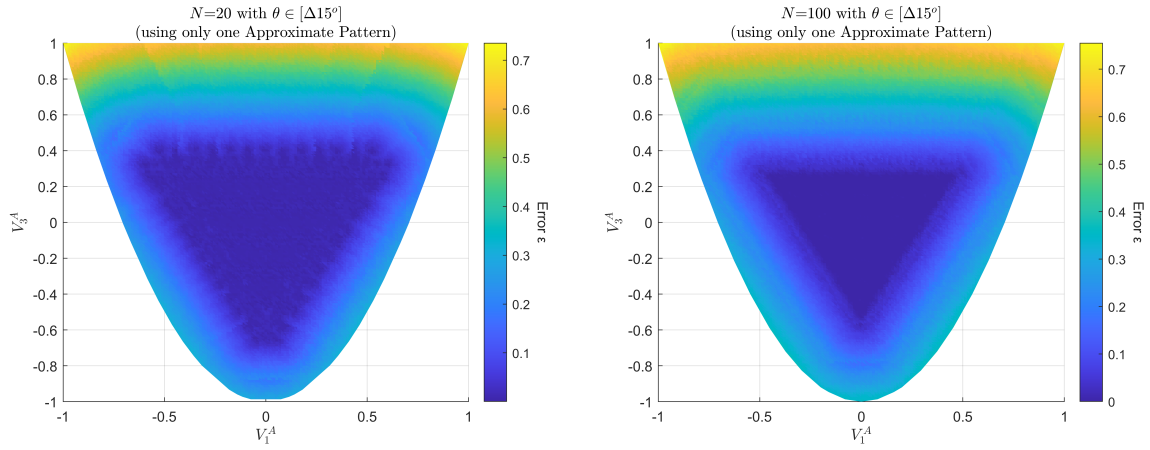

Figure 10.2: Error Profile of FFT-based method using only one Approximate Pattern (from Table 7.8)

For clarity, the approximate pattern used to make this error profile (in Table 7.8) is restated here:

Table 10.1: Non-Uniform Approximate Signal Pattern corresponding to the $V^A_{1,3} = [0.17, -0.1]$; Unsampled timestamps are marked with an 'X'

$T=0$	$T=1$	$T=2$	$T=3$	$T=4$	$T=5$	$T=6$
1	V^A_1	V^A_3	X	$-V^A_3$	$-V^A_1$	X

In Figure 10.2, the FADs obtained for each $V^A_{1,3}$ combination is rounded such that all $|\theta|$ have integer ply counts, and the balancing constraints are not imposed. When ε is less than 0.1[1], a solution is said to match the given target closely. As such, a closely matching solution can only be found within a visible triangular-shaped domain, outside which mismatch errors are as high as 0.7. Thus, these error profiles can be considered the design domain of the above-mentioned approximate pattern: indicating the region where the pattern provides a closely-matching solution. However, the triangular design domain appears to be reduced in size for $N = 100$ compared to $N = 20$. This is because, while making an approximate pattern, the contribution of certain $|\theta|$(s) are involuntarily fixed, while others vary in terms of the three known quantities (unity, and $V^A_{1,3}$). These fixed ply counts need not help match any given $V^A_{1,3}$; there will be cases where they can cause LP mismatch. With smaller values of N, the rounding procedures decrease the value of these fixed ply counts to minimise mismatch. However, this effect is less pronounced with increasing values of N, as only the last digit of the ply counts are rounded up/down. Hence, with increasing N, the design domain of a given approximate pattern slowly contracts due to an increase in mismatch error.

Nevertheless, new approximate patterns are needed to provide closely matching solutions outside the triangular domain. The FADs belonging to the regions outside this domain were designed with [$\Delta 15°$] using an open-source GA (OptiBLESS [90]). By plotting their cosine signals and identifying more approximate patterns, the triangular design domain of closely matching solutions was incrementally increased to span more of the $V^A_{1,3}$ space. As such, 23 approximate patterns were totally made and added to the tool. When using multiple signal patterns[2], FFTs are performed with all of them to infer multiple unique FADs. Among them, the solution with the least ε is chosen and plotted in the error profile, as shown here for $N = [20, 100]$:

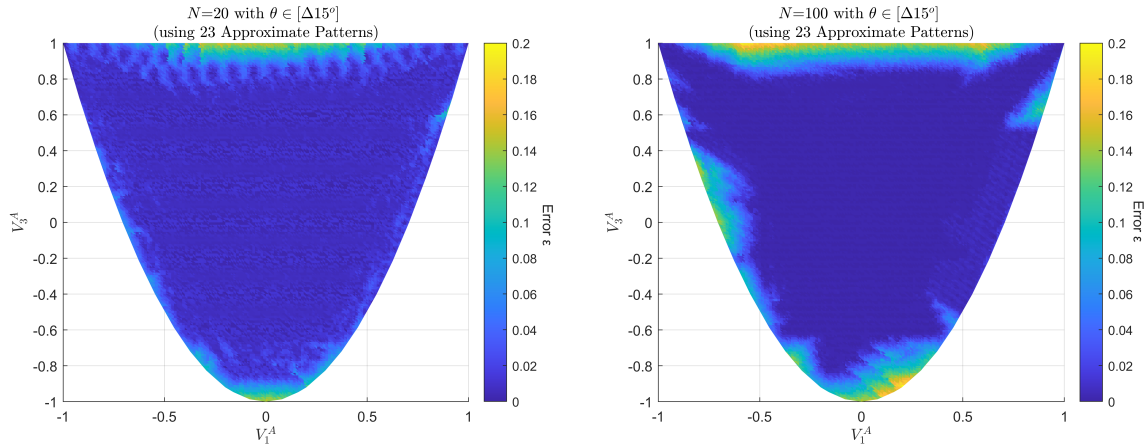

Figure 10.3: Error Profile of FFT-based Method with 23 Approximate Patterns

Over here, especially with increasing N, poorly performing regions can still be identified close to the periphery of the feasible domain. However, this was understood to happen because more than three-ply orientations are not necessarily needed in a FAD to match the LP values of those regions. As seen from Miki's diagram in the literature review (Figure 3.1), the LP values along the feasible design domains' periphery can be matched with only one $|\theta|$ value. Consequently, it is understood that regions closer to the periphery can be matched with fewer numbers of $|\theta|$'s. Hence, 23 approximate patterns[3] were

[1] The value of 0.1 was conservatively chosen based on the permissible LP mismatch values inferred from Macquart et al.'s aeroelastic design study of a blended composite wingbox [91].

[2] For the interested reader, the design domain of all 23 approximate patterns are presented in the Appendix (in section B.5).

[3] The complete list of these Approximate Patterns can be referred from the Appendix (in section B.4).

deemed sufficient for the In-Plane Stiffness design of FADs with $[\Delta 15°]$. Regardless, the Exact Patterns are known to design FAD with at most three $|\theta|$'s. So, by performing FFTs with the 23 Approximate Patterns and 35 exact patterns, the following error profile was generated:

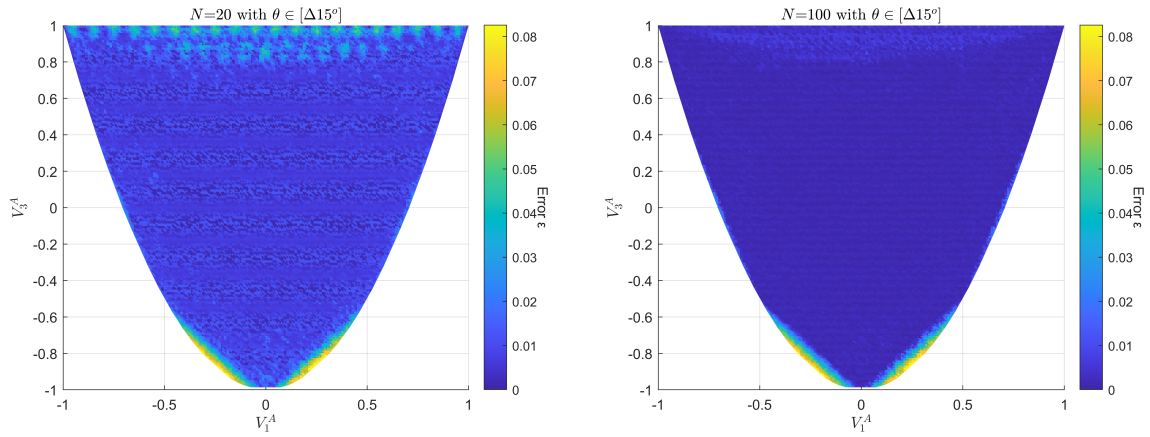

Figure 10.4: Error Profile of FFT-based Method with 23 Approximate Patterns and 35 Exact Patterns

From this point onwards, unless specified otherwise, error profiles will be generated using all known approximate and exact patterns. Consequently, the FFT-based method is now capable of converting a $V_{1,3}^A$ into multiple unique FADs (with $[\Delta 15°]$). Even with 58 signal patterns, the time taken to convert a $V_{1,3}^A$ combination into a FAD (not yet balanced) was always within a second ($\approx 0.3s$), irrespective of N.

10.2. Design Performance for Symmetric-Balanced Fibre Angle Distributions

Using the pool of 58 signal patterns for $[\Delta 15°]$, and the procedure described in chapter 7, any feasible combination of $V_{1,3}^A$ can be converted into a closely-matching N-layered symmetric-balanced FAD. Hence, the 2D-benchmark (in Figure 10.1) was used to validate this implementation. This was done by providing the targets from this dataset for increasing N values. Since a distribution of 2000+ ε points is obtained for every N, they were planned to be presented using box plots. Plots such as these are called the 'Error Distributions' for convenience.

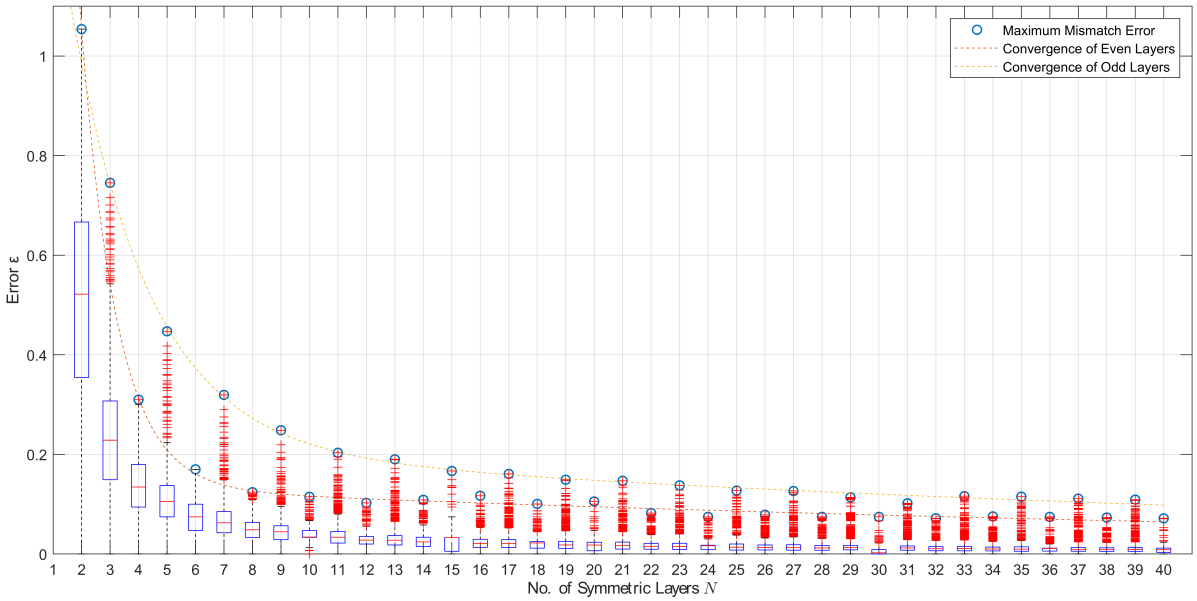

Figure 10.5: Error Distribution of the FFT-based method for the Design of Symmetric-Balanced FADs

As expected, the maximum observed ε's are outliers in a distribution[4]. Moreover, the median and overall range of ε's exponentially decreases with increasing layers in a FAD. However, when only focusing on the maximum ε of each distribution, it was seen to decrease in a fluctuating manner. Then, it was realised that ε for odd and even-numbered FADs exponentially decreases with an offset. To understand why, the error profiles for three consecutive N ($5, 6$ and 7) was observed:

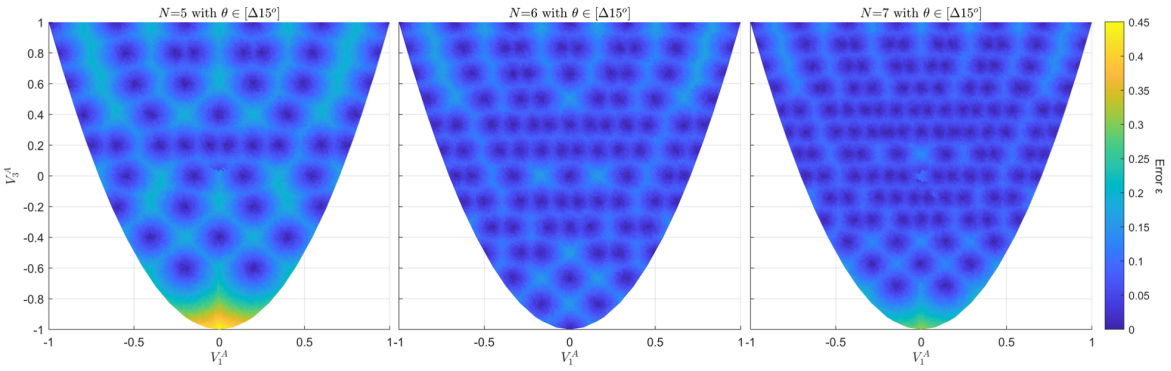

Figure 10.6: Error Profile for Symmetric-Balanced FADs with $N = 5$ (left), $N = 6$ (middle), and $N = 7$ (right)

With increasing N, more feasible $V^A_{1,3}$ can be matched using a Symmetric-Balanced FAD consisting $[\Delta 15°]$. However, for the odd-numbered $N = 5$ and 7, it can be observed that the bottom portion of the $V^A_{1,3}$ space can never be matched as well as the cases in the even-numbered $N = 6$. From a visual perspective, it is clear that $V^A_{1,3} = [0, -1]$ can be matched using a FAD only made of 45° plies[5]. However, when a FAD is designed with odd-numbered layers, it is impossible for off-axis $|\theta|$'s to exist as balanced pairs of $+\theta$ and $-\theta$. Due to this reason, the balanced rounding procedure adds a 0° or 90° ply to the FAD. This causes the offset in performance between the Symmetric-Balanced FADs of odd and even-numbered layers. More specifically, the maximum ε of even-numbered Symmetric-Balanced FADs converged faster than the odd-layered ones. Nonetheless, the rounding procedure ensures that the closest possible solution is provided without violating the Symmetry-Balanced rules. The time taken to convert any given $V^A_{1,3}$ combination into an N-layer Symmetric-Balanced FAD was still performed within a second. For completeness, these values [6] are tabulated as shown here:

Table 10.2: Time-efficiency of the FFT-based method to design Symmetric-Balanced FADs using $[\Delta 45°]$ and $[\Delta 15°]$ orientations

Average Time Taken (s)	
Conventional Orientations $[\Delta 45°]$	**Non-Conventional Orientations** $[\Delta 15°]$
0.06	0.3011

The conversion using $[\Delta 45°]$ is faster as only one signal pattern is sufficient to describe them. However, only within $0.3s$ the FFT-based method can use different signal patterns and generate multiple unique FADs with $[\Delta 15°]$. This capability can be demonstrated for the first example case used in chapter 7 ($V_{1,3} = [0.5232, 0.1500]$ and $N = 20$). These targets were generated from a real Symmetric-Balanced FAD ($[0_4,\ +15_3, -15_3, +30_3, -30_3, +45, -45, +75, -75]_S$), and they were exactly matched by the only approximate pattern present in the implementation back then. Now that more patterns are present, multiple unique solutions can be generated. Five closely matching solutions among them are tabulated as follows:

[4] High values of ε's are inevitable with very low N as many regions of the mathematically feasible $V^A_{1,3}$ space are practically unattainable with finite N. Such regions can be identified for a given N, using the relations described by Setoodeh [19].

[5] In the literature review, the Miki's diagram (Figure 3.1) showed that the periphery of the LP design domain can be matched only using one ply orientation. In this case, that $\theta = 45^\circ$.

[6] These average computation times were documented while testing the implementation with the 2D benchmark.

Table 10.3: Five Closely-matching Symmetric-Balanced FADs for the targets $V^A_{1,3} = [0.5232, 0.1500]$ and $N = 20$

Symmetric-Balanced FAD	Mismatch Error ε
$[-75, -45, -30_3, -15_3, 0_4, +15_3, +30_3, +45, 75]_S$	0
$[-30_4, -15_5, +15_5, +30_4, 90_2]_S$	9E-3
$[-60_2, -45_1, -15_7, +15_7, +45_1, +60_2]_S$	1E-2
$[-45_1, -30_3, -15_4, 0_2, +15_4, +30_3, +45_1]_S$	2E-2
$[-60_2, -45_2, -30_2, -15_1, 0_8, +15_1, +30_2, +45_1, +60_2]_S$	3E-2

In this way, the FFT-based method provides a designer with a selection of FADs that closely match the same LP combination. Offering a range of choices becomes particularly advantageous when attempting to satisfy particular design guidelines, possibly providing a laminate that is easier to certify, and especially when designing for variable stiffness (VS)[7].

10.3. Design Performance for Unbalanced Fibre Angle Distributions

Using a pool of 58 signal patterns for $[\Delta 15°]$, and the procedure described in chapter 8, any feasible combination of $V^A_{1,2,3,4}$ can be converted into a N-layered Symmetric-unbalanced FAD. To validate this implementation, four dimensional targets of $V^A_{1,2,3,4}$ were required. Hence, a test dataset from the literature [81] and a more thorough custom-made benchmark was used to evaluate performance.

10.3.1. Validation with Benchmark from Literature

The inverse problem has been handled using decision tree-based tools in literature [75, 81, 92]. Among them, one of the most successful implementations has been LAYLA (LAY-ups for LAminates) by Fedon et al.[81]. To validate the performance of LAYLA, they created a test dataset with 200 different SS. They were Symmetric-Balanced or Unbalanced laminates with $N = 100$ and made of the conventional $[\Delta 45^\circ]$ orientations. As such, LPs in this dataset are practically realisable at $N = 100$. Moreover, these laminates were manually generated to have diverse LPs, as seen in the following diagrams:

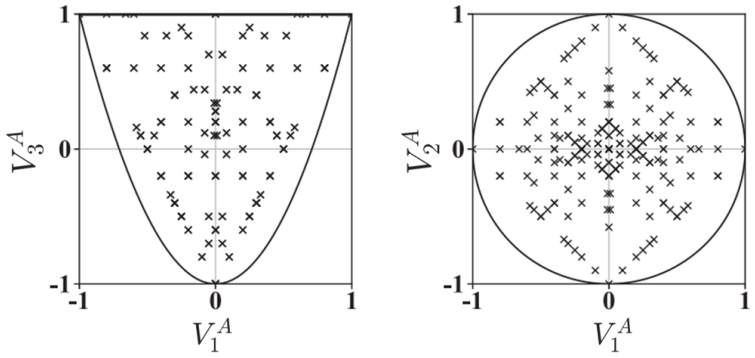

Figure 10.7: Bristol Dataset: Diverse set of LPs that belong to 200 different SS (Figure Modified from Fedon et al.[81])

This dataset, owing to its origin from the Bristol Composite Institute, is conveniently referred to as the 'Bristol Dataset'. The published results of LAYLA indicated that they need $\approx 3.4s$ for designing a FAD only with $V^A_{1,2,3,4}$ targets [81]. Hence, the Bristol dataset was used to test the FFT-based method and OptiBLESS[8], such that their solution accuracy and time efficiency can be compared with LAYLA.

Table 10.4: FAD Design Performance for the Bristol Dataset

	FFT-based Method	**LAYLA** [81]	**OptiBLESS**
Time taken (s)	0.28	3.4	89.11
Mismatch Error ε	0	0	0

[7]While patching together different laminates using blending or by generating steered fibre paths, it is possible to incur infeasibilities like butted edge formations or steering radius limit violation, respectively. However, having multiple laminate choices for the same LP combination allows for reducing these infeasibilities by exploring alternate solutions.

[8]The parameters used to operate OptiBLESS can be referred from the Appendix (in section B.2).

The formulations used to represent LP mismatch vary for all these techniques, but they were all capable of designing perfectly matching FADs for all 200 targets in the dataset. This was attributed to the fact that the LP values in this dataset were practically realisable when $N = 100$. Nevertheless, it must be highlighted that the FFT-based method can be faster than other solutions and provide multiple unique solutions simultaneously.

10.3.2. Validation with Custom Benchmark

The LP targets from the Bristol dataset are sourced from real SS made of conventional orientations ($\theta \in [0, \pm 45, 90]$). However, this set has only one off-axis orientation ($45°$). As such, the Bristol Dataset fails to test a tool's capability to design unbalanced FADs with multiple off-axis orientations. Hence, a new dataset with 4-dimensional $V^A_{1,2,3,4}$ targets was desired.

While creating such a benchmark dataset, obtaining a diverse set of targets is essential, as the obtained results can better represent the robustness of a tool. However, generating a diverse set of FADs with $[\Delta 15°]$, or uniformly sampling $V^A_{1,2,3,4}$ space, constitutes significant computational effort. Hence, a method involving quasi-random sampling[9] was used to generate this 4D benchmark. They are explained as follows:

1. Describe a 4D hypercube of edge length 1, such that their coordinate values span from $[0, 1]$.
2. Obtain a desired number of 4D coordinates using the Sobol Sampling Technique.
3. Re-scale the 4D coordinates such that they span from $[0, 1]$ to $[-1, 1]$.
4. Remove infeasible $V^A_{1,2,3,4}$ combinations using the Fukunaga Constraint[51] that describes the feasible region of all In-Plane LPs.

$$2\left(1+V_3^A\right)\left(V_2^A\right)^2 - 4V_1^A V_2^A V_4^A + \left(V_4^A\right)^2 - \left(V_3^A - 2\left(V_1^A\right)^2 + 1\right)\left(1 - V_3^A\right) \leq 0$$

Since certain (infeasible) points are removed from the quasi-random samples, their diversity is indeed affected. However, given the nature of the LPs, this exercise was considered appropriate to obtain a set of mathematically feasible $V^A_{1,2,3,4}$ combinations[10]. Upon generating over 200 samples, the design space projections of the 4D benchmark looked as such when compared to the Bristol dataset. This benchmark dataset can be accessed from the GitHub Repository of this thesis.

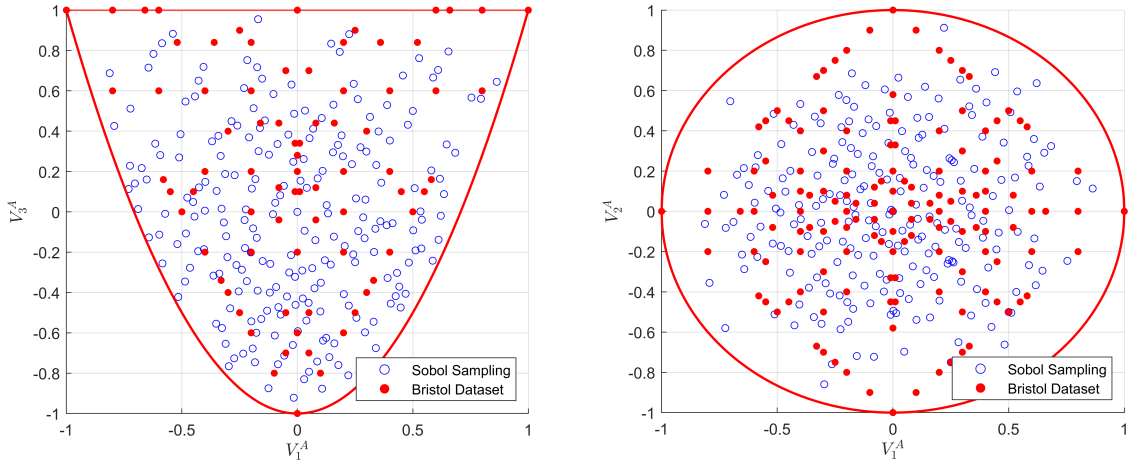

Figure 10.8: Comparing the Custom Benchmark(4D) generated with Sobol Sampling to the Bristol Dataset

Using this 4D benchmark, the design implementation for Unbalanced FAD was tested. For every N with increasing steps of five, an Error Distribution plot was made:

[9] Quasi-Random Sampling: Methods to describe a sequence of numbers with low discrepancy between them.

[10] For the interested reader, the comparison between the samples obtained from Sobol Sampling and Latin Hypercube Sampling is illustrated in the Appendix (in section B.6).

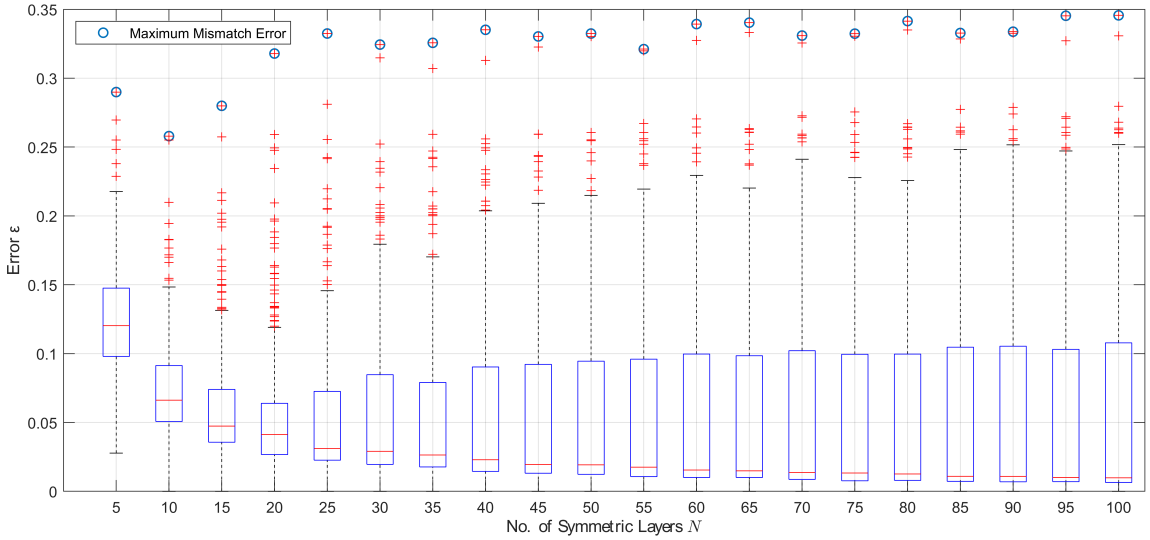

Figure 10.9: Error Distribution of the FFT-based method for the Design of Symmetric-Unbalanced FADs

With the distributions, it is clear that the maximum ε's for all the cases are outliers. Furthermore, the median ε exponentially decreases with increasing N. Thus, the capability of this implementation to design an Unbalanced FAD was validated. Nonetheless, the maximum seems to increase with increasing N, seemingly converging around 0.34. To understand why, the FAD corresponding to the worst-matching case ($V_{1,2,3,4} = [0.5117, -0.5039, -0.1914, -0.9335]$, and $N = 100$) was analysed. Using OptiBLESS, it was understood that a closely matching solution does not exist for this case while using $[\Delta 15°]$. Hence, the FAD was also attempted to be designed using $[\Delta 5°]$, and all results were tabulated and compared:

Table 10.5: Results for the worst performing case in 4D Benchmark ($V_{1,2,3,4} = [0.5117, -0.5039, -0.1914, -0.9335]$, and $N = 100$), using the FFT-based method and OptiBLESS

Approach	Fibre Angle Distribution	Mismatch Error ε	Time Taken (s)
FFT-based method with $[\Delta 15°]$	$[-75_2, -30_{69}, -15_6, +60_{20}, +75_3]$	0.34351	0.1991
OptiBLESS with $[\Delta 15°]$	$[-30_{53}, -15_{32}, +60_{11}, +75_4]$	0.10352	177.06
OptiBLESS with $[\Delta 5°]$	$[-30_{13}, -25_{47}, -20_{24}, -15_2, +50_2, +55_6, +60_5, +65_1]$	0.0098212	261.25

From these solutions, it can be understood that the outlier cases exist due to the FFT-based method's inability to design an Unbalanced FAD with more than three off-axis ply orientations and use $[\Delta 5°]$. In cases like this, a computationally expensive GA can help obtain closely matching solutions. Nonetheless, the time efficiency of the FFT-based method is still commendable. For completeness, these values[11] are tabulated as follows

Table 10.6: Time-efficiency of the FFT-based method to design Symmetric-Unbalanced FADs using $[\Delta 45°]$ and $[\Delta 15°]$ orientations

Average Time Taken (s)	
Conventional Orientations $[\Delta 45°]$	**Non-Conventional Orientations** $[\Delta 15°]$
0.05	0.2080

Even though more number of LPs are handled in this part of the implementation, the average time to design FADs is faster than in the Symmetric-Balanced case. This was attributed to the fact that the balanced rounding procedure is more exhaustive than the unbalanced rounding.

10.4. Discussion

The first stage of this Hierarchical design framework pertains to the design of FADs, which is powered by the FFT-based method. As their effectiveness became evident from the results, their time complexity,

[11] These average computation times were documented while testing the implementation with the 4D benchmark.

handling the Inverse Problem in this manner, and the benefits of using non-conventional orientations are discussed in more detail.

10.4.1. Time efficiency of the FFT-based method

In the previous sections, the FFT-based method was thoroughly tested using the 2D and 4D benchmarks for the design of Symmetric-Balanced and Symmetric-Unbalanced FADs, respectively. During these tests, the time efficiency was documented for increasing N, and it was understood that, on average, LPs could be converted into a FAD within a second ($\approx 0.3s$). For completeness, these time efficiency values are now plotted and shown for increasing N:

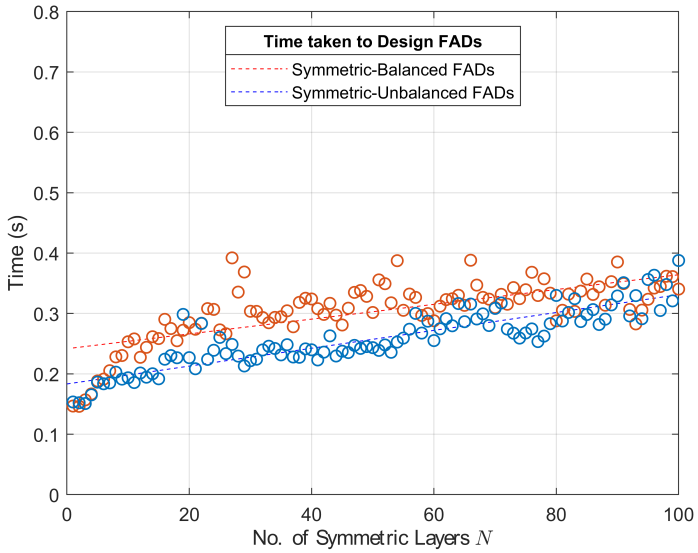

Figure 10.10: Time taken by the FFT-based method to design Symmetric-Balanced and Symmetric-Unbalanced FADs

As N increases, the time taken by the FFT-based method to design FADs seems to increase linearly, implying they have a linear time complexity ($O(N)$). Although, the computational time increases with N by a practically insignificant amount. This can be explained by the fact that the number of FFT evaluations remains consistent for any given N, and the post-processing operations primarily involve rounding the last digit of the ply counts. Additionally, it is worth noting that the time needed to design Symmetric-Balanced FADs is slightly greater than in the case of Unbalanced FADs. As pointed out earlier, this was because the balanced rounding operations are relatively more exhaustive.

10.4.2. Approach to handle the Inverse Problem: Simultaneous vs Hierarchical

In the literature review (chapter 3), it was observed that combinatorial optimisers like the decision tree-based tools ([81, 92]) or GAs ([45, 90]) can simultaneously handle all LPs to design an SS. However, these one-step implementations were shown to be less-informed and greedy optimisation procedures. Consequently, this thesis focused on better utilising the LPs as targets. This was achieved by developing a hierarchical SS design framework involving multiple steps: Initially, information about FAD is acquired from $V^A_{1,2,3,4}$, after which their SS is determined while trying to match $V^D_{1,2,3,4}$. Although the latter aspect has not been implemented in this thesis, the computational efficiency of a hierarchical procedure is evident from the results presented for the Bristol Dataset (in Table 10.4).

Nevertheless, a combinatorial optimiser needs to handle the conversion of a FAD into SS. The literature study showed that the decision tree implementation of Fedon et al.[81] was computationally efficient with increasing N. However, their solution accuracy could have been better when designing with more θ's (Non-Conventional Orientations). Regardless, such a limitation can be circumvented in a hierarchical framework. Since the FAD is designed by the FFT-based method, a combinatorial optimiser only needs to design the sequence in which they are placed within a laminate. Hence, an SS can be efficiently designed from a FAD. As such, the hierarchical framework holds the potential to outperform simultaneous procedures in terms of both solution accuracy and computational efficiency.

10.4.3. Benefits of using $[\Delta 15°]$ over $[\Delta 45°]$

The FFT-based method can efficiently design FADs with $[\Delta 15°]$. Therefore, the benefits of using them over the conventional $[\Delta 45°]$ can be visually observed through the following error profiles for Symmetric FADs with $N = [4, 5, 6, 7]$:

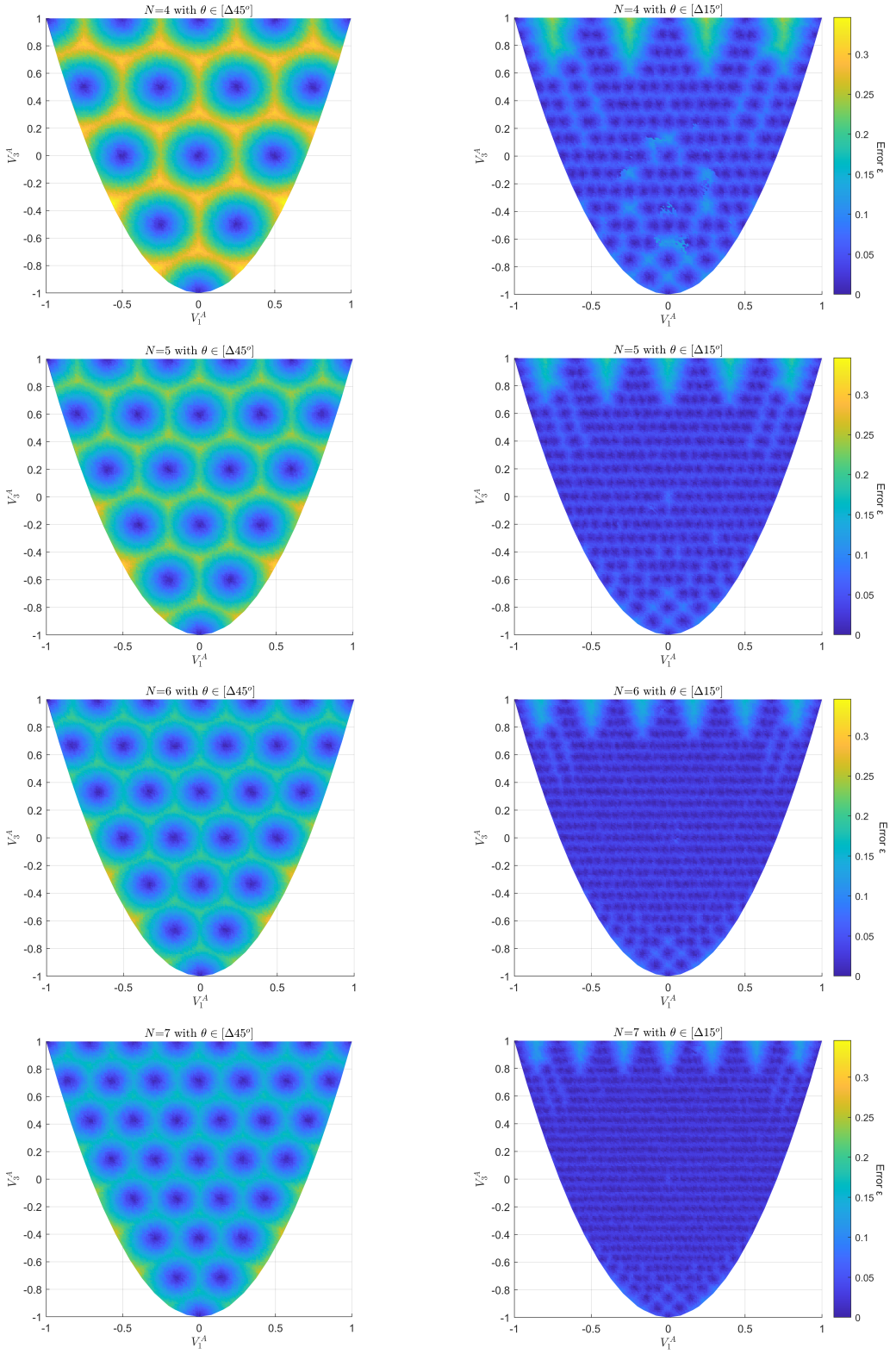

Figure 10.11: Error Profiles for Symmetric FADs with $N = [4, 5, 6, 7]$, compared between $[\Delta 45°]$(left) and $[\Delta 15°]$(right)

When compared with $[\Delta 45°]$, the FADs made of $[\Delta 15°]$ can match more of the feasible $V^A_{1,3}$ space with lesser N. The same trend is expected for Symmetric-Balanced FAD, albeit at a slightly higher N value. As such, the benefits of using a set for ply orientations with smaller increments are evident. Nonetheless, these results were analysed further to understand how many unique $|\theta|$'s from $[\Delta 15°]$ are required to provide a good solution. The FFTs can design FAD using two different signal patterns: the Exact Pattern can design a FAD with a maximum of three $|\theta|$'s, while Approximate Patterns can design with more $|\theta|$'s. Hence, error profiles without and with the solutions from Approximate patterns were made:

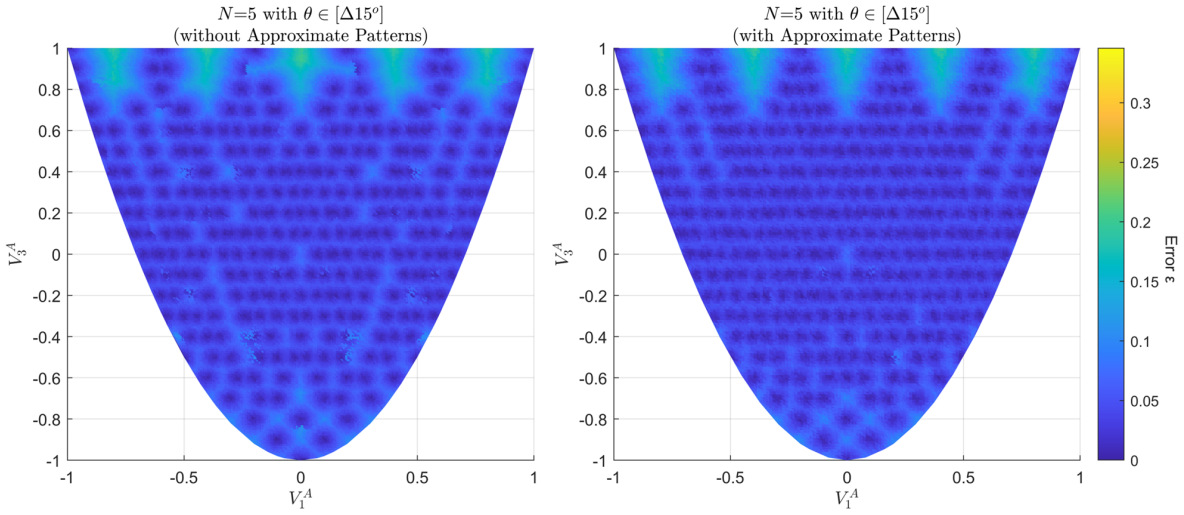

Figure 10.12: Error Profiles for Symmetric FADs with $N = [5]$ and $[\Delta 15°]$: without Approximate Patterns (left) and with Approximate Patterns(right)

For the case shown here ($N = 5$), one could observe that Approximate Patterns populate the design space with a few more exactly matching solutions. To visualise this better, the reduction in mismatch error upon using approximate patterns is plotted below.

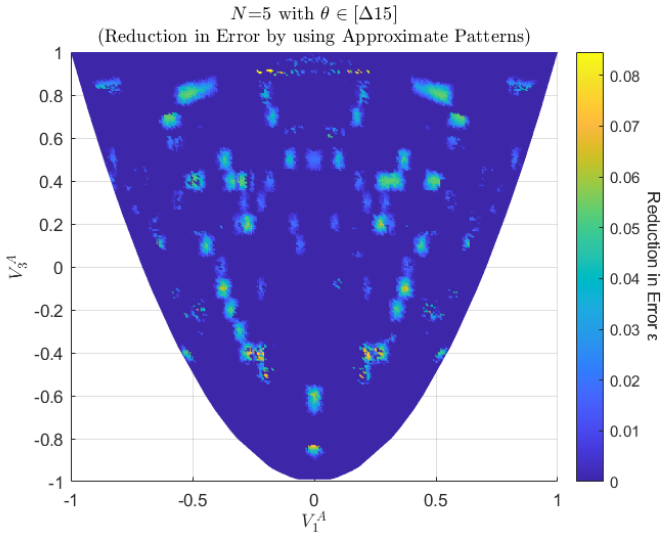

Figure 10.13: Reduction in mismatch error upon using Approximate Patterns, for Symmetric FADs with $N = [5]$ and $[\Delta 15°]$

Here, the brighter spots indicate the regions that benefit from lower mismatch error upon using approximate patterns. To understand how this attribute varies across increasing N, the reduction in mismatch error was documented from error profiles of increasing N and plotted in the following figure:

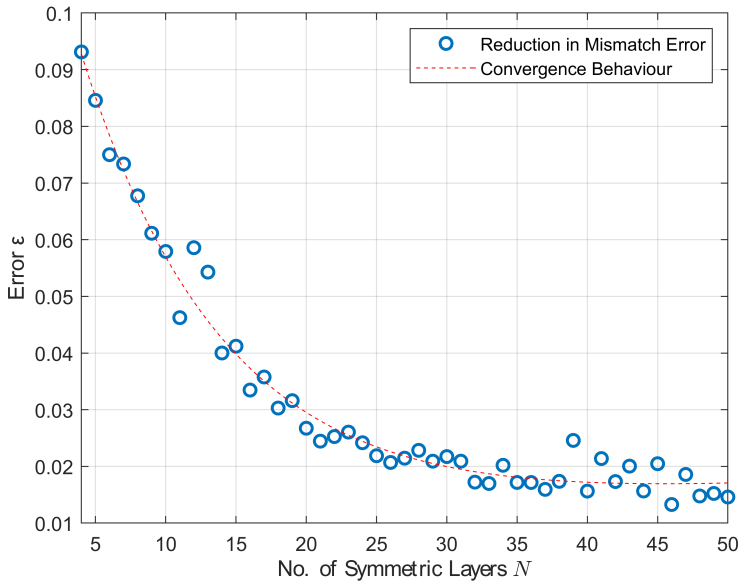

Figure 10.14: Benefits of using more than three $|\theta|$'s to design a FAD

The benefits of using approximate patterns and designing with more than three $|\theta|$'s are significant (≈ 0.1) for $N = [4, 5, 6]$. However, as N increases, these benefits reduce exponentially. This was attributed to the general fact that better matching of $V^A_{1,3}$ is possible with increasing N. For completeness, it will be acknowledged that a small but irregular fluctuating trend can be observed with the error reductions. However, this behaviour could not be explained with any attributable cause.

Therefore, the following can be concluded from this discussion. The In-Plane Stiffness Design of Laminates can be significantly improved when using $[\Delta 15°]$ instead of $[\Delta 45°]$. At the same time, the benefits of using more than three orientations from $[\Delta 15°]$ are more pronounced only for $N \leq 10$. Nevertheless, it has to be said that the benefits of designing with more than three $|\theta|$'s may be more pronounced while attempting to design for Out-of-Plane Stiffness ($V^D_{1,2,3,4}$) and/or help satisfy any empirical SS design guidelines.

This discussion claims that the design of a laminate's In-Plane Stiffness properties is better off with only three $|\theta|$'s, as long as they belong to a more extensive set of orientations like $[\Delta 15°]$. The findings of a study from 1999 can also back up this claim. Hammer et al.[52] state that a two-ply laminate(with unique $|\theta|$'s) is mathematically sufficient to match a given $V^A_{1,3}$ combination, while a three-ply laminate is sufficient to match a $V^A_{1,2,3,4}$ combination. Although their findings draw an interesting parallel to the ones presented in this thesis, their approach was different and practically less viable. They allow ply thickness to be a continuous design variable for optimum $|\theta|$ values to match $V^A_{1,2,3,4}$. While their solutions are theoretically sound, it is not straightforward to realise them using commercially available ply thicknesses. Moreover, their approach inherently allows less room to enforce empirical design guidelines.

11

Conclusions and Recommendations

> "A scientist is never certain.... We absolutely must leave room for doubt or there is no progress and there is no learning."
>
> *Richard P. Feynman*

This thesis addresses the 'Inverse Problem' of converting LPs into SS while considering non-conventional $[\Delta 15^\circ]$. For this, a hierarchical design procedure was proposed: first, the FAD of a laminate with non-conventional $[\Delta 15^\circ]$ orientations is to be designed, and by using them as a basis, a SS can be designed. As this is the first step in a new direction, the thesis concentrated on the FAD design, for which a novel FFT-inspired approach was introduced. As seen in chapter 10, the solution accuracy and time efficiency of the implementations were unparalleled in literature. As such, the hierarchical design framework holds the potential to outperform current techniques to solve the Inverse Problem. This chapter will briefly conclude the findings from the implementations made for FAD design (in section 11.1), answer the research questions (in section 11.2) and provide recommendations for future work (in section 11.3).

11.1. Conclusions

All laminates designed in this thesis are symmetric. This was achieved by designing fibre orientations of the layers only in the symmetric half of the laminate. Initially, using the FFTs (as seen in chapter 7), a target $V_{1,3}^A$ combination is converted into a FAD ($\forall\ |\theta|$). If a balanced laminate is to be designed, the ply counts of all the off-axis $|\theta|$ are equally split among the corresponding $+\theta$ and $-\theta$, respectively. On the other hand, if an unbalanced laminate is to be designed, a $V_{2,4}^A$ combination is accounted for in the already known FAD solution, using a system of linear equations (as seen in chapter 8).

Given that neither FFTs nor a system of linear equations ensures integer outputs, a rounding operation was always implemented along with them. This ensured integer ply counts to be present in all the designed FADs. As such, the hierarchical framework introduced in this thesis can design Symmetric-Balanced and Symmetric-Unbalanced FADs. By thoroughly testing their capabilities, the following conclusions were drawn:

- Design of Symmetric-Balanced FADs: A custom-made 2D benchmark dataset of several uniformly sampled $V_{1,3}^A$ targets were used to test the design performance for Symmetric-Balanced FADs. The FFT-based method could design multiple unique solutions, all within a second ($\approx 0.3s$). Based on the error profiles obtained from these tests, it was understood that all $V_{1,3}^A$ values that can be practically matched using $[\Delta 15^\circ]$ orientations could be obtained. Moreover, unlike other techniques in literature, their time efficiency stays almost the same with increasing N.
- Design of Symmetric-Unbalanced FADs: A benchmark dataset from literature (the Bristol Dataset [81]), and a custom-made 4D benchmark dataset of several quasi-randomly sampled $V_{1,2,3,4}^A$ targets were used to test the design performance for Symmetric-Unbalanced FADs. The FFT-based

procedure, along with the system of linear equations, maintained their commendable time efficiency. This, combined with their solution accuracy, outperformed all other techniques in the literature that handle the Inverse Problem.

- $[\Delta 45°]$ vs $[\Delta 15°]$: Compared to the conventional $[\Delta 45°]$ ply orientations, the non-conventional $[\Delta 15°]$ allows more area of the feasible $V^A_{1,3}$ design space to be matched using a FAD with less number of N, paving way for lighter designs. By analysing the results further, it was understood that a $V^A_{1,3}$ combination can be well-matched only with three $|\theta|$'s, as long as they belong to a more extensive set of orientations like $[\Delta 15°]$ and not the conventional $[\Delta 45°]$. However, it has to be acknowledged that the benefits of using more than three $|\theta|$'s from $[\Delta 15°]$ were seen for $N \leq 10$.
- Design Limitations: For the case of Symmetric-Unbalanced FADs, they can be designed with a maximum of three off-axis $|\theta|$'s. Hence, the solution accuracy of this framework is inferior to a GA for $V^A_{1,2,3,4}$ combinations that can only be achieved with more than three off-axis $|\theta|$'s.

11.2. Research Questions

During the implementation phase of this thesis, the limitation of using FFTs in laminate design was recognised: it was viable to use FFTs only with the $V^A_{1,3}$ LPs. Furthermore, a system of linear equations and rounding procedures were embedded with this FFT implementation to design Symmetric-Balanced and Symmetric-Unbalanced FADs efficiently. So, with the knowledge acquired from this thesis and the findings derived from the results, informed answers can be provided for the research questions of this master's thesis (presented in the following page).

Main Research Question

What is a computationally efficient method to convert LPs into SS of a given number of layers with Non-Conventional Orientations?

Sub-Question I

How can FFTs be used to handle the Inverse Problem?

Sub-Sub-Question i

How can the Inverse Problem be parameterised as a signal processing problem?
By incorporating a fictitious time domain within the definition of LPs, the notion of Laminate Signals was introduced in this thesis. Such a parameterisation meant that frequencies within these signals are ply orientations, and their respective amplitudes are the Sum of Weights.

Sub-Sub-Question ii

What are the consequences of using a time-domain-based parameterisation?
All LPs are mathematically correlated but independently defined using two different sinusoids, weighted differently to describe three different stiffnesses. Hence, multiple laminate signals were required to represent multiple different LPs. As this thesis only worked for designing symmetric laminates, four different laminate signals $L_{1,2}^{A,D}$ were parameterised: L_1^A represents the In-Plane Cosine based LPs ($V_{1,3}^A$), L_2^A represents the In-Plane Sine based LPs ($V_{2,4}^A$), L_1^D represents the Out-of-Plane Cosine based LPs ($V_{1,3}^D$), and L_2^D represents the Out-of-Plane Sine based LPs ($V_{2,4}^D$). Moreover, the multi-modality of the inverse problem meant that many laminate signals could correspond to the same LPs. Nonetheless, this parameterisation implies that by performing FFT on laminate signals, the Sum of Weights (amplitudes) for all ply orientations (frequencies) can be obtained. The Sum of Weights from $L_{1,2}^A$ constitutes the FAD of a laminate. Although, the Sum of Weights from $L_{1,2}^D$ could not be intuitively associated with a laminate. Therefore, FFTs can be effectively used to design a laminate's FAD.

Sub-Question II

What steps should be followed for converting LPs into SS?
A step-by-step operation was desired to effectively use LPs as targets and design a SS. This was termed the Hierarchical SS Design Framework. Initially, the FAD of a laminate is designed using $V_{1,2,3,4}^A$, upon which their SS can be designed using $V_{1,2,3,4}^D$. During this thesis, it was realised that performing FFTs was practically feasible only on the $V_{1,3}^A$ laminate signals (L_1^A). Moreover, by taking advantage of multi-modality, signal samples of different L_1^A that correspond to the same $V_{1,3}^A$ could be constructed. Since a Symmetric-Balanced FAD only relies on these LPs, multiple unique solutions can be designed for them using FFTs. For Symmetric-Unbalanced designs, the FAD designed using FFTs was modified using a System of Equations to account for $V_{2,4}^A$. After this, the SS must be designed by rearranging the FAD to match a given $V_{1,2,3,4}^D$. The latter step could not be implemented within the timeline of this master thesis.

Sub-Question III

Considering both result quality and computational effort, what is a good performance metric for evaluating this conversion method with others?
Upon analysing the results, it was understood that the time taken to produce them and the LP mismatch error are the only practical and reliable ways to compare different techniques. A good technique is the one that produces the least LP mismatch and consumes less time. The amount of evaluations a technique performs also relates to the computational effort (computational complexity O). However, the evaluations performed by different techniques are not comparable, as they perform different numerical calculations/operations. Moreover, these calculations may be looped, vectorised, or parallelised within the implementation. Hence, they were not considered a performance metric. Such a statement might sound paradoxical, given that the time taken by every technique is also not comparable on equal grounds. This is why it was suggested that the time taken needs to be assessed along with the LP mismatch error to assess a technique's performance practically. With this in mind, the results obtained using the Hierarchical Procedure for FAD design were analysed. They were capable of swiftly designing an N-layered Symmetric-Balanced FADs (around $0.3s$). Moreover, the framework is capable of providing multiple closely matching results at the same time. The framework was also tested using a benchmark dataset from the literature. It was made by Fedon et al.[81] to benchmark several methods in the literature that handle the Inverse Problem. Along with this, a custom-made and more thorough benchmark dataset was made in this thesis (4D benchmark). The performance metrics for both these benchmark tests are shown as follows:

Table 11.1: FAD Design Performance for the Bristol Dataset and 4D Benchmark while using $[\Delta 15°]$

	Bristol Dataset		**4D Benchmark**	
	Max Error ε	**Time taken (s)**	**Max Error ε**	**Time taken (s)**
FFT-based Method	0	0.28	0.34	0.21
LAYLA [81]	0	3.40	-	-
OptiBLESS	0	89.11	0.10	177.06

With the results from the Bristol dataset, it was understood that the hierarchical framework outperforms other techniques in terms of solution accuracy and time taken. However, with the 4D benchmark, the GA outperforms the hierarchical framework in terms of solution accuracy, albeit slowly. Hence, none of these methods are computationally efficient for the latter case.

11.3. Recommendations for Future Work

This thesis focused on providing a computationally efficient solution for the Inverse Problem. Given the master thesis timeline, exploring and implementing every idea in-depth was not practically feasible. As such, these ideas and the framework's limitations can be considered recommendations for future work. By addressing the following points, the hierarchical procedure becomes complete and has the potential to become more robust:

1. Automatic recognition of Signal Patterns: A set of Exact Patterns can be mathematically derived for any given $[\Delta\theta]$. However, finding Approximate Patterns remains a completely manual exercise. Using a GA's design space exploration capabilities, a FAD belonging to many parts of the LP space are obtained. Their L_1^A signals are then plotted to identify patterns manually. Among them, many patterns are removed concerning redundancy (the extent of their design domain). Hence, by automating these steps, a pool of signal patterns can be designed for any given $[\Delta\theta]$. This makes setting up a hierarchical framework less intensive and the overall approach more robust.
2. Out-of-plane Stiffness Design: While the FFTs proved helpful only to design FADs, they act as

partial solutions, using which an SS can be designed. However, as stated in chapter 9, this thesis has not implemented the conversion of FAD into a SS. Nonetheless, the branch and bound method with an efficient search algorithm similar to the work of Fedon et al.[81] seems to be the computationally efficient way to handle this step. The design of SS, as such, completes the hierarchical procedure. Furthermore, this will also answer the question: Does the Out-of-Plane Stiffness Design improve when using more than three $|\theta|$'s from $[\Delta 15^\circ]$?

3. Empirical Design Guidelines: In this thesis, guidelines such as Symmetry and Balancing were accounted for while designing FAD(s). However, several other guidelines are yet to be accounted for during the design of SS: minimise bend-twist coupling, disorientation, contiguity, damage tolerance, and internal continuity. Hence, the step that converts FAD into a SS must account for them while designing θ for every layer. The 10% rule is not mentioned here since it only pertains to the In-Plane Stiffness properties. Moreover, they can be implicitly accounted for using LPs[93].
4. Blending and Steering: Upon implementing the conversion of a FAD to an SS, the hierarchical framework is complete and can handle the Inverse Problem for a given $[\Delta\theta]$. In order to extend them into the design of variable stiffness laminates, they need to be incorporated into the design procedures of blended and fibre-steered laminates. As explained in the literature review (in Figure 2.13), their design procedures involve converting LPs into SS using a GA. Hence, the hierarchical framework can replace the GA for this purpose. Upon doing so, variable stiffness structures can be more efficiently designed.

References

[1] *BP Statistical Review of World Energy*. Tech. rep. 2022.

[2] Airbus. *A350 Less Operating Cost. More Capabilities.* URL: https://aircraft.airbus.com/en/aircraft/a350-clean-sheet-clean-start/a350-less-operating-cost-more-capabilities.

[3] Bob Griffiths. *Boeing sets pace for composite usage in large civil aircraft*. Jan. 2005. URL: https://www.compositesworld.com/articles/boeing-sets-pace-for-composite-usage-in-large-civil-aircraft.

[4] M.W. Hyer and H.H. Lee. "The use of curvilinear fiber format to improve buckling resistance of composite plates with central circular holes". en. In: *Composite Structures* 18.3 (Jan. 1991), pp. 239–261. ISSN: 02638223. DOI: 10.1016/0263-8223(91)90035-W.

[5] Christos Kassapoglou. *Design and Analysis of Composite Structures: With Applications to Aerospace Structures*. en. 1st ed. Wiley, May 2013. ISBN: 978-1-118-40160-6 978-1-118-53693-3.

[6] Zafer Gürdal, Raphael T. Haftka, and Prabhat Hajela. *Design and optimization of laminated composite materials*. New York: Wiley, 1999. ISBN: 978-0-471-25276-4.

[7] *Towards zero-emission aviation-DLR's new aviation strategy*. Tech. rep. Deutsches Zentrum für Luft- und Raumfahrt, 2021.

[8] Hossein Ghiasi, Damiano Pasini, and Larry Lessard. "Optimum stacking sequence design of composite materials Part I: Constant stiffness design". en. In: *Composite Structures* 90.1 (Sept. 2009), pp. 1–11. ISSN: 02638223. DOI: 10.1016/j.compstruct.2009.01.006.

[9] RZG Bohrer and I Kim. "Concurrent topology and stacking sequence optimization of composite laminate plates using lamination parameters". In: *COMPOSITE STRUCTURES* 276 (Nov. 2021). ISSN: 0263-8223. DOI: 10.1016/j.compstruct.2021.114556.

[10] Hossein Ghiasi et al. "Optimum stacking sequence design of composite materials Part II: Variable stiffness design". en. In: *Composite Structures* 93.1 (Dec. 2010), pp. 1–13. ISSN: 02638223. DOI: 10.1016/j.compstruct.2010.06.001.

[11] T.R. Tauchert and S. Adibhatla. "Design of Laminated Plates for Maximum Stiffness". en. In: *Journal of Composite Materials* 18.1 (Jan. 1984), pp. 58–69. ISSN: 0021-9983, 1530-793X. DOI: 10.1177/002199838401800105.

[12] Reynaldo Olmedo and Zafer Gurdal. "Buckling Response of Laminates with Spatially Varying Fiber Orientations". en. In: *34th Structures, Structural Dynamics and Materials Conference*. La Jolla,CA,U.S.A.: American Institute of Aeronautics and Astronautics, Apr. 1993. DOI: 10.2514/6.1993-1567.

[13] Mazen A. Albazzan et al. "Efficient design optimization of nonconventional laminated composites using lamination parameters: A state of the art". In: *COMPOSITE STRUCTURES* 209 (Feb. 2019), pp. 362–374. ISSN: 0263-8223. DOI: 10.1016/j.compstruct.2018.10.095.

[14] Stephen W. Tsai and Nicholas J. Pagano. "Invariant Properties of Composite Materials". In: (1968).

[15] Terence Macquart et al. "Optimisation of composite structures – Enforcing the feasibility of lamination parameter constraints with computationally-efficient maps". en. In: *Composite Structures* 192 (May 2018), pp. 605–615. ISSN: 02638223. DOI: 10.1016/j.compstruct.2018.03.049.

[16] Vladimir Balabanov et al. "Optimal Design of a Composite Sandwich Structure Using Lamination Parameters". en. In: Honolulu, Hawaii: American Institute of Aeronautics and Astronautics, Apr. 2012. ISBN: 978-1-60086-937-2. DOI: 10.2514/6.2012-1520.

[17] Panos Y. Papalambros and Douglass J. Wilde. *Principles of Optimal Design: Modeling and Computation*. 3rd ed. Cambridge University Press, Jan. 2017. ISBN: 978-1-107-13267-2 978-1-316-45103-8. DOI: 10.1017/9781316451038.

[18] ST Ijsselmuiden. “Optimal Design of Variable Stiffness Composite Structures using Lamination Parameters”. PhD thesis. 2011.

[19] Shahriar Setoodeh. “Optimal Design of Variable-Stiffness Fiber-Reinforced Composites Using Cellular Automata”. PhD thesis. 2005.

[20] ZM Wu, G Raju, and PM Weaver. “Framework for the Buckling Optimization of Variable-Angle Tow Composite Plates”. In: *AIAA JOURNAL* 53.12 (Dec. 2015), pp. 3788–3804. ISSN: 0001-1452. DOI: 10.2514/1.J054029.

[21] Mohammad Gomaa. *Laminate Blending Demonstrator: A buckling experimental campaign of a physical laminate blending demonstrator*. MSc Thesis. 2019.

[22] Gustavo Gonzalez Lozano et al. “A review on design for manufacture of variable stiffness composite laminates”. en. In: *Proceedings of the Institution of Mechanical Engineers, Part B: Journal of Engineering Manufacture* 230.6 (June 2016), pp. 981–992. ISSN: 0954-4054, 2041-2975. DOI: 10.1177/0954405415600012.

[23] D.M.J. Peeters. “Design Optimisation of Practical Variable Stiffness and Thickness Laminates”. PhD thesis. Delft University of Technology, 2017.

[24] A.W Blom. “Structural Performance of Fiber-Placed, Variable-Stiffness Composite Conical and Cylindrical Shells”. PhD thesis. 2010.

[25] Israel O. Ayodele et al. “Characterization of steered fiber laminates: Perspectives and a survey of the state of the art on principal considerations”. en. In: *Composites Part C: Open Access* 4 (Mar. 2021), p. 100118. ISSN: 26666820. DOI: 10.1016/j.jcomc.2021.100118.

[26] Paul Mattheij, Konrad Gliesche, and Dirk Feltin. “Tailored Fiber Placement-Mechanical Properties and Applications”. en. In: *Journal of Reinforced Plastics and Composites* 17.9 (June 1998), pp. 774–786. ISSN: 0731-6844, 1530-7964. DOI: 10.1177/073168449801700901.

[27] Max Hijne. *A Fibre-Path Generation Algorithm for Fibre-Steered Variable Stiffness Laminates*. en. MSc Thesis. 2022.

[28] Michael J. Van Tooren, Ifat Jahangir, and Ali Elham. “Optimization of variable stiffness composite plates with cut-outs subjected to compression, tension and shear using an adjoint formulation”. en. In: *57th AIAA/ASCE/AHS/ASC Structures, Structural Dynamics, and Materials Conference*. San Diego, California, USA: American Institute of Aeronautics and Astronautics, Jan. 2016. ISBN: 978-1-62410-392-6. DOI: 10.2514/6.2016-1970.

[29] Byung Chul Kim, Kevin Potter, and Paul M. Weaver. “Continuous tow shearing for manufacturing variable angle tow composites”. en. In: *Composites Part A: Applied Science and Manufacturing* 43.8 (Aug. 2012), pp. 1347–1356. ISSN: 1359835X. DOI: 10.1016/j.compositesa.2012.02.024.

[30] B. Kristinsdottir and Z. Zabinsky. “Including manufacturing tolerances in composite design”. en. In: *35th Structures, Structural Dynamics, and Materials Conference*. Hilton Head,SC,U.S.A.: American Institute of Aeronautics and Astronautics, Apr. 1994. DOI: 10.2514/6.1994-1495.

[31] David B. Adams, Layne T. Watson, and Zafer Gürdal. “Optimization and Blending of Composite Laminates Using Genetic Algorithms with Migration”. en. In: *Mechanics of Advanced Materials and Structures* 10.3 (July 2003), pp. 183–203. ISSN: 1537-6494, 1537-6532. DOI: 10.1080/15376490306741.

[32] Thore Roepman. *Patching a Fuselage: Application of Straight Fiber Variable Stiffness Laminates in Large Aerospace Structures*. MSc Thesis. 2022.

[33] Julien van Campen et al. “General Blending Definitions for Stacking Sequence Design of Composite Laminate Structures”. In: *49th AIAA/ASME/ASCE/AHS/ASC Structures, Structural Dynamics, and Materials Conference*. Structures, Structural Dynamics, and Materials and Co-located Conferences. American Institute of Aeronautics and Astronautics, Apr. 2008. DOI: 10.2514/6.2008-1798.

[34] François-Xavier Irisarri et al. “Optimal design of laminated composite structures with ply drops using stacking sequence tables”. en. In: *Composite Structures* 107 (Jan. 2014), pp. 559–569. ISSN: 02638223. DOI: 10.1016/j.compstruct.2013.08.030.

[35] Yasser M. Meddaikar, François-Xavier Irisarri, and Mostafa M. Abdalla. “Laminate optimization of blended composite structures using a modified Shepard’s method and stacking sequence tables”. en. In: *Structural and Multidisciplinary Optimization* 55.2 (Feb. 2017), pp. 535–546. ISSN: 1615-147X, 1615-1488. DOI: 10.1007/s00158-016-1508-0.

[36] Ellen van Den Oord. *Overcoming the curse of dimensionality in composite laminate blending: A CA-based algorithm for blending laminated composite plates with a large amount of sections*. Tech. rep. MSc Thesis. 2018.

[37] Scott Beckwith. “Designing with Composites: Suggested “Best Practices” Rules”. In: *SAMPE Journal* 45 (2009), pp. 36–37.

[38] Daniël Peeters and Mostafa Abdalla. “Design Guidelines in Nonconventional Composite Laminate Optimization”. In: *Journal of Aircraft*. American Institute of Aeronautics and Astronautics 54.4 (2017), pp. 1454–1464. ISSN: 0021-8669. DOI: 10.2514/1.C034087.

[39] Christopher B. York. “Unified Approach to the Characterization of Coupled Composite Laminates: Benchmark Configurations and Special Cases”. In: *JOURNAL OF AEROSPACE ENGINEERING* 23.4 (Oct. 2010), pp. 219–242. ISSN: 0893-1321. DOI: 10.1061/(ASCE)AS.1943-5525.0000036.

[40] Marco Montemurro et al. “Least-weight composite plates with unconventional stacking sequences: Design, analysis and experiments”. en. In: *Journal of Composite Materials* 53.16 (July 2019), pp. 2209–2227. ISSN: 0021-9983, 1530-793X. DOI: 10.1177/0021998318824783.

[41] G. Caprino and I. Crivelli Visconti. “A Note on Specially Orthotropic Laminates”. en. In: *Journal of Composite Materials* 16.5 (Sept. 1982), pp. 395–399. ISSN: 0021-9983, 1530-793X. DOI: 10.1177/002199838201600504.

[42] Stephen Tsai. “Double–Double: New Family of Composite Laminates”. en. In: *AIAA Journal* 59.11 (Nov. 2021), pp. 4293–4305. ISSN: 0001-1452, 1533-385X. DOI: 10.2514/1.J060659.

[43] T Macquart et al. “Derivation and application of blending constraints in lamination parameter space for composite optimisation”. In: *COMPOSITE STRUCTURES* 135 (Jan. 2016), pp. 224–235. ISSN: 0263-8223. DOI: 10.1016/j.compstruct.2015.09.016.

[44] Zhi Hong, Daniël Peeters, and Sergio Turteltaub. “An enhanced curvature-constrained design method for manufacturable variable stiffness composite laminates”. en. In: *Computers & Structures* 238 (Oct. 2020), p. 106284. ISSN: 00457949. DOI: 10.1016/j.compstruc.2020.106284.

[45] Frederico Sousa Vicente. *Stacking Sequence Retrieval of Large Composite Structures in Bi-step Optimization Strategies Using Mechanical Constraints*. MSc Thesis. 2019.

[46] Mitsunori Miki. “Material design of composite laminates with required in-plane elastic properties”. In: *Progress in science and engineering of composites* (1982).

[47] Mitsunori Miki. “Sandwich-type composite material optimal design of beams”. In: (1983). DOI: 10.34401/zairyosystem.2.0_81.

[48] Raphael T. Haftka and Zafer Gürdal. *Elements of structural optimization*. 3rd rev. and expanded ed. Solid mechanics and its applications v. 11. Dordrecht ; Boston: Kluwer Academic Publishers, 1992. ISBN: 978-0-7923-1504-9.

[49] Julien van Campen and Zafer Gürdal. “Retrieving Variable Stiffness Laminates from Lamination Parameters Distribution”. en. In: *50th AIAA/ASME/ASCE/AHS/ASC Structures, Structural Dynamics, and Materials Conference*. Palm Springs, California: American Institute of Aeronautics and Astronautics, May 2009. ISBN: 978-1-60086-975-4. DOI: 10.2514/6.2009-2183.

[50] Hisao Fukunaga and Hideki Sekine. “Stiffness design method of symmetric laminates using lamination parameters”. en. In: *AIAA Journal* 30.11 (Nov. 1992), pp. 2791–2793. ISSN: 0001-1452, 1533-385X. DOI: 10.2514/3.11304.

[51] Hisao Fukunaga and Hideki Sekine. “A Laminate Design for Elastic Properties of Symmetric Laminates with Extension-Shear or Bending-Twisting Coupling”. en. In: *Journal of Composite Materials* 28.8 (May 1994), pp. 708–731. ISSN: 0021-9983, 1530-793X. DOI: 10.1177/002199839402800802.

[52] Velaja B. Hammer et al. “Parametrization in laminate design for optimal compliance”. en. In: *International Journal of Solids and Structures* 34.4 (Feb. 1997), pp. 415–434. ISSN: 00207683. DOI: 10.1016/S0020-7683(96)00023-6.

[53] Maija Autio. “Optimization of coupled thermal-structural problems of laminated plates with lamination parameters”. en. In: *Structural and Multidisciplinary Optimization* 21.1 (Mar. 2001), pp. 40–51. ISSN: 1615-147X, 1615-1488. DOI: 10.1007/s001580050166.

[54] Moritz Sprengholz et al. “Rapid transformation of lamination parameters into stacking sequences”. In: *COMPOSITE STRUCTURES* 276 (Nov. 2021). ISSN: 0263-8223. DOI: 10.1016/j.compstruct.2021.114514.

[55] Alden H. Wright. “Finding all solutions to a system of polynomial equations”. en. In: *Mathematics of Computation* 44.169 (1985), pp. 125–133. ISSN: 0025-5718, 1088-6842. DOI: 10.1090/S0025-5718-1985-0771035-4.

[56] Andrew D. Viquerat. “A continuation-based method for finding laminated composite stacking sequences”. In: *COMPOSITE STRUCTURES* 238 (Apr. 2020). ISSN: 0263-8223. DOI: 10.1016/j.compstruct.2020.111872.

[57] SFM de Almeida, APCS Ferreira, and G. Bonet. “Buckling optimization using lamination parameters”. In: *Proceedings of the 5th international conference on advanced computational engineering and experimenting 2011*. Algarve, Portugal.

[58] Rubens Zolar Gehlen Bohrer, Sérgio Frascino Müller de Almeida, and Mauricio Vicente Donadon. “Optimization of composite plates subjected to buckling and small mass impact using lamination parameters”. en. In: *Composite Structures* 120 (Feb. 2015), pp. 141–152. ISSN: 02638223. DOI: 10.1016/j.compstruct.2014.09.043.

[59] Michel Grediac. “A procedure for designing laminated plates with required stiffness properties. Application to thin quasi-isotropic quasi-homogeneous uncoupled laminates”. In: *JOURNAL OF COMPOSITE MATERIALS* 33.20 (1999), pp. 1939–1956. ISSN: 0021-9983. DOI: 10.1177/002199839903302005.

[60] Michel Grediac. “On the stiffness design of thin woven composites”. In: *COMPOSITE STRUCTURES* 51.3 (Mar. 2001), pp. 245–255. ISSN: 0263-8223. DOI: 10.1016/S0263-8223(00)00135-5.

[61] Daniël Peeters, Zhi Hong, and Mostafa Abdalla. “A compliance approximation method applied to variable stiffness composite optimisation”. en. In: *Structural and Multidisciplinary Optimization* 58.5 (Nov. 2018), pp. 1981–2001. ISSN: 1615-147X, 1615-1488. DOI: 10.1007/s00158-018-2007-2.

[62] Julien van Campen. “Optimum Lay-Up Design of Variable Stiffness Composite Structures”. PhD thesis. 2011.

[63] Paulo Cortez. “Population Based Search”. en. In: *Modern Optimization with R*. Cham: Springer International Publishing, 2021, pp. 89–151. ISBN: 978-3-030-72818-2 978-3-030-72819-9.

[64] A. Rama Mohan Rao and N. Arvind. “Optimal stacking sequence design of laminate composite structures using tabu embedded simulated annealing”. In: *Structural Engineering and Mechanics* 25.2 (Jan. 2007), pp. 239–268. DOI: 10.12989/SEM.2007.25.2.239.

[65] Mark Bloomfield, J. Herencia, and Paul Weaver. “Optimisation of Anisotropic Composite Plates Incorporating Non-Conventional Ply Orientations”. en. In: Schaumburg, IL: American Institute of Aeronautics and Astronautics, Apr. 2008. ISBN: 978-1-60086-993-8. DOI: 10.2514/6.2008-1918.

[66] Nozomu Kogiso et al. “Genetic Algorithms with Local Improvement for Composite Laminate Design”. In: *Structural Optimization* 7.4 (June 1994), pp. 207–218. ISSN: 0934-4373. DOI: 10.1007/BF01743714.

[67] Noémie Fedon et al. “A repair algorithm for composite laminates to satisfy lay-up design guidelines”. en. In: *Composite Structures* 259 (Mar. 2021), p. 113448. ISSN: 02638223. DOI: 10.1016/j.compstruct.2020.113448.

[68] WG Zhu et al. “Optimization Design for Laminated Composite Structure Based on Kriging Model”. In: ed. by XH Liu et al. Vol. 217-219. 2012, pp. 179–183. ISBN: 1660-9336. DOI: 10.4028/www.scientific.net/AMM.217-219.179.

[69] A Todoroki and T Ozawa. “Warping thermal deformation constraint for optimization of a blade stiffened composite panel using GA”. In: *INTERNATIONAL JOURNAL OF AERONAUTICAL AND SPACE SCIENCES* 14.4 (Dec. 2013), pp. 334–340. ISSN: 2093-274X. DOI: 10.5139/IJASS.2013.14.4.334.

[70] Xiaoyang Liu et al. “Design optimization of laminated composite structures using artificial neural network and genetic algorithm”. In: *COMPOSITE STRUCTURES* 305 (Feb. 2023). ISSN: 0263-8223. DOI: 10.1016/j.compstruct.2022.116500.

[71] François-Xavier Irisarri, Mostafa M. Abdalla, and Zafer Gürdal. “Improved Shepard’s Method for the Optimization of Composite Structures”. In: *AIAA JOURNAL* 49.12 (Dec. 2011), pp. 2726–2736. ISSN: 0001-1452. DOI: 10.2514/1.J051109.

[72] Akira Todoroki, Naonobu Sasada, and Mitsunori Miki. “Object-Oriented Approach to Optimize Composite Laminated Plate Stiffness with Discrete Ply Angles”. en. In: *Journal of Composite Materials* 30.9 (June 1996), pp. 1020–1041. ISSN: 0021-9983, 1530-793X. DOI: 10.1177/002199839603000904.

[73] Y. Narita. “Layerwise optimization for the maximum fundamental frequency of laminated composite plates”. en. In: *Journal of Sound and Vibration* 263.5 (June 2003), pp. 1005–1016. ISSN: 0022460X. DOI: 10.1016/S0022-460X(03)00270-0.

[74] Y. Narita and J.M. Hodgkinson. “Layerwise optimisation for maximising the fundamental frequencies of point-supported rectangular laminated composite plates”. en. In: *Composite Structures* 69.2 (July 2005), pp. 127–135. ISSN: 02638223. DOI: 10.1016/j.compstruct.2004.05.021.

[75] Yuichiro Terada, Akira Todoriki, and Yoshinobu Shimamura. “Stacking Sequence Optimizations Using Fractal Branch and Bound Method for Laminated Composites”. In: (2001). DOI: https://doi-org.tudelft.idm.oclc.org/10.1299/jsmea.44.490.

[76] Akira Todoroki and Yuichiro Terada. “Improved Fractal Branch and Bound Method for Stacking-Sequence Optimizations of Laminates”. en. In: *AIAA Journal* 42.1 (Jan. 2004), pp. 141–148. ISSN: 0001-1452, 1533-385X. DOI: 10.2514/1.9038.

[77] Ryosuke Matsuzaki and Akira Todoroki. “Stacking-sequence optimization using fractal branch-and-bound method for unsymmetrical laminates”. en. In: *Composite Structures* 78.4 (June 2007), pp. 537–550. ISSN: 02638223. DOI: 10.1016/j.compstruct.2005.11.015.

[78] Xiaoyang Liu, CA Featherston, and D Kennedy. “Two-level layup optimization of composite laminate using lamination parameters”. In: *COMPOSITE STRUCTURES* 211 (Mar. 2019), pp. 337–350. ISSN: 0263-8223. DOI: 10.1016/j.compstruct.2018.12.054.

[79] Xiaoyang Liu, Carol A. Featherston, and David Kennedy. “Buckling optimization of blended composite structures using lamination parameters”. en. In: *Thin-Walled Structures* 154 (Sept. 2020), p. 106861. ISSN: 02638231. DOI: 10.1016/j.tws.2020.106861.

[80] Xiaoyang Liu, Carol A. Featherston, and David Kennedy. “A Novel Parallel Method for Layup Optimization of Composite Structures with Ply Drop-offs”. en. In: *Composite Structures* (Feb. 2023), p. 116853. ISSN: 02638223. DOI: 10.1016/j.compstruct.2023.116853.

[81] N Fedon et al. “A method using beam search to design the lay-ups of composite laminates with many plies”. In: *COMPOSITES PART C: OPEN ACCESS* 4 (Mar. 2021). ISSN: 2666-6820. DOI: 10.1016/j.jcomc.2020.100072.

[82] Steven W. Smith. *Digital Signal Processing: a Practical Guide for Engineers and Scientists*. eng. 3rd ed. Saint Louis: Elsevier Science & Technology, 2013. ISBN: 978-0-08-047732-9.

[83] Qingkai Kong, Timmy Siauw, and Alexandre M. Bayen. *Python programming and numerical methods: a guide for engineers and scientists*. eng. London: Elsevier, Academic Press, 2021. ISBN: 978-0-12-819549-9.

[84] A. Douglas. “Seismic Source Identification: A Review of Past and Present Research Efforts”. In: *Identification of Seismic Sources — Earthquake or Underground Explosion*. Ed. by Eystein S. Husebye and Svein Mykkeltveit. Dordrecht: Springer Netherlands, 1981, pp. 1–48. ISBN: 978-94-009-8533-9 978-94-009-8531-5.

[85] James W. Cooley and John W. Tukey. “An algorithm for the machine calculation of complex Fourier series”. en. In: *Mathematics of Computation* 19.90 (1965), pp. 297–301. ISSN: 0025-5718, 1088-6842. DOI: 10.1090/S0025-5718-1965-0178586-1.

[86] Konrad Knopp. *Theory of functions*. eng. Dover ed. Dover books on mathematics. Mineola, N.Y: Dover Publications, 1996. ISBN: 978-0-486-69219-7.

[87] James H. McClellan, Ronald W. Schafer, and M. A. Yoder. *DSP first*. Second edition. Always learning. Boston: Pearson, 2016. ISBN: 978-0-13-601925-1.

[88] W. Heisenberg. “Uber den anschaulichen Inhalt der quantentheoretischen Kinematik und Mechanik”. de. In: *Zeitschrift fur Physik* 43.3-4 (Mar. 1927), pp. 172–198. ISSN: 1434-6001, 1434-601X. DOI: 10.1007/BF01397280.

[89] *MATLAB nufft (Nonuniform fast Fourier transform) Release 2020a*. Natick, Massachusetts, United States, 2019. URL: https://nl.mathworks.com/help/matlab/ref/double.nufft.html.

[90] Terence Macquart. *OptiBLESS (Optimisation of BLEnded Stacking Sequence) toolbox*. 2015. URL: https://github.com/TMacquart/OptiBLESS.

[91] T Macquart, N Werter, and R De Breuker. “Aeroelastic Design of Blended Composite Structures Using Lamination Parameters”. In: *JOURNAL OF AIRCRAFT* 54.2 (Mar. 2017), pp. 561–571. ISSN: 0021-8669. DOI: 10.2514/1.C033859.

[92] Dianzi Liu et al. “Bilevel Optimization of Blended Composite Wing Panels”. In: *JOURNAL OF AIRCRAFT* 48.1 (Jan. 2011), pp. 107–118. ISSN: 0021-8669. DOI: 10.2514/1.C000261.

[93] Mostafa Abdalla, Zafer Gurdal, and Christos Kassapoglu. “Formulation of Composite Laminate Robustness Constraint in Lamination Parameters Space”. In: *50th AIAA/ASME/ASCE/AHS/ASC Structures, Structural Dynamics, and Materials Conference*. Structures, Structural Dynamics, and Materials and Co-located Conferences. American Institute of Aeronautics and Astronautics, May 2009. DOI: 10.2514/6.2009-2478.

[94] Marissa Renardy et al. “To Sobol or not to Sobol? The effects of sampling schemes in systems biology applications”. en. In: *Mathematical Biosciences* 337 (July 2021), p. 108593. ISSN: 00255564. DOI: 10.1016/j.mbs.2021.108593.

Part IV

Appendix

A

Theoretical Background

A.1. Classical Laminated Plate Theory

A composite ply is an orthotropic and multi-phase material: reinforcement(continuous or discontinuous) bound together by a matrix. For the discussions in this thesis, the reinforcement agent is always assumed to be a continuous unidirectional fibre. Given that the thickness of a ply is usually in the order of a tenth of a mm, a significant disparity exists between the thickness and other planar dimensions. As such, the governing equations describing the elastic medium heavily use the plane stress assumption and classical laminated plate theory [5]. The stiffness of a ply is usually represented using a reduced material stiffness matrix $Q_{Base\ Ply}$ as shown below:

$$Q_{Base\ Ply} = \begin{bmatrix} \frac{E_1}{1-\nu_{12}\nu_{21}} & \frac{\nu_{12}E_2}{1-\nu_{12}\nu_{21}} & 0 \\ \frac{\nu_{12}E_2}{1-\nu_{12}\nu_{21}} & \frac{E_1}{1-\nu_{12}\nu_{21}} & 0 \\ 0 & 0 & G_{12} \end{bmatrix} \tag{A.1}$$

From here, it is understood that the reduced material stiffness can be characterised using five material properties from uniaxial mechanical tests: E_1 (Young modulus in longitudinal (fibre) direction), E_2 (Young modulus in transverse (matrix) direction, G_{12} (In-Plane Shear modulus), ν_{12}, and ν_{12} (Poisson's ratio). The (1-2) notation used here represents the principal directions of orthotropy:

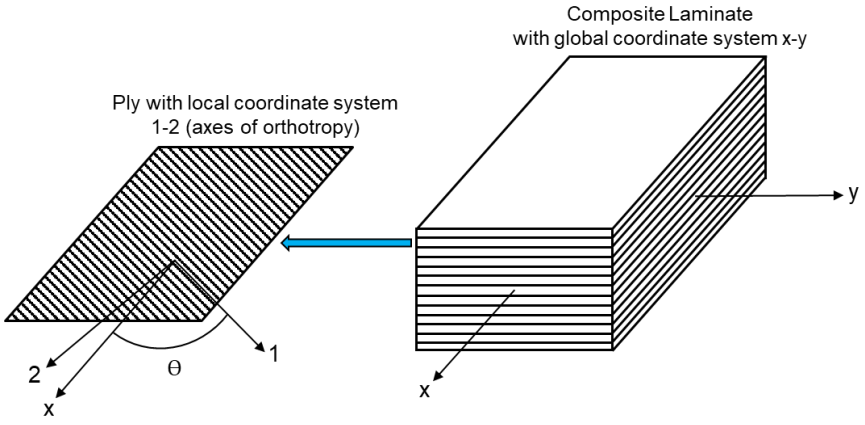

Figure A.1: Coordinate system notations followed for the laminate and off-axis plies

Using the base ply stiffness (Equation A.7), the reduced stiffness matrix of any k^{th} ply (Q^k) inside a laminate can be obtained using appropriate tensor transformations (with θ_k, and fibre orientation in the k^{th} ply):

$$Q^k = \begin{bmatrix} m^2 & n^2 & 2mn \\ n^2 & m^2 & -2mn \\ -mn & nm & \left(m^2 - n^2\right) \end{bmatrix}^k Q_{BasePly} \begin{bmatrix} m^2 & n^2 & mn \\ n^2 & m^2 & -mn \\ -2mn & 2nm & \left(m^2 - n^2\right) \end{bmatrix}^k \tag{A.2}$$

Here, m and n are direction cosines ($m = cos(\theta_k)\ and\ n = sin(\theta_k)$). While this Q matrix could be used to represent plane stress ($\sigma = Q\epsilon$), it is practically convenient to relate strains using force (N_x,N_y,N_{xy}) and moment resultants (M_x,M_y,M_{xy}). They are illustrated as follows:

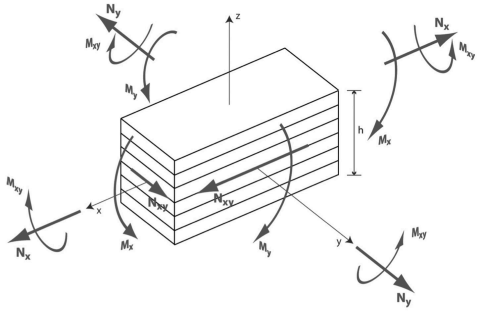

Figure A.2: Force and moment resultants on a composite laminate (Figure courtesy:[5])

These quantities are obtained by integrating loads through the laminate thickness (z) as shown below:

$$\begin{aligned} N_x &= \int_{-\frac{h}{2}}^{\frac{h}{2}} \sigma_x \, \mathrm{d}z & M_x &= \int_{-\frac{h}{2}}^{\frac{h}{2}} \sigma_x z \, \mathrm{d}z \\ N_y &= \int_{-\frac{h}{2}}^{\frac{h}{2}} \sigma_y \, \mathrm{d}z & M_y &= \int_{-\frac{h}{2}}^{\frac{h}{2}} \sigma_y z \, \mathrm{d}z \\ N_{xy} &= \int_{-\frac{h}{2}}^{\frac{h}{2}} \tau_{xy} \, \mathrm{d}z & M_{xy} &= \int_{-\frac{h}{2}}^{\frac{h}{2}} \tau_{xy} z \, \mathrm{d}z \end{aligned} \tag{A.3}$$

The x-y notation here refers to the laminate coordinate system (as illustrated in Figure A.1). Since fibres in every ply can be oriented differently, stiffness must be described in a three-fold manner: Extensional Stiffness (A), Flexural Stiffness (D), and Coupling Stiffness (B) (couples in-plane extensional and out-of-plane flexural responses). These stiffness matrices are then calculated as shown below:

$$A_{ij} = \sum_{k=1}^{N} Q_{ij}^k \left(z_k - z_{k-1}\right) \tag{A.4}$$

$$B_{ij} = \sum_{k=1}^{N} \frac{Q_{ij}^k}{2} \left(z_k^2 - z_{k-1}^2\right) \tag{A.5}$$

$$D_{ij} = \sum_{k=1}^{N} \frac{Q_{ij}^k}{3} \left(z_k^3 - z_{k-1}^3\right) \tag{A.6}$$

Here, N is the number of plies in a laminate, and z_k and z_{k-1} are the top and bottom coordinates of the k^{th} ply, respectively. The numbering system followed for the plies is shown in the following figure:

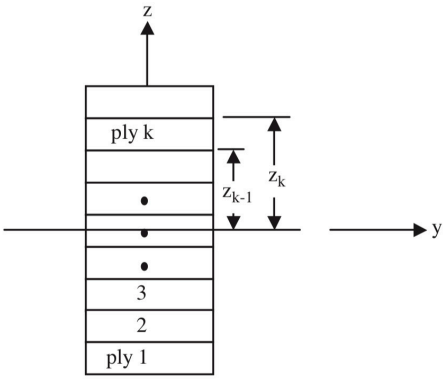

Figure A.3: Numbering convention followed for plies in a laminate (Figure courtesy:[5])

These laminate stiffness matrices are collectively called the ABD matrices in common literature. They relate the applied loads and mid-plane strains of a laminate (as written below in a compact format):

$$\begin{bmatrix} N \\ M \end{bmatrix} = \begin{bmatrix} A & B \\ B & D \end{bmatrix} \begin{bmatrix} \varepsilon^{\circ} \\ \kappa \end{bmatrix} \tag{A.7}$$

The usual norm in industry is to eliminate the membrane/bending coupling effect($B = 0$) by having a symmetric SS of plies in a laminate. When a sequence of plies is mirrored about a mid-plane, the out-of-plane responses for an in-plane load and vice-versa get eliminated. Hence, the above system can be simplified, rearranged, and solved for the mid-plane strains as shown below:

$$\begin{bmatrix} N_x \\ N_y \\ N_{xy} \end{bmatrix} = \begin{bmatrix} A_{11} & A_{12} & A_{16} \\ A_{12} & A_{22} & A_{26} \\ A_{16} & A_{26} & A_{66} \end{bmatrix} \begin{bmatrix} {\varepsilon_x}^{\circ} \\ {\varepsilon_y}^{\circ} \\ {\gamma_{xy}}^{\circ} \end{bmatrix} \qquad \begin{bmatrix} M_x \\ M_y \\ M_{xy} \end{bmatrix} = \begin{bmatrix} D_{11} & D_{12} & D_{16} \\ D_{12} & D_{22} & D_{26} \\ D_{16} & D_{26} & D_{66} \end{bmatrix} \begin{bmatrix} \kappa_x \\ \kappa_y \\ \kappa_{xy} \end{bmatrix}$$

$$(or)$$

$$\left[\begin{array}{c} {\varepsilon_x}^{\circ} \\ {\varepsilon_y}^{\circ} \\ {\gamma_{xy}}^{\circ} \\ \hdashline \kappa_x \\ \kappa_y \\ \kappa_{xy} \end{array}\right] = \left[\begin{array}{ccc:ccc} a_{11} & a_{12} & a_{16} & 0 & 0 & 0 \\ a_{12} & a_{22} & a_{26} & 0 & 0 & 0 \\ a_{16} & a_{26} & a_{66} & 0 & 0 & 0 \\ \hdashline 0 & 0 & 0 & d_{11} & d_{12} & d_{16} \\ 0 & 0 & 0 & d_{12} & d_{22} & d_{26} \\ 0 & 0 & 0 & d_{16} & d_{26} & d_{66} \end{array}\right] \left[\begin{array}{c} N_x \\ N_y \\ N_{xy} \\ \hdashline M_x \\ M_y \\ M_{xy} \end{array}\right]$$

Depending on the failure theory used, the mid-plane strains for a given load case could be directly used to predict laminate failure, or a ply-level stress analysis can be performed. The latter is achieved by using the mid-plane strains to evaluate the lamina strains and stresses, as shown here:

$$\begin{aligned} \varepsilon_x^k &= {\varepsilon_x}^{\circ} + z_k \kappa_x & \sigma_x^k &= Q^k \left[{\varepsilon_x}^{\circ} + z_k \kappa_x \right] \\ \varepsilon_y^k &= {\varepsilon_y}^{\circ} + z_k \kappa_y & \sigma_y^k &= Q^k \left[{\varepsilon_y}^{\circ} + z_k \kappa_y \right] \\ \gamma_{xy}^k &= {\varepsilon_{xy}}^{\circ} + z_k \kappa_{xy} & \tau_{xy}^k &= Q^k \left[{\varepsilon_{xy}}^{\circ} + z_k \kappa_{xy} \right] \end{aligned}$$

The x-y global (laminate) system measures these stresses and strains. Hence, they are usually converted to the 1-2 principal(lamina/ply) system before using them on a failure criterion. This is achieved using tensor transformations with the same direction cosines as mentioned before:

$$\begin{bmatrix} \sigma_1 \\ \sigma_2 \\ \tau_{12} \end{bmatrix}^k = \begin{bmatrix} m^2 & n^2 & 2mn \\ n^2 & m^2 & -2mn \\ -mn & nm & \left(m^2 - n^2\right) \end{bmatrix}^k \begin{bmatrix} \sigma_x \\ \sigma_y \\ \tau_{xy} \end{bmatrix}^k \qquad \begin{bmatrix} \varepsilon_1 \\ \varepsilon_2 \\ \gamma_{12} \end{bmatrix}^k = \begin{bmatrix} m^2 & n^2 & mn \\ n^2 & m^2 & -mn \\ -2mn & 2nm & \left(m^2 - n^2\right) \end{bmatrix}^k \begin{bmatrix} \varepsilon_x \\ \varepsilon_y \\ \gamma_{xy} \end{bmatrix}^k$$

A.2. Material Invariants

$$\Gamma_0 = \begin{bmatrix} U_1 & U_4 & 0 \\ U_4 & U_1 & 0 \\ 0 & 0 & U_5 \end{bmatrix} \quad \Gamma_1 = \begin{bmatrix} U_2 & 0 & 0 \\ 0 & -U_2 & 0 \\ 0 & 0 & 0 \end{bmatrix} \quad \Gamma_2 = \frac{1}{2}\begin{bmatrix} 0 & 0 & U_2 \\ 0 & 0 & U_2 \\ U_2 & U_2 & 0 \end{bmatrix}$$

$$\Gamma_3 = \begin{bmatrix} U_3 & -U_3 & 0 \\ -U_3 & U_3 & 0 \\ 0 & 0 & -U_3 \end{bmatrix} \quad \Gamma_4 = \begin{bmatrix} 0 & 0 & U_3 \\ 0 & 0 & -U_3 \\ U_3 & -U_3 & 0 \end{bmatrix}$$

Where,

$$\begin{aligned} U_1 &= \frac{1}{8}\left(3Q_{11} + 3Q_{22} + 2Q_{12} + 4Q_{66}\right) \\ U_2 &= \frac{1}{2}\left(Q_{11} - Q_{22}\right) \\ U_3 &= \frac{1}{8}\left(Q_{11} + Q_{22} - 2Q_{12} - 4Q_{66}\right) \\ U_4 &= \frac{1}{8}\left(Q_{11} + Q_{22} + 6Q_{12} - 4Q_{66}\right) \\ U_5 &= \frac{1}{8}\left(Q_{11} + Q_{22} - 2Q_{12} + 4Q_{66}\right) \end{aligned}$$

The Q entities shown above are the reduced material stiffness values (for the base ply).

A.3. Empirical Guidelines followed in SS Design

The below-mentioned guidelines are commonly followed in the aerospace industry while designing SS of laminated composites [5, 37, 38].

i. To nullify in-plane and out-plane coupling stiffness (B matrix), mid-plane **symmetry** of a stacking sequence can be enforced. Eliminating coupling behaviour without mid-plane symmetry is explored by the work of York et al. [39].

ii. To nullify coupling responses within the A matrix (extension-shear coupling), the off-axis plies (orientations apart from 0 and 90) need to be **balanced**, that is, every $+\theta$ should have a $-\theta$. Eliminating In-Plane coupling effects without the balancing rule is explored by the work of Montemurro et al. [40].

iii. To nullify coupling responses within the D matrix (bend-twist coupling), the SS can be **anti-symmetric** about midplane. Since this guideline cannot be realised along with the symmetry guideline, the coupling effect is usually minimised by closely placing all balanced pairs ($+\theta$ and $-\theta$) [41].

iv. The **10% Rule** demands 10% of the plies in any given SS to be aligned along the four principal in-plane directions (0,$\pm$45,90). This commonly followed empirical rule explicitly ensures a minimum in-plane stiffness level in all directions to protect a structure against secondary load cases. However, for laminates with Non-Conventional orientations, the robust 10% rule [38, 93] can be used to check if a minimum stiffness value (depending on the material used) is present in the uni-axial states (4 principal directions), and in non-uni-axial states.

v. To induce less residual stresses in laminate while curing and reduce chances of delamination, the **disorientation** guideline does not allow the change of orientation between consecutive layers to be greater than 45°. A lower and upper bound for the difference in consecutive layer's ply orientations can also be formulated from the materials Poisson's ratio [38].

vi. To avoid bridging cracks, **contiguity** guideline does not allow more than 0.6mm of material with the same orientation to be placed together.

vii. For **damage tolerance** and improved buckling performance, the laminate's surface layers should have a $\pm$45 ply.

viii. **Plydrop** guidelines are as follows:

   (a) External ply drops need to be avoided to reduce the tendency of delamination.

(b) It is advised to drop symmetric pairs of plies about the midplane together.
(c) To minimise stress concentrations due to stiffness change at one point, more than 0.5mm worth of plies must not be dropped at one location. They must be staggered at a distance of at least 10-15 times the height of the dropped plies.

ix. The **internal continuity** guideline ensures structural continuity by demanding at least one of every three consecutive layers in a multi-segmented structure to be shared.

From Table A.1 shown below, it is clear that all coupling behaviour in a laminate can be eliminated by nullifying $V^{\{A,D\}}_{[2,4]}$ and $V^{B}_{[1,2,3,4]}$.

Table A.1: Relation between ABD matrix entities and lamination parameters

LPs / A, B, D $terms$	$V_0^{\{A,\sim,D\}}$	$V_1^{\{A,B,D\}}$	$V_2^{\{A,B,D\}}$	$V_3^{\{A,B,D\}}$	$V_4^{\{A,B,D\}}$
$\{A_{11}, B_{11}, D_{11}\}$	U_1	U_2	0	U_3	0
$\{A_{22}, B_{22}, D_{22}\}$	U_1	$-U_2$	0	U_3	0
$\{A_{12}, B_{12}, D_{12}\}$	U_4	0	0	$-U_3$	0
$\{A_{66}, B_{66}, D_{66}\}$	U_5	0	0	$-U_3$	0
$2\{A_{16}, B_{16}, D_{16}\}$	0	0	U_2	0	$2U_3$
$2\{A_{26}, B_{26}, D_{26}\}$	0	0	U_2	0	$-2U_3$

Here, V_0 refers to the normalisation term associated with different LPs. However, completely eliminating coupling responses within the D matrix is difficult in practice, as the guidelines explain. So, the simplification of nullifying $V^{D}_{[2,4]}$ remains an incorrect practice.

A.4. Overview of Designing Steered Fibre Laminates

When the Bi-level design procedure is implemented for steered-fiber laminates, using a finite element paradigm, the process overview will appear as seen below Figure A.4.

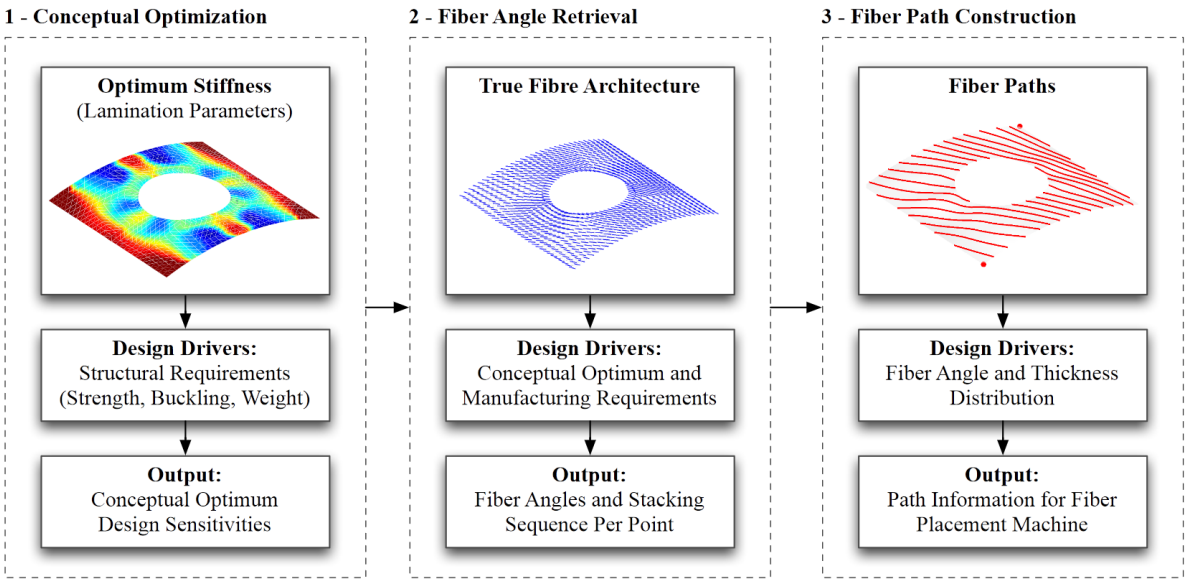

Figure A.4: Design process for steered fibre laminates in a finite element paradigm (Figure Courtesy: [18])

A.5. Fractal patterns of feasible SS with Conventional Orientations

For laminates with conventional orientations, the self-repeating (fractal) nature of feasible design points in all LP space can be observed in the following image:

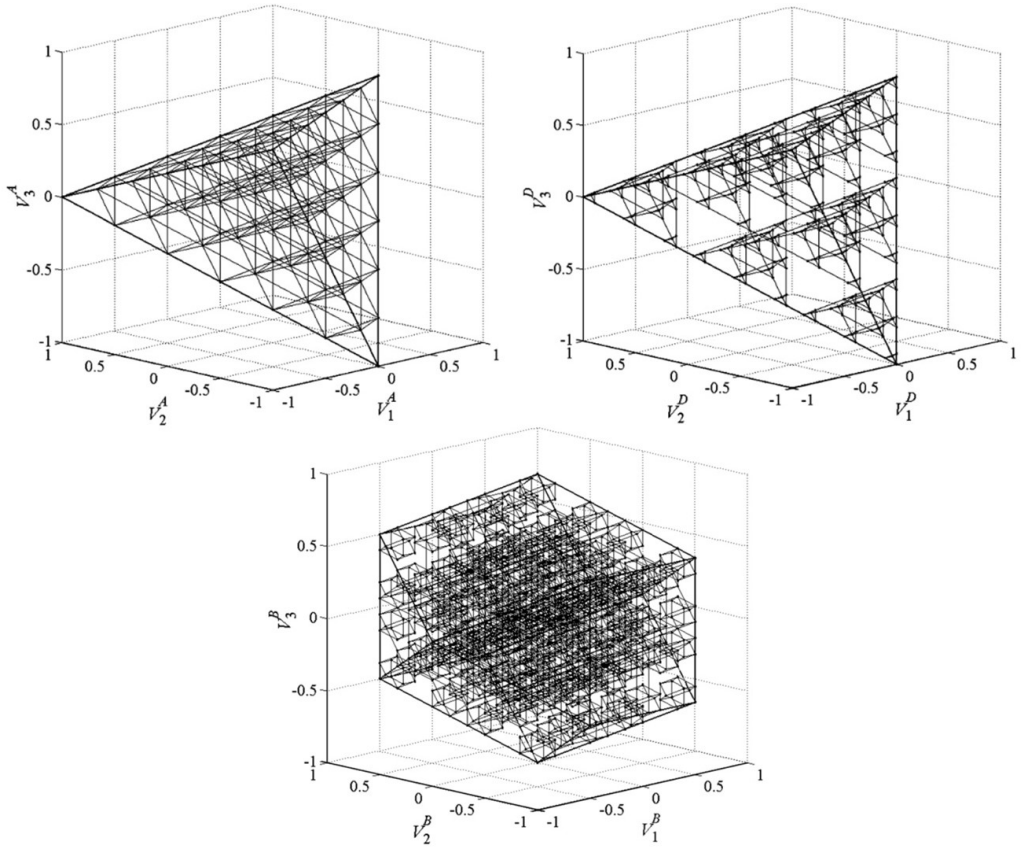

Figure A.5: Realised fractal patterns for a 6-ply laminate with conventional orientations (Figure Courtesy: [77])

B

Research Implementation

B.1. Alternate Time-Domain Parameterisations Considered

The macro-mechanical behaviour of laminated composites is influenced by: (1) the orientation of fibres θ within each layer and (2) the position of each layer with respect to the laminate mid-plane z. Hence, a signal must ideally capture these two characteristics. In a signal made with a set of designed LPs, if the frequencies present within them are z, and their associated amplitudes are the θ, an FFT can instantaneously provide the orientations associated with all layers. However, such a signal cannot be well-described using LPs. This is because the frequency is an argument of the sinusoidal function present within the definition of LPs. Hence, this parameterisation was not mathematically possible.

Another approach is parameterising the phase difference ϕ as θ and keeping frequency constant. However, FFTs decompose a signal using frequency, meaning all information about ϕ will be imposed over one frequency. This would add a more complex problem to the procedure: decomposing the phase differences into a SS. Hence, such parameterisations were also not considered for further studies.

B.2. Parameters used for Genetic Algorithm

For all the case studies within the thesis and to help generate more signal patterns, FAD and SS for a set of target LPs were designed using the open-source GA OptiBLESS [90]. The following parameters were used while operating this MATLAB program.

Table B.1: OptiBLESS GA setting values

OptiBLESS Options	Value
Population Size	200
Minimum No. of Generation	500
Maximum No. of Generation	2000
Probability of Crossover	0.8
Elitism (%)	30
Objective Function	Root Mean Square Error

B.3. Complete list of Exact Patterns made using $[\Delta 15^{\circ}]$

Presented in the following page.

Table B.2: Exact Signal Patterns for Laminates made of $[\Delta 15^\circ]$ orientations

Orientations	$T=0$	$T=1$	$T=2$	$T=3$	$T=4$	$T=5$	$T=6$
$[0,15,30]$	1	V_1^A	V_3^A	$6.46-10.19V_1^A+4.73V_3^A$	$20.39-30.58V_1^A+11.19V_3^A$	$35.32-51.98V_1^A+17.66V_3^A$	$41.78-61.17V_1^A+20.39V_3^A$
$[0,15,45]$	1	V_1^A	V_3^A	$3.73-6.46V_1^A+3.73V_3^A$	$7.46-12.93V_1^A+6.46V_3^A$	$7.46-13.93V_1^A+7.46V_3^A$	$6.46-12.92V_1^A+7.46V_3^A$
$[0,15,60]$	1	V_1^A	V_3^A	$1-2.73V_1^A+2.73V_3^A$	$-2.73V_1^A+3.73V_3^A$	$-3.73V_1^A+4.73V_3^A$	$1+5.46(V_3^A-V_1^A)$
$[0,15,75]$	1	V_1^A	V_3^A	$-1+2V_3^A$	$-2+V_3^A$	$-2-V_1^A+4V_3^A$	$-3+4V_3^A$
$[0,15,90]$	1	V_1^A	V_3^A	$-1.73+V_1^A+1.73V_3^A$	$-2+V_3^A$	$-3.46+V_1^A+3.46V_3^A$	$-3+4V_3^A$
$[0,30,45]$	1	V_1^A	V_3^A	$3-5V_1^A+3V_3^A$	$4-6V_1^A+3V_3^A$	V_1^A	$-3+6V_1^A-2V_3^A$
$[0,30,60]$	1	V_1^A	V_3^A	$1-2V_1^A+2V_3^A$	V_3^A	V_1^A	1
$[0,30,75]$	1	V_1^A	V_3^A	$-0.46+0.19V_1^A+1.26V_3^A$	$-0.39+0.58V_1^A+0.8V_3^A$	$0.68-0.02V_1^A+0.34V_3^A$	$0.21+1.17V_1^A-0.39V_3^A$
$[0,30,90]$	1	V_1^A	V_3^A	$-1+V_1^A+V_3^A$	V_3^A	V_1^A	1
$[0,45,60]$	1	V_1^A	V_3^A	$1-V_1^A+V_3^A$	$2V_1^A-V_3^A$	V_1^A	$1-2V_1^A+2V_3^A$
$[0,45,75]$	1	V_1^A	V_3^A	$0.26+0.46V_1^A+0.26V_3^A$	$0.53+0.92V_1^A-0.46V_3^A$	$0.53-0.07V_1^A+0.53V_3^A$	$-0.46+0.92V_1^A+0.53V_3^A$
$[0,45,90]$	1	V_1^A	V_3^A	V_1^A	1	V_1^A	V_3^A
$[0,60,75]$	1	V_1^A	V_3^A	$1+0.73V_1^A-0.73V_3^A$	$0.73V_1^A+0.26V_3^A$	$-0.26V_1^A+1.26V_3^A$	$1+1.46V_1^A-1.46V_3^A$
$[0,60,90]$	1	V_1^A	V_3^A	$1+V_1^A-V_3^A$	V_3^A	V_1^A	1
$[0,75,90]$	1	V_1^A	V_3^A	$1.73+V_1^A-1.73V_3^A$	$-2+V_3^A$	$3.46+V_1^A-3.46V_3^A$	$-3+4V_3^A$
$[15,30,45]$	1	V_1^A	V_3^A	$2.73-4.73V_1^A+2.73V_3^A$	$2.73-4.73V_1^A+1.73V_3^A$	$-2.73+3.73V_1^A-2.73V_3^A$	$-6.46+9.46V_1^A-5.46V_3^A$
$[15,30,60]$	1	V_1^A	V_3^A	$0.86-2V_1^A+1.73V_3^A$	-0.5	$-0.86+V_1^A-1.73V_3^A$	$-2V_3^A$
$[15,30,75]$	1	V_1^A	V_3^A	$-0.5+V_3^A$	-0.5	$0.5-V_1^A-V_3^A$	$-2V_3^A$
$[15,30,90]$	1	V_1^A	V_3^A	$-1+0.73V_1^A+0.73V_3^A$	$-0.73V_1^A+0.26V_3^A$	$-0.26V_1^A-1.26V_3^A$	$1-1.46V_1^A-1.46V_3^A$
$[15,45,60]$	1	V_1^A	V_3^A	$0.73-1.26V_1^A+0.73V_3^A$	$-0.73+1.26V_1^A-1.73V_3^A$	$-0.73+0.26V_1^A-0.73V_3^A$	$0.46-2.53V_1^A+1.46V_3^A$
$[15,45,75]$	1	V_1^A	V_3^A	0	$-V_3^A$	$-V_1^A$	-1
$[15,45,90]$	1	V_1^A	V_3^A	$-0.26+0.46V_1^A-0.26V_3^A$	$0.53-0.93V_1^A-0.46V_3^A$	$-0.53-0.07V_1^A-0.53V_3^A$	$-0.46-0.92V_1^A+0.53V_3^A$
$[15,60,75]$	1	V_1^A	V_3^A	$0.5-V_3^A$	-0.5	$0.5-V_1^A+V_3^A$	$-2V_3^A$
$[15,60,90]$	1	V_1^A	V_3^A	$0.46+0.19V_1^A-1.26V_3^A$	$-0.39-0.58V_1^A+0.8V_3^A$	$-0.67-0.02V_1^A-0.34V_3^A$	$0.21-1.17V_1^A-0.39V_3^A$
$[15,75,90]$	1	V_1^A	V_3^A	$1-2V_3^A$	$-2+V_3^A$	$2-V_1^A-4V_3^A$	$-3+4V_3^A$
$[30,45,60]$	1	V_1^A	V_3^A	$-2V_1^A$	$-2+V_3^A$	V_1^A	$3+4V_3^A$
$[30,45,75]$	1	V_1^A	V_3^A	$-0.73-1.26V_1^A-0.73V_3^A$	$-0.73-1.26V_1^A-1.73V_3^A$	$0.73+0.26V_1^A+0.73V_3^A$	$0.46+2.53V_1^A+1.46V_3^A$
$[30,45,90]$	1	V_1^A	V_3^A	$-1-V_1^A-V_3^A$	$-2V_1^A-V_3^A$	V_1^A	$1+2V_1^A+2V_3^A$
$[30,60,75]$	1	V_1^A	V_3^A	$-0.86-2V_1^A-1.73V_3^A$	-0.5	$0.86+V_1^A+1.73V_3^A$	$-2V_3^A$
$[30,60,90]$	1	V_1^A	V_3^A	$-1-2V_1^A-2V_3^A$	V_3^A	V_1^A	1
$[30,75,90]$	1	V_1^A	V_3^A	$-1-2.73V_1^A-2.73V_3^A$	$2.73V_1^A+3.73V_3^A$	$-3.73V_1^A-4.73V_3^A$	$1+5.46(V_3^A+V_1^A)$
$[45,60,75]$	1	V_1^A	V_3^A	$-2.73-4.73V_1^A-2.73V_3^A$	$2.73+4.73V_1^A+1.73V_3^A$	$2.73+3.73V_1^A+2.73V_3^A$	$-6.46-9.46V_1^A-5.46V_3^A$
$[45,60,90]$	1	V_1^A	V_3^A	$-3-5V_1^A-3V_3^A$	$4+6V_1^A+3V_3^A$	V_1^A	$-3-6V_1^A-2V_3^A$
$[45,75,90]$	1	V_1^A	V_3^A	$-3.73-6.46V_1^A-3.73V_3^A$	$7.46+12.92V_1^A+6.46V_3^A$	$-7.46-13.93V_1^A-7.46V_3^A$	$6.46+12.93V_1^A+7.46V_3^A$
$[60,75,90]$	1	V_1^A	V_3^A	$-6.46-10.19V_1^A-4.73V_3^A$	$20.39+30.58V_1^A+11.19V_3^A$	$-35.32-51.98V_1^A-17.66V_3^A$	$41.78+61.17V_1^A+20.39V_3^A$

B.4. Complete list of Approximate Patterns made for $[\Delta 15^{\circ}]$

Presented in the following page.

Table B.3: Approximate Signal Patterns for Laminates made of more than three orientations within the set $[\Delta 15°]$. Unsampled timestamps are marked with an X.

Approximate Pattern	$T=0$	$T=1$	$T=2$	$T=3$	$T=4$	$T=5$	$T=6$
1	1	V_1^A	V_3^A	X	$-V_3^A$	$-V_1^A$	X
2	1	V_1^A	V_3^A	X	V_3^A	V_1^A	X
3	1	V_1^A	V_3^A	X	$1-V_3^A$	$1-V_1^A$	X
4	1	V_1^A	V_3^A	X	V_3^A	V_3^A	X
5	1	V_1^A	V_3^A	X	$2V_1^A$	V_1^A	X
6	1	V_1^A	V_3^A	$-V_3^A$	$V_1^A - V_3^A$	V_1^A	$-V_1^A$
7	1	V_1^A	V_3^A	$-V_3^A$	$V_3^A - V_1^A$	V_1^A	$-V_1^A$
8	1	V_1^A	V_3^A	V_1^A	V_3^A	V_1^A	$-V_1^A$
9	1	V_1^A	V_3^A	X	X	V_1^A	$-V_1^A$
10	1	V_1^A	V_3^A	V_1^A	V_3^A	V_1^A	V_1^A
11	1	V_1^A	V_3^A	$0.5V_3^A$	$-V_3^A$	$-0.85V_3^A$	V_1^A
12	1	V_1^A	V_3^A	V_3^A	$0.5V_3^A$	$0.5(V_1^A + V_3^A)$	$0.5V_3^A$
13	1	V_1^A	V_3^A	$0.36(V_3^A - V_1^A)$	$0.34V_1^A$	V_1^A	$0.33V_1^A$
14	1	V_1^A	V_3^A	$1 + V_1^A - V_3^A$	V_3^A	V_1^A	1
15	1	V_1^A	V_3^A	$0.84V_1^A + 0.34V_3^A$	$0.59V_3^A$	$0.87V_1^A + 0.59V_3^A$	$0.43V_3^A$
16	1	V_1^A	V_3^A	$-2V_1^A$	$-0.5(V_1^A + V_3^A)$	V_1^A	$0.5(V_3^A - V_1^A)$
17	1	V_1^A	V_3^A	$0.36(V_3^A - V_1^A)$	$-0.34V_1^A$	$-V_1^A$	-0.6
18	1	V_1^A	V_3^A	$V_1^A + V_3^A$	$-V_1^A$	V_1^A	$-2V_1^A$
19	1	V_1^A	V_3^A	V_1^A	$0.5(V_1^A + V_3^A)$	V_1^A	$-0.5(V_1^A + V_3^A)$
20	1	V_1^A	V_3^A	$-2V_1^A$	$0.2V_3^A$	V_1^A	$-0.8V_3^A$
21	1	V_1^A	V_3^A	$-2V_1^A$	$5V_3^A$	V_1^A	$4V_3^A$
22	1	V_1^A	V_3^A	0	$1.66V_3^A$	$-V_1^A$	0
23	1	V_1^A	V_3^A	$V_3^A - 0.5$	-0.5	$0.5 - (V_1^A + V_3^A)$	$-2V_3^A$

B.5. Design Domain of Approximate Signal Patterns

From the Miki's diagram in the literature review (from Figure 3.1), it was understood that every $V^A_{1,3}$ combination along the periphery of the feasible domain can be associated with a laminate only made of one $|\theta|$. For Exact Patterns it is known that they can design a FAD with three $|\theta|$'s. Hence, their design domain are the polygon inscribed between three points corresponding to the three $|\theta|$'s on the Miki's diagram. Such an analogy cannot be repeated to judge the design domain of the Approximate Patterns, as they inherently fix the contribution of certain $|\theta|$'s. Hence, their design domains can be visualised only by plotting error profiles for different N. The following set of 23 plots are the design domains for the 23 Approximate Patterns that have been found for designing with $[\Delta 15°]$ (as seen in section 10.2).

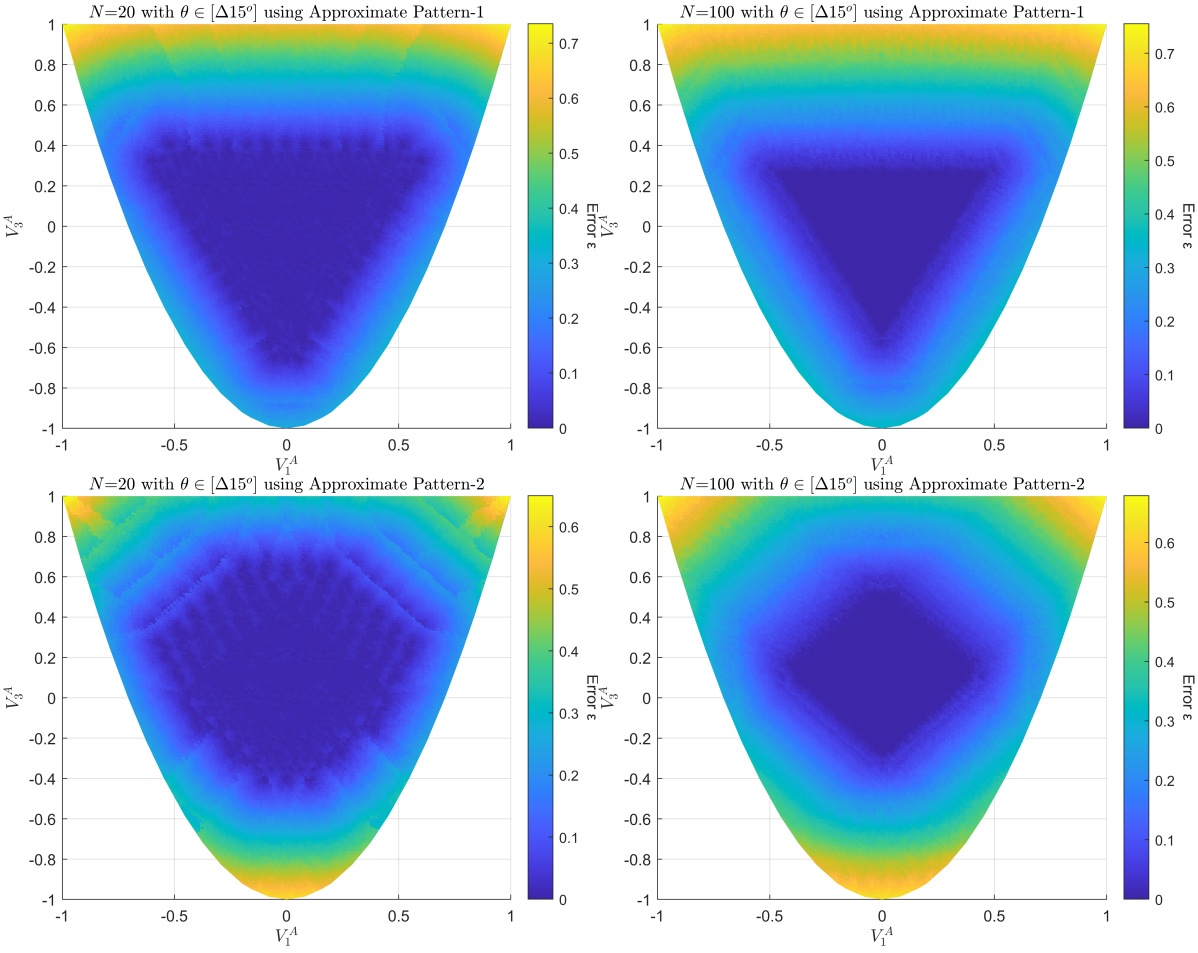

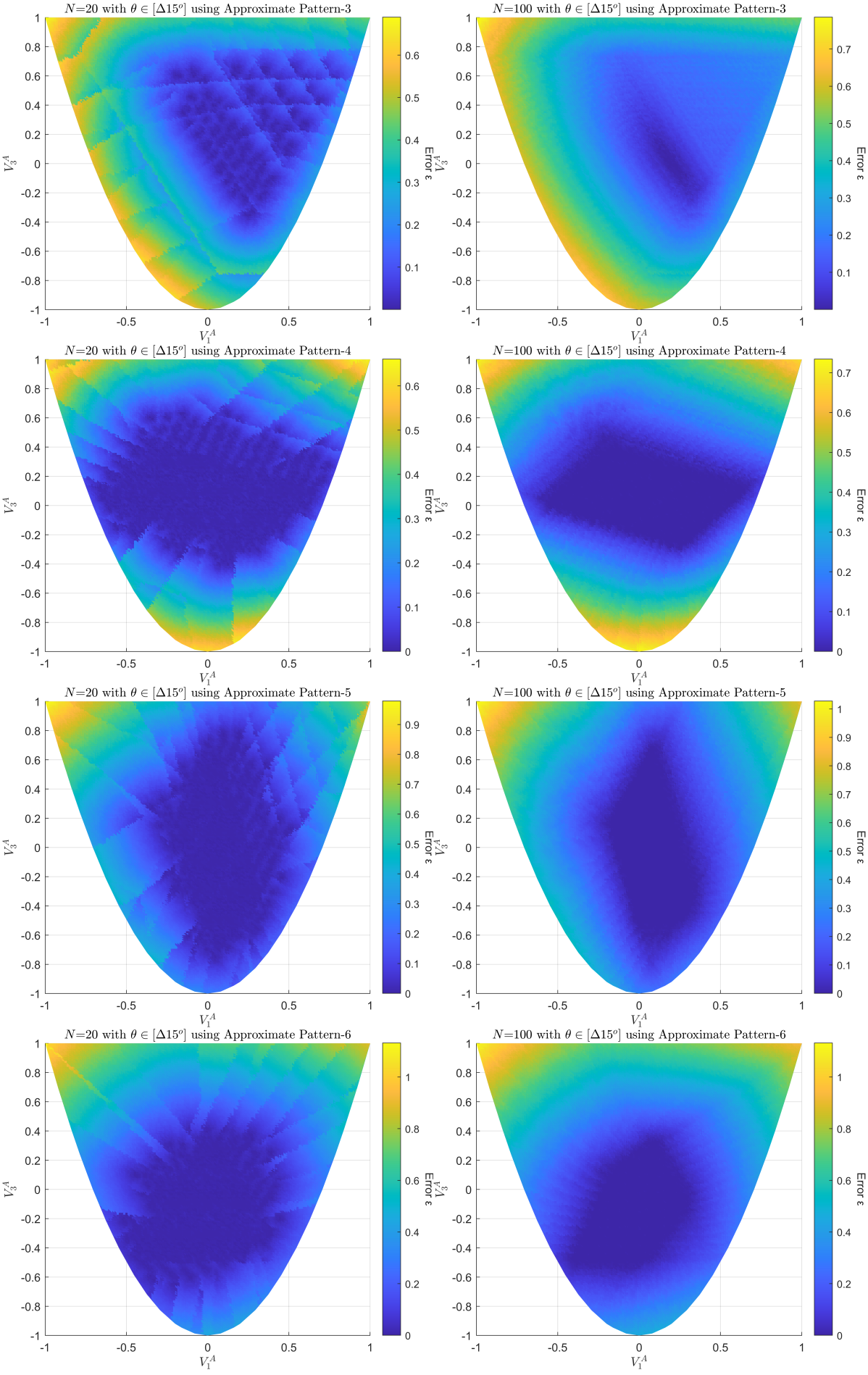
N=20 with $\theta \in [\Delta 15^o]$ using Approximate Pattern-3
N=100 with $\theta \in [\Delta 15^o]$ using Approximate Pattern-3
N=20 with $\theta \in [\Delta 15^o]$ using Approximate Pattern-4
N=100 with $\theta \in [\Delta 15^o]$ using Approximate Pattern-4
N=20 with $\theta \in [\Delta 15^o]$ using Approximate Pattern-5
N=100 with $\theta \in [\Delta 15^o]$ using Approximate Pattern-5
N=20 with $\theta \in [\Delta 15^o]$ using Approximate Pattern-6
N=100 with $\theta \in [\Delta 15^o]$ using Approximate Pattern-6
V_1^A
V_3^A
Error ε

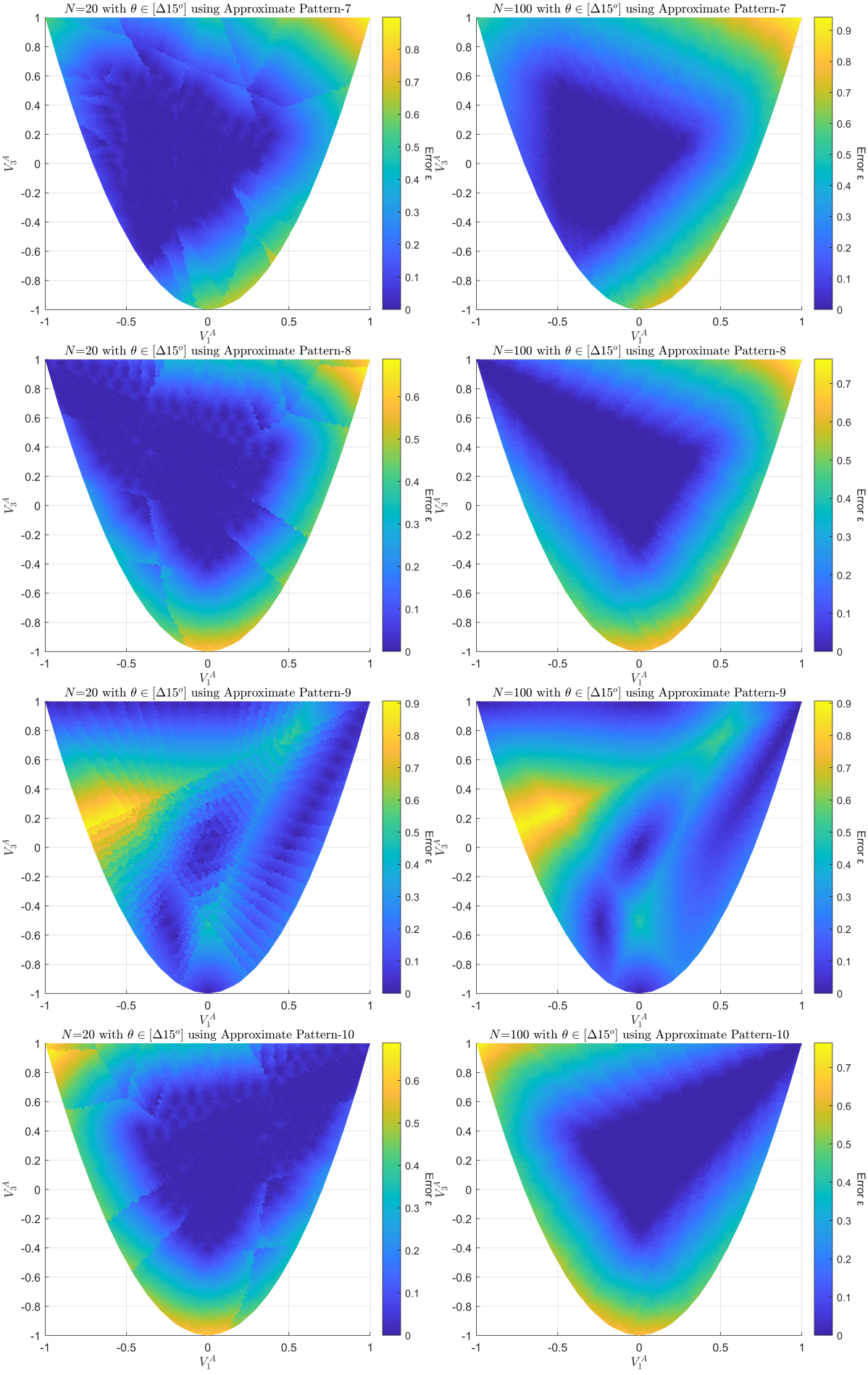
N=20 with $\theta \in [\Delta 15^o]$ using Approximate Pattern-7
N=100 with $\theta \in [\Delta 15^o]$ using Approximate Pattern-7
N=20 with $\theta \in [\Delta 15^o]$ using Approximate Pattern-8
N=100 with $\theta \in [\Delta 15^o]$ using Approximate Pattern-8
N=20 with $\theta \in [\Delta 15^o]$ using Approximate Pattern-9
N=100 with $\theta \in [\Delta 15^o]$ using Approximate Pattern-9
N=20 with $\theta \in [\Delta 15^o]$ using Approximate Pattern-10
N=100 with $\theta \in [\Delta 15^o]$ using Approximate Pattern-10
V_1^A
V_3^A
Error ε

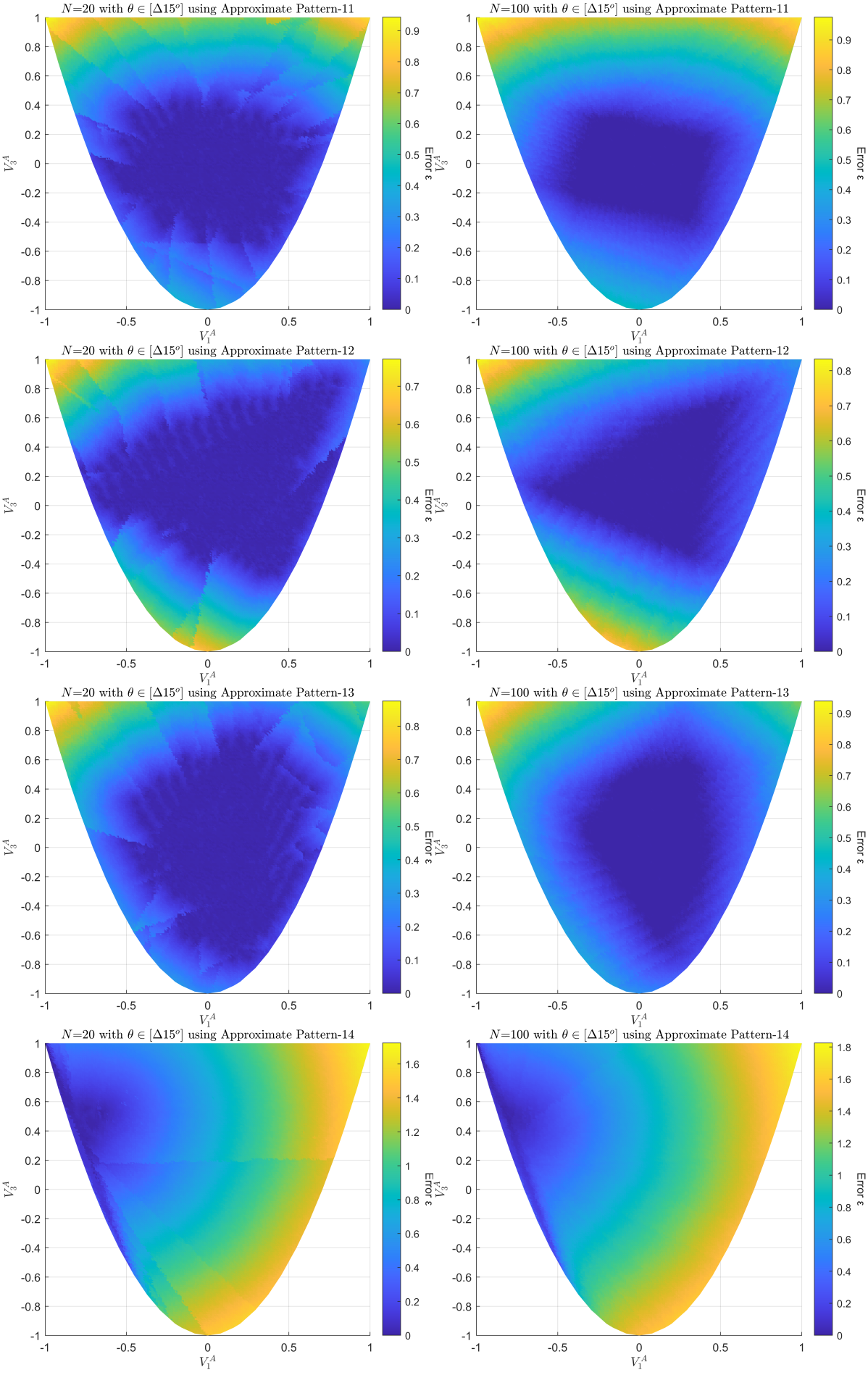
N=20 with $\theta \in [\Delta 15^o]$ using Approximate Pattern-11
N=100 with $\theta \in [\Delta 15^o]$ using Approximate Pattern-11
N=20 with $\theta \in [\Delta 15^o]$ using Approximate Pattern-12
N=100 with $\theta \in [\Delta 15^o]$ using Approximate Pattern-12
N=20 with $\theta \in [\Delta 15^o]$ using Approximate Pattern-13
N=100 with $\theta \in [\Delta 15^o]$ using Approximate Pattern-13
N=20 with $\theta \in [\Delta 15^o]$ using Approximate Pattern-14
N=100 with $\theta \in [\Delta 15^o]$ using Approximate Pattern-14
V_1^A
V_3^A
Error ε

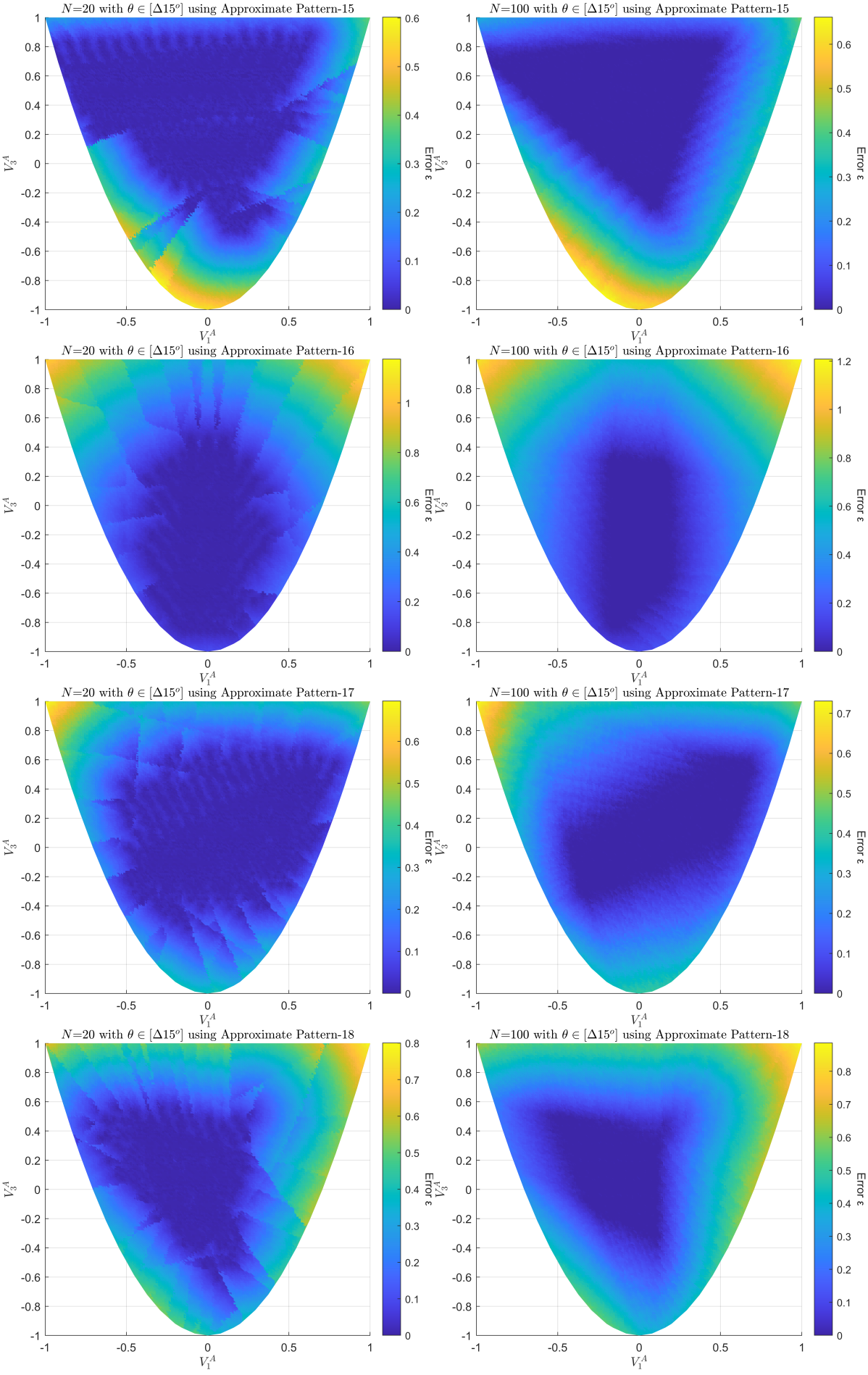
N=20 with $\theta \in [\Delta 15^o]$ using Approximate Pattern-15
N=100 with $\theta \in [\Delta 15^o]$ using Approximate Pattern-15
N=20 with $\theta \in [\Delta 15^o]$ using Approximate Pattern-16
N=100 with $\theta \in [\Delta 15^o]$ using Approximate Pattern-16
N=20 with $\theta \in [\Delta 15^o]$ using Approximate Pattern-17
N=100 with $\theta \in [\Delta 15^o]$ using Approximate Pattern-17
N=20 with $\theta \in [\Delta 15^o]$ using Approximate Pattern-18
N=100 with $\theta \in [\Delta 15^o]$ using Approximate Pattern-18
V_1^A
V_3^A
Error ε

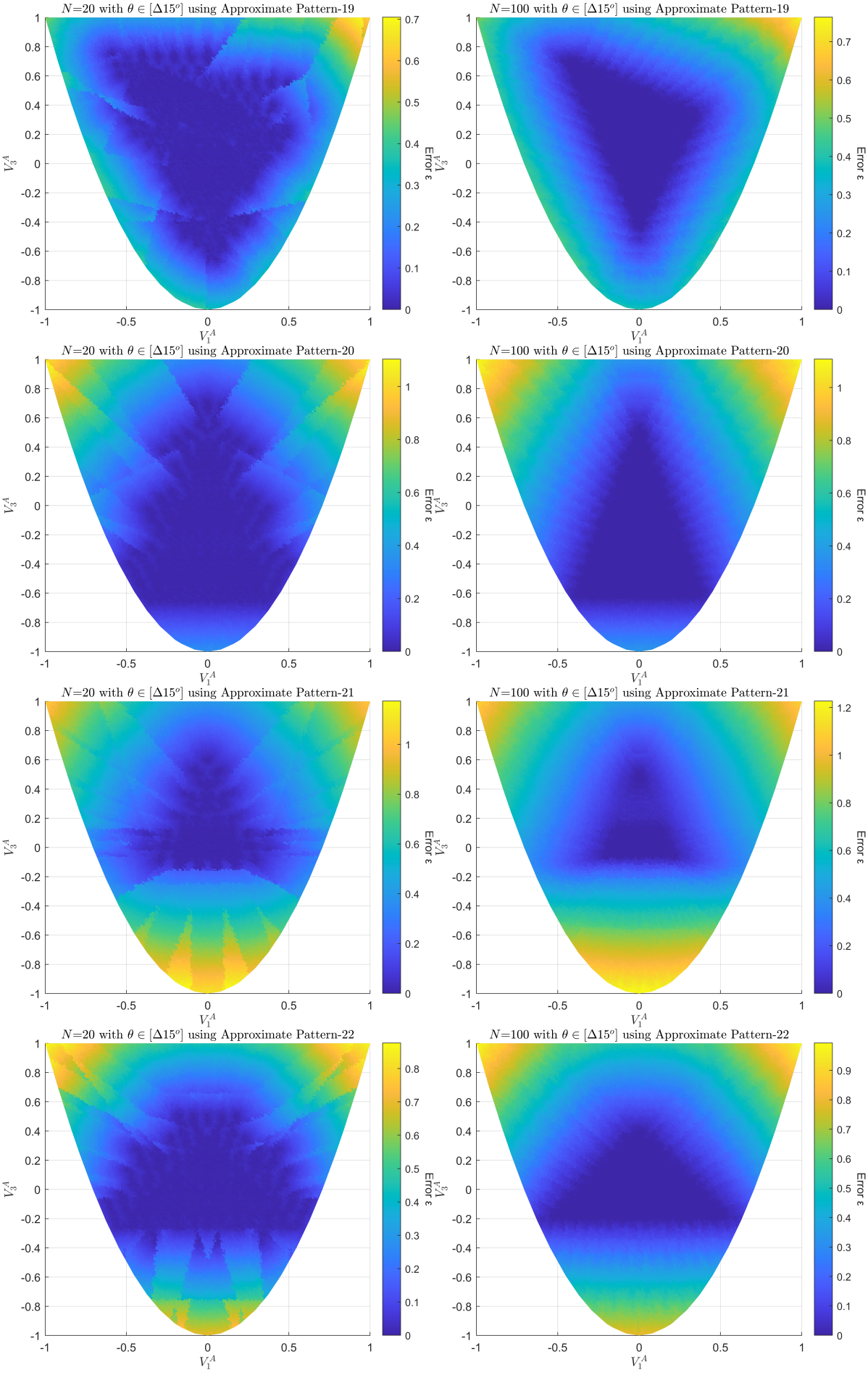
N=20 with $\theta \in [\Delta 15^o]$ using Approximate Pattern-19
N=100 with $\theta \in [\Delta 15^o]$ using Approximate Pattern-19
N=20 with $\theta \in [\Delta 15^o]$ using Approximate Pattern-20
N=100 with $\theta \in [\Delta 15^o]$ using Approximate Pattern-20
N=20 with $\theta \in [\Delta 15^o]$ using Approximate Pattern-21
N=100 with $\theta \in [\Delta 15^o]$ using Approximate Pattern-21
N=20 with $\theta \in [\Delta 15^o]$ using Approximate Pattern-22
N=100 with $\theta \in [\Delta 15^o]$ using Approximate Pattern-22
V_1^A
V_3^A
Error ε

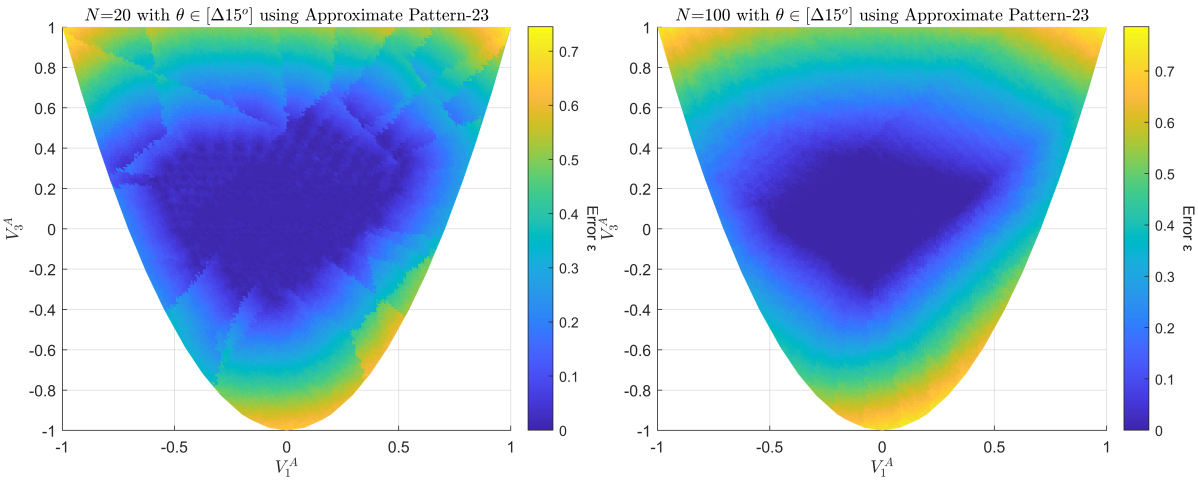

Figure B.1: Design Domains of all 23 Approximate Patterns for $[\Delta 15°]$: $N = 20$ (left) and $N = 100$ (right)

B.6. Sampling Scheme to make 4D benchmark dataset of $V^A_{1,2,3,4}$

For a quasi-random sampling of a design space, the Sobol and Latin hypercube sampling (LHS) methods are popularly used in the literature [94]. In order to choose one method over the other, the design space projections of the samples generated by both of them were compared. Sobol is a deterministic method, and the LHS was implemented with a seed value of 5466210 (TU Delft Student Number).

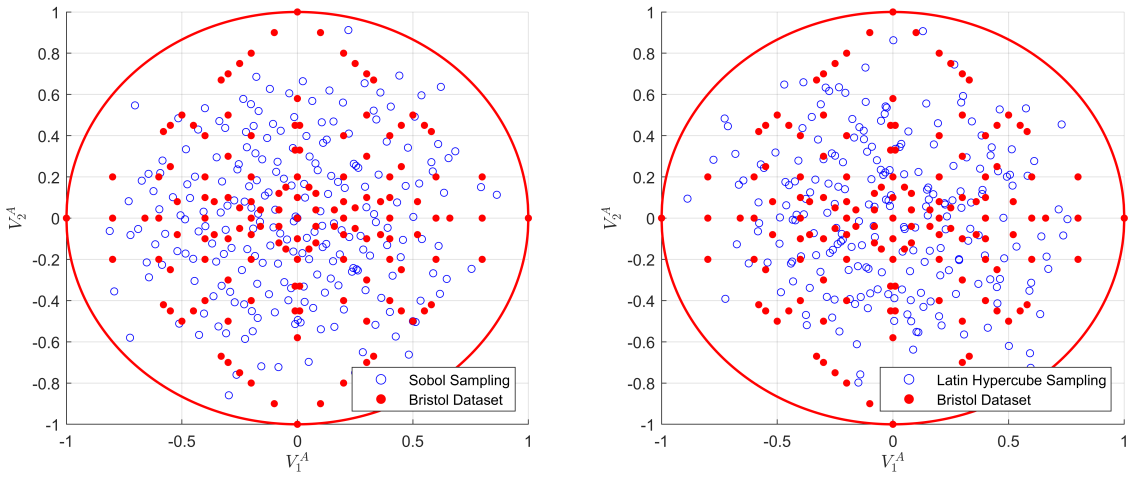

Figure B.2: $V_1^A - V_2^A$ projections of the samples generated by Sobol Sampling (left) and LHS (right)

Compared to the Bristol dataset, both the quasi-random sample sets have a better spread over the design space. However, the Sobol sampling method had less tendency to over-sample a particular region. Hence, they were chosen over LHS for the benchmarking exercise (in subsection 10.3.2).